Internal and External Light Trapping for Solar Cells and Modules

Cover image: artistic impression of an external light trap. Light is focused through an aperture by a parabolic mirror and travels several times through the solar cell (red). This results in an increase of the absorption in the solar cell.

ISBN 978-90-393-6566-3

Internal and External Light Trapping for Solar Cells and Modules

Interne en Externe Lichtopsluiting voor Zonnecellen en Zonnepanelen

(met een samenvatting in het Nederlands)

Proefschrift

ter verkrijging van de graad van doctor aan de Universiteit Utrecht
op gezag van de rector magnificus, prof. dr. G.J. van der Zwaan,
ingevolge het besluit van het college voor promoties in het
openbaar te verdedigen op 30 mei 2016
des middags te 12.45 uur

door

Lourens van Dijk

geboren op 7 januari 1987 te Leusden

Promotoren: Prof. dr. R. E. I. Schropp
Prof. dr. A. Polman
Copromotor: Dr. M. Di Vece

The work described in this thesis is supported by NanoNextNL, a micro and nano-technology consortium of the Government of the Netherlands and 130 partners.

Abstract

Renewable energy resources are essential to realize a sustainable society and a clean environment. In virtually all energy scenarios, solar power will supply a significant fraction of the world energy demand within a few decades. This energy transition can be significantly supported and accelerated when the power conversion efficiency of solar cells improves. This will bring down the costs per delivered unit of energy and thereby solar cells become even more financially competitive with burning fossil fuels. The efficiency of solar cells is related to their absorptance. Conventional solar cells do not absorb all the sunlight; instead they reflect a fraction to space. This reflection loss is one of the causes preventing solar modules from achieving their potential energy conversion efficiency.

This thesis focuses on two optical solutions for improved absorptance of light in solar modules: internal and external light trapping. For internal light trapping the solar cell is internally modified to guide the light, while for external light trapping optical elements are applied on top of the cell.

Internal light trapping is demonstrated in a nano-crystalline silicon solar cell by applying an array of glass nano-cylinders that is over-coated by silver at the backside of the cell (chapter 3). Due to the geometry and refractive index contrast of these three materials, the light scatters when it interacts with this back reflector. By total internal reflection in the silicon, most of the scattered light will travel a much longer distance through the cell compared to a flat cell. This leads to a significant increase in the absorptance and thereby an increase in cell efficiency.

The second part of this thesis describes various aspects of external light trapping. In an external light trap the light that reflects from the solar cell is recycled in a cage between the solar cell and a mirror above the solar cell. A lens is used to guide the light into this cage through a small aperture in the mirror. The light reflecting from the solar cell is now reflected back to the cell leading to an enhanced efficiency. A successful demonstration is shown of a 3D-printed external light trap on top of a nano-crystalline silicon solar cell (chapter 4). Furthermore, the opportunities for external light trapping on a large area are explored by making an array of lenses which is tested on an organic solar cell (chapter 5). Finally, a series

of external light traps is fabricated by an industrial milling process and tested on top of a crystalline silicon solar cell (chapter 6). The results pave the way towards the commercial application of external light trapping on solar modules (chapter 7).

Contents

Chapter 1

General Introduction

The earth is a beautiful and hospitable planet to live on. However, some solutions are urgently required to ensure the earth remains equally livable for the time to come. Our current energy management puts a heavy burden on the environment. To sustain a clean environment it is key to adapt our energy generation and consumption. The availability of powerful, clean, and economical viable technology is essential to establish a renewable energy infrastructure. Solar panels are one of the most promising technologies to facilitate this energy transition. The goal of this thesis is to explore novel methods for light trapping in solar panels that can improve their power conversion efficiency and economic competitiveness. Here, we first briefly explain the consequences of our current energy system and discuss several motivations to work on renewable energy before we focus on the potential of solar energy as a source for renewable energy for the future.

1.1 Global Environmental and Energy Challenges

Important motivations to further develop renewable energy resources (renewables) are the environmental benefits, low-cost availability, and the abundance of these resources, as will be described here.

Environmental Benefits. Figure 1.1a shows the increase of the global carbon-dioxide (CO_2) level of more than 40 percent during the last centuries. This increase is mainly attributed to the burning of fossil fuels[1] and such an increase does not come without environmental impact. A major fraction of the CO_2 is dissolved into oceans and affects the ocean's wild life due to acidification by the uptake of CO_2. The CO_2 that remains in the atmosphere results in a radiative imbalance of the earth, thereby increasing the global temperature. Figure 1.1b shows the measured

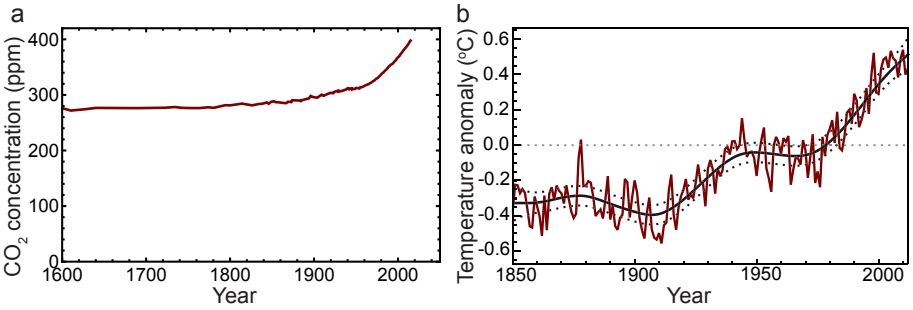

Figure 1.1: **(a)** Measured CO_2 level (ppm) in the atmosphere over the last centuries. Data obtained from reference.[3] **(b)** Global average temperature since the year 1850. The red curve shows the global mean surface temperature anomaly. The data is relative to the "normal" climate conditions between 1961 and 1990. The black solid curve is a smoothing spline through the data. Figure adapted from IPCC report.[1]

increase in global average temperature after the industrial revolution. The global temperature increased by ~0.8 °C since the year 1880. The radiative imbalance is expected to result in more extreme climate conditions than we have experienced so far.[2] Besides these negative global environmental effects, the burning of fossil fuels results in severe smog in cities, which severely impacts the life expectancy of many people.

To prevent these negative consequences from occurring, it would be wise to prevent climate change from becoming even more extreme in the next decades. The effective emission of CO_2 and that of other greenhouse gases has therefore to be reduced, and finally to be virtually eliminated. The net CO_2 (equivalent) emission from renewables is much lower than that of fossil fuels and therefore they are well suited to achieve this (close to) zero emission target.

Low-cost and Abundant Availability. It is becoming increasingly more difficult to exploit fossil fuels: the cost and energy required to extract them from the earth has increased significantly over the years and this is not expected to change in the future. Interestingly, the energy stored in the natural reserves of coal, oil, and gas is equivalent to no more than the global irradiance by the sun in just around 20 days. The current way of generating energy from fossil fuels can thus only be sustained on a short time-scale. On the other hand, renewable energy resources are sustainable and abundantly available. Moreover, their exploitation cost will drop over time due to progressing technology and economies of scale. The local deployment of renewable energy makes countries (energy) independent. Thereby, it prevents abuse of political power between different nations and ensures energy security.

Most readers of this thesis will be accustomed to the present-day relatively low and affordable prices of energy. However, the contrary is true for many people

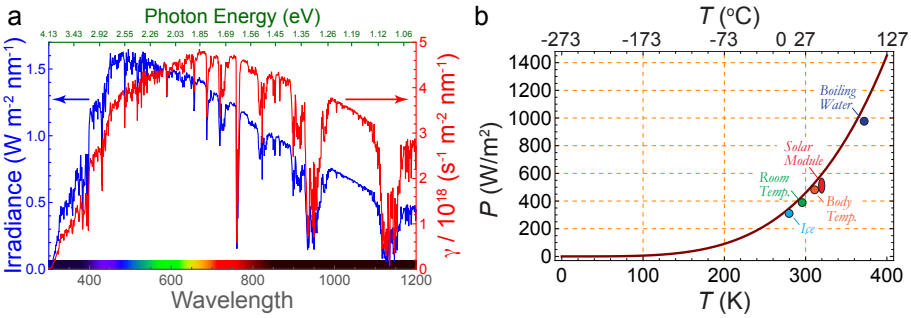

Figure 1.2: **(a)** Spectrum of the sun as a function of the wavelength (and photon energy). The blue curve shows the power spectrum and the red curve shows the photon spectrum. **(b)** Thermal emission of a black body according to the Stefan-Boltzmann law as a function of the temperature. For reference, the emission by several "daily objects" is roughly indicated (assuming an emissivity of 0.9). Generally, the emissivity of such objects (except metals) is 5-20% lower than that of a black body. The indicated temperature of a solar module indicates a typical nominal operating cell temperature (NOCT) of 48 ° C at an irradiance of 800 W/m^2.

living in developing countries that pay much more per unit of electrical energy coming from diesel-fired power plants. Cheap availability of renewable energy can resolve energy poverty and enable a sustainable economic growth of these countries, and thereby the global economy becomes more resilient.

1.1.1 Thermal Radiation and Climate

Thermal Emission - From the Universe to the Earth and Back Again. Due to thermonuclear fusion at the core of the sun, the surface of the sun has a temperature of around 5800 K. At this temperature, the charged particles continuously oscillate, the associated acceleration results in electromagnetic radiation. Figure 1.2a shows a standardized solar spectrum[4] as received at earth. The blue curve shows the irradiance (or energy intensity) in units of W/m^2/nm and the red curve the photon flux in units of number of photons/s/m^2/nm. The highest irradiance of the spectrum is at a wavelength of ~500 nm and the highest photon flux is at ~650 nm.

Fig 1.2b shows the thermal radiation of a black body according to the Stefan-Boltzmann law: $P = A\epsilon\sigma T^4$, for an emitting area (A) of 1 m^2 with an emissivity (ϵ) of 1. It also shows the radiative emission by a solar cell at typical outdoor conditions; a large fraction of the sunlight not converted into electricity heats the module and escapes via radiation (assuming[5,6] ϵ=0.8 to 0.9); another major part is lost via convection. The surface of the sun emits an impressive intensity of around 63 MW/m^2 due to its extremely high temperature.

On the ~150 million kilometer long journey of the sunlight towards the earth,

the light diverges and the intensity is reduced to ~1.35 kW/m^2 at the top of the earth's atmosphere. As the light travels through the atmosphere, the (direct) flux is reduced further due to absorption and scattering in the air. A fraction of the incoming radiation is reflected by both the atmosphere and the earth surface to outer space. The remaining fraction is absorbed by the earth, and thermally radiated at much longer wavelengths of ~5-50 μm.

The transmission of light by the earth's atmosphere depends on the wavelength of light. For example, CO_2 is relatively transparent for wavelengths up to 1.5 μm, but it has several absorption bands at longer wavelengths where the earth is radiating. For this reason, CO_2 forms one of the essential greenhouse gases that enable a hospitable temperature on a large area of the world; without these gases it would be around 33 °C colder than it currently is. An increase of the level of CO_2 (and/or that of other greenhouse gases such as methane) results in a (temporal) radiative imbalance: the incoming power exceeds the power emitted by the earth (as a system) and thus the global temperature will rise. This increase in temperature results in an increase of the thermal emission by the earth (Fig. 1.2b).

Due to the imbalance of the incoming and outgoing radiation, the earth heats up until a new equilibrium (or radiative balance) has been reached. The earth's surface is currently absorbing ~0.85 W/m^2 more than it is emitting;[7] this power is roughly comparable to the power consumption of four mobile phones on *every* square meter of earth's surface. Thereby, the temperature and the associated thermal emission (Fig. 1.2b) of the earth increases until a new (time-averaged) radiative equilibrium has been established. Therefore, even if we stop emitting greenhouses gas today, the temperature (and the sea level) will still continue to rise for several decades in the future.[7]

1.1.2 The (Only) Solution: Making Supply and Demand of Energy Sustainable

The following three action points need to be realized to establish a more sustainable energy supply and demand of our society.

1. **Reduce CO_2 Emission per Generated Joule.** For example, the emission of CO_2 per unit of energy can be reduced by improving the power conversion efficiency of power plants and by switching from coal to (less polluting) natural gas. The use of renewables (almost) eliminates the emission of CO_2.
2. **Improve Energy Efficiency of Systems.** Make energy consuming devices more efficient to get more useful work per unit of energy. Examples are improved energy efficiency of car engines, lighting, computers, and improved insulation.
3. **Smart Energy Usage by End Consumer.** The energy consumption can be significantly reduced by adapting our lifestyle and by using smart(er)

control systems. Energy conservation can be most effective for people living in developed countries,[8] as it is relatively easy for them to reduce their consumption without severely impacting their quality of life. Examples of smart energy usage are car sharing; reduced consumption and recycling of goods; smart heating and cooling management of buildings; and taking a bike instead of a car.

Each of these points can make a significant contribution to a sustainable society and therefore they all deserve serious attention. Research on renewable electricity generation addresses the first action point. Among the most promising renewable energy conversion techniques are wind energy, hydro-power, sustainable biomass combustion, and solar power. This thesis envisages making a contribution to the development of solar energy by exploring new concepts for reaching enhanced conversion efficiencies.

Implementation of New Technologies. The worldwide introduction of several modern technologies in society happened within a relatively short time span of a few years to a decade. However, such a fast transition is not expected for the relatively conservative energy market if current policies do not change drastically. It is a common misconception that a breakthrough is needed to give the deployment of photovoltaics (PV) a boost. Currently, renewable energy can be generated fairly economically and it will only become even more competitive. Therefore, the success of integration of renewables is becoming more and more dependent on political hurdles than on technological barriers. Fortunately, the political will to make the transition towards renewables is increasing as was highlighted by the *United Nations Climate Change Conference 2015* (COP21).[9]

Cost of Photovoltaics and Advantage of High Efficiency. Over the last decade, relatively small, incremental improvements of solar cells found their way into the market. No major, fundamental changes were made to the module design of the bulk solar market. Similar incremental progress towards higher conversion efficiency is expected in the next decade.[10] This incremental progress of c-Si technology becomes increasingly more difficult to continue as we are closing the gap with the theoretical maximum efficiency; to make a big leap in efficiency a radical change to the current solar module design needs to be implemented. The largest change in the solar cell market was the impressive reduction of cost, mostly driven by economies of scale. With increase of market size, the module cost will be pushed downwards even more along the PV learning curve: historically, for every doubling in production the module cost dropped by about 21%.[11] The average efficiency of the sold solar modules increased by around 0.3% (absolute) per year.[12]

In the end, the price of solar electricity will not become as cheap as that of fossil fuel based electricity; it will become *much cheaper*. Experts forecast that the price of solar power will drop to 4-6 €ct/kWh in 2025, and 2-4 €ct/kWh in 2050 in many regions of the world and thereby it will be the cheapest form of electricity.[13]

Currently, the cost of the module forms around 20 to 40% of the total system cost. The remaining fraction comes from the cost from the *balance of system* (BOS) components, such as the cost for mounting of the solar modules, the wiring and the power inverter. Due to this all-time low cost-share of the solar module in the total cost, the potential costs reduction of solar electricity coming from a further cost reduction of the solar module is limited. Consider this extreme example: if the solar module would be for free, the cost of the generated electricity would "only" reduce by 20 to 40%. On the other hand, the cost per unit of electricity (e.g. kWh) scales (in first order) inversely proportional to the efficiency of the solar module. For this reason, increasing the power conversion efficiency is currently a very important cost leverage for the total system cost of installed solar power.[14,15]

1.2 Solar Irradiance

Solar Irradiance Map. Figure 1.3 shows a world map of the global horizontal irradiation (GHI). The GHI includes both the direct and diffuse illumination. In the Netherlands the GHI is ∼1 000 kWh/m^2/year, while in the Sahara ∼2 700 kWh/m^2/year. For comparison, the global average energy consumption per person is ∼22 100 kWh/year and for people living in the Netherlands the average is ∼54 000 kWh/year.[16]

The current world energy consumption is ∼18 TW[16] and is expected to grow by one-third to 2040.[8] To cover the current world's energy consumption using solar modules with an efficiency of 20% in geographical areas with high irradiance (2 700 kWh/m^2/year), an area in the order of ∼630×630 km^2 would be sufficient, which is just 4% of the Sahara. Solar energy thus not only offers a solution for our current energy needs, but can also meet the growing energy demand from the developing countries.

1.3 Conversion Technologies of Solar Energy

The radiation from the sun can be converted into other useful forms such as heat and electricity in several ways, I describe four of them.

Solar Thermal. Using solar energy to make hot water for domestic and industrial usage is relatively simple and also efficient; as a rough indication ∼40% to 50% efficiency can be realized for a flat plate collector in the Netherlands. A flat plate collector or evacuated tube collector can be used to absorb a large fraction of the sunlight to heat water that can be used residentially and industrially. The hot water can also be used to power air-conditioning, for example by using an absorption refrigerator. The power conversion efficiency of solar thermal is generally significantly higher than that of solar panels, although this depends

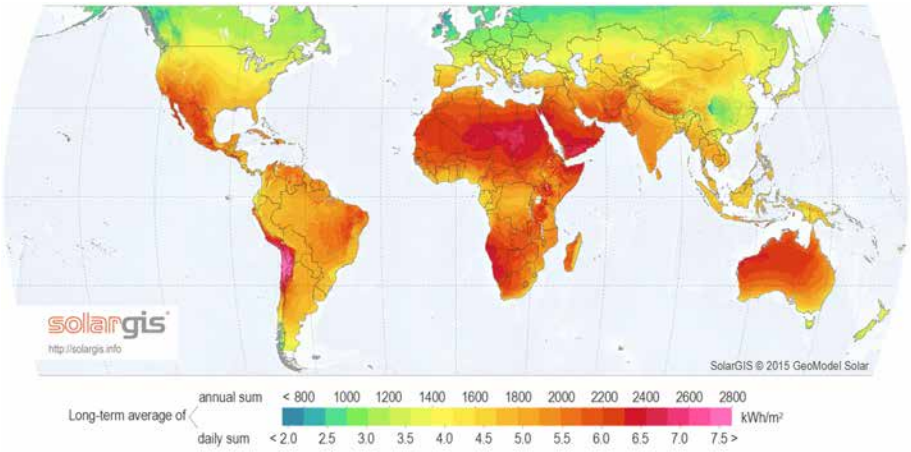

Figure 1.3: Geographical map of the global horizontal irradiance.[17] The yearly irradiance is determined by the local climate and the geographical location. Used under ⓒ license.

significantly on how efficiently the hot water is used. However, heat is a much less versatile form of energy than (entropy-free[18]) electricity. The direct use of solar heat can therefore only cover a limited fraction of our energy need.

Concentrated Solar Power (CSP, or Concentrated Solar Thermal). For CSP, mirrors are used to concentrate light on a small area that obtains a high temperature. The heat is used to power a heat engine, such as a steam turbine or Stirling engine. The limiting thermal efficiency[†] of these systems is around 85%.[18] However, in practice the efficiency is around 15-32% due to various losses. Diffuse light cannot be concentrated.[18] Therefore, CSP is mostly interesting for geographic regions[17] with a high amount of direct irradiance.

Photovoltaics (PV). The operating mechanism of photovoltaics is fundamentally different than that of solar thermal and CSP. Instead of being based on heat, it is based on the energy distribution of the electrons in the semiconductor material of a solar cell. The photovoltaic effect thereby offers a more direct energy conversion to electricity than CSP and can be effectively applied in most geographical regions; also in regions which a high amount of diffuse light. Crystalline silicon is the widest deployed material for photovoltaics. Photovoltaics can be combined with solar thermal in a single module, but this hybrid form is currently not widely deployed. Hybrid solutions combining PV and CSP are being explored.[19]

Concentrated Photovoltaics (CPV). Higher conversion efficiencies can be

[†]The thermal efficiency (η_{thermal}) is given by $\eta_{\text{thermal}}=1-\frac{T_C}{T_H}$, with T_H the temperature of the heat entering the engine and T_C that of its surroundings. However, due to the presence of an absorber (which also radiates back to the sun) the optimal temperature of the absorber should be used instead of the T_{Sun}.

obtained by concentrating sunlight on a highly efficient (but generally also relatively expensive) solar cell. However, this CPV technology is slightly more complicated than conventional photovoltaics and its current market share is relatively small. It also requires a high amount of direct irradiance as for CSP.

Need for Storage. To have dispatchable[‡] solar energy, the availability of low-cost energy storage is essential. Without energy storage, the economic value per kWh of photovoltaic electricity reduces significantly when the regionally generated solar power is in the order of the regionally consumed power. Finding a low-cost technology for energy storage is therefore essential to continue the successful development of photovoltaics. Furthermore, it is likely that electricity prices for the end-consumers will be flexible in the future. This stimulates demand site power management and thereby improves the balance between generation and demand of electricity. Alternatively, the balance between supply and demand of electricity can be improved by connecting different electricity grids to form larger super grids.

1.4 Light Trapping in Solar Cells

The absorption of sunlight is one of the factors that determine the power conversion efficiency of a solar cell. To improve the absorption of light in a silicon solar cell one generally guides the light such that a large fraction of the light is internally trapped within the solar cell.

Incoupling and Refraction of Light. Figure 1.4 shows the interaction of an un-polarized beam of light at the interface of air and a (absorption-free) material with a refractive index (n) of 3.5 (resembling a slab of silicon). Figure 1.4a shows a series of rays coming from the air at different angles of incidence. The color of the reflected and refracted rays corresponds to the associated incoming ray. The length of the arrows represents the intensity of the rays. Around 70% of the light is transmitted into the silicon for most angles and the remaining light is reflected.

Figure 1.4b shows a series of rays coming from the silicon at a range of angles of incidence. Light coming from an angle smaller than the critical angle (θ_c) is both refracted out of the cell (roughly 70%) and internally reflected (roughly 30%). Light with an angle larger than the critical angle is completely internally reflected at the flat air-Si interface. In a flat solar cell the propagation direction of light within the solar cell does not exceed (θ_c) and therefore the light is not internally trapped (radiatively emitted photons form an exception to this statement). In chapter 3 we show a method to scatter the light within the solar cell which enables total internal reflection leading to enhanced absorption.

[‡] *Dispatchable* power means that one can provide the required amount of power to the grid regardless of e.g. the time of day and weather conditions.

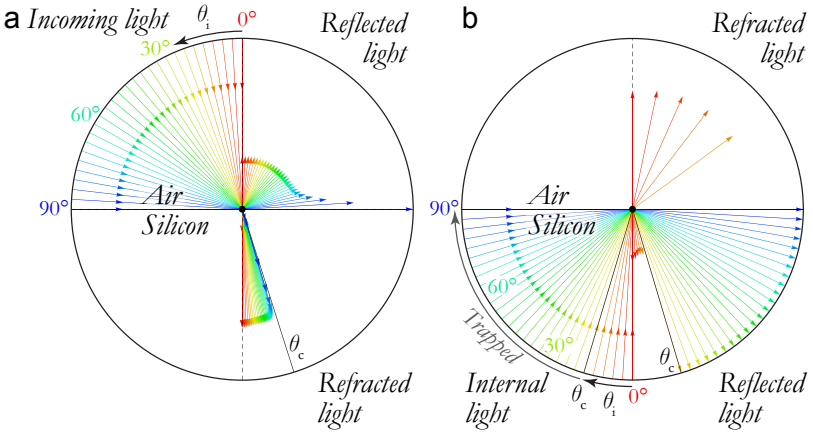

Figure 1.4: Interaction of unpolarized light with a flat interface of air and a medium with a refractive index n=3.5, which roughly resembles silicon for wavelengths from 700-1200 nm. The interaction is shown for both light coming from the air (a) and silicon (b) side of the interface, for a range of angles of incidence (θ_i) indicated by different colors (the colors do not represent physical colors). **(a)** Incoming light on an air-Si interface is both reflected and refracted. The length of the arrows represents their (interface) intensity with respect to the incoming light (outer ring is 100%). Corresponding colors represent (fractions of) the same incoming ray. The intensity of the reflected light increases with θ_i, while the intensity of the refracted light decreases with θ_i. The angle of the refracted light does not exceed the critical angle θ_c. **(b)** Light coming from the Si side with $\theta_i < \theta_c$ is partly refracted out of the Si and internally reflected. Rays coming from larger angles ($\theta_i < \theta_c$) are totally internally reflected.

Reciprocity Principle. One of the properties of light is its *reciprocity*, which has important implications for the optics within a solar cell. The reciprocity principle can be illustrated as follows. Consider a ray with intensity I_i and fixed polarization that is traveling from position A to B (for example from air to silicon, see figure 1.4a) and arrives with a fraction f of intensity at B. If the direction of light is now reversed and we start with intensity I_i and same polarization at point B, than an equal fraction f will end up at A. This principle will be used in chapter 4 of this thesis to illustrate that if the (angular averaged) probability for light to enter the solar cell is reduced then, due to this reciprocity principle, the probability for light to escape from the light trap is equally reduced.

Illustration of the Critical Angle. Figure 1.5a shows a photo taken from the bottom of a swimming pool by a fish eye camera. Rays coming from above the water surface can enter the water and only propagate to the camera if they hit the water within the acceptance cone, see the circular area marked by (θ_c). The reciprocity principle dictates that if the camera emits a light ray, then it can only escape out of the water within this cone. This cone is therefore also called the escape cone; outside this cone the light is completely internally reflected by the water surface.

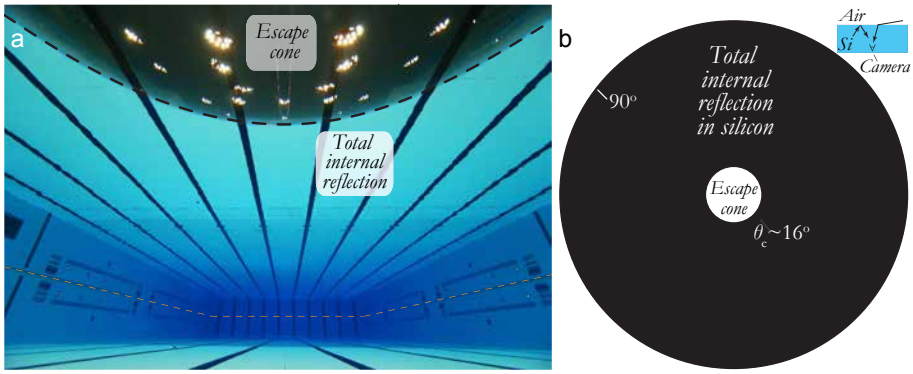

Figure 1.5: **(a)** Underwater photo of a swimming pool.[20] Light entering the water within the escape cone (circular area above the dashed black line) is partly transmitted into the water and thereby you can look outside the pool (you see the lamps on the ceiling of the building). The critical escape angle for water is ∼42°. Outside this cone, the light is totally internally reflected: one can see the image of the stripes on the bottom of the pool at the water surface due to reflection. The dashed orange line marks the outer border of the water surface, which is a symmetry plane in this photo. **(b)** Sketch of the view in a flat slab of a material with a refractive index (n) of 3.5 (this roughly resembles a slab of silicon) in air. For most angular directions the light is completely internally reflected at the Si-Air interface; only the light that travels in a relatively small angular cone of ∼16° will partly escape outwards.

Total internal reflection also occurs in a slab of silicon. However, a much larger fraction of the light is totally internally reflected due to the relatively high refractive index of 3.5 of silicon. If we could take a photo from inside a flat slab of silicon facing a light source, it would look like the illustration shown in Figure 1.5b: an illuminated center within a completely dark surrounding.

Light can be trapped in the solar cell by total internal reflection. If light is completely randomized within the solar cell, the averaged path length of light within the cell can be enhanced by a factor of $4n^2$.[21] However, this enhancement limit is only valid if there is no absorption; in case of absorption the path length enhancement is significantly less than $4n^2$. Light can be randomized in the solar cell in various ways. Generally, a pyramidal texture is realized by etching the surface of c-Si solar cells. Incoming light is refracted into oblique angles into the solar cell at the pyramid facets. This mechanism is based on geometrical optics. However, this type of texturing cannot be applied to solar cells with a thickness less than the typical dimensions of the etched texture. Moreover, the texturing also has a negative effect on the electrical characteristics and thereby reduces the cell performance as will be explained in the next chapters.

In the first part of this thesis we demonstrate a nano-structure that scatters the light internally and can be applied on solar cells that cannot be effectively surface-

textured. The scattering by this nano-structure is not based on geometrical optics but on scattering of light due the refractive index contrast of the different materials. In the second part of this thesis, we demonstrate a novel alternative approach of light trapping. Instead of modification on the solar cell level, we focus the sunlight by a parabolic concentrator through an aperture in a highly reflective cage. This external light trap is placed on top of the solar cell and directs the reflected light back to the solar cell and improves the power conversion efficiency.

Chapter 2

Experimental Techniques

The optical components presented in this thesis are not off-the-shelf available, therefore the components were fabricated in-house. Some companies offer glass lenses and parabolic concentrators. However, to make an external light trap one has to properly connect the concentrator to a reflective cage. The use of a 3D-printer and an industrial milling machine were found to offer high design flexibility. In this chapter we provide some background information on these fabrication processes and the measurements of the solar cells with an external light trap.

2.1 3D-Printing External Light Traps

Figure 2.1 shows an Ultimaker Original 3D-printer. A thermoplastic filament is located at the backside of the printer. A material feeder presses the thermoplastic into the bowden tube, which is connected to the extrusion head. This extrusion head moves in the horizontal plane and is powered by the indicated engines for the x and y direction. The heated thermoplastic is printed on the printing platform. To obtain a proper bonding of the plastic, *Scotch 3M Blue Tape 2090* is applied to the platform. The print was cut loose from the platform and cleaned with ethanol to remove any residual tape. This platform moves in the vertical direction by the leadscrew.

The thermoplastic is printed on a platform that moves one step (of $\sim$100 μm) downwards after finishing each layer. The width of the print line is among others determined by the diameter of the nozzle (ø$\sim$400 μm). The print head heats a thermoplastic called Acrylonitrile Butadiene Styrene (ABS) to a temperature of around 260 °C. The molten thermoplastic is extruded and deposited as a line on the printing platform. The track of the head depends on several settings like the diameter of the nozzle, layer height and filling fraction. The thermoplastic attaches

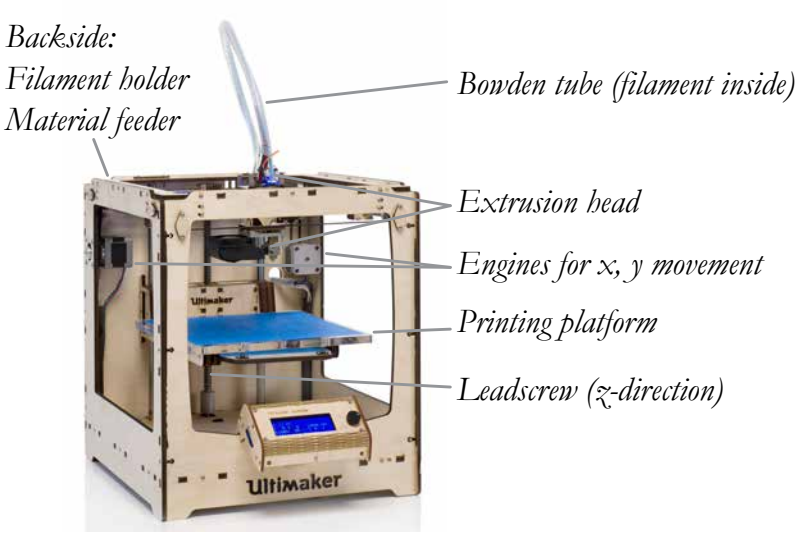

Figure 2.1: An Ultimaker Original 3D-printer. The indicated components are described in the main text. Figure adapted with permission from Ultimaker.

to the platform and/or the already printed part and solidifies. The compound parabolic concentrators (CPCs) and the cage as presented in the thesis are printed from ABS. A movie of the printing process can be seen here.[22] More details on the printing process can be found in the assembling manual.[23]

The printing process starts by making a CAD design of the external light trap for which we used OpenSCAD.[24] Cura,[25] a so-called *slicer*, converts the CAD file to $\sim 10^5$ print lines depending on various print settings such as the diameter of the nozzle and the speed of the extrusion head. For example, the extrusion speed of the molten plastic is calculated by the slicer as a function of these settings.

2.1.1 Smoothening & Silver Coating

Chemical Smoothening. For the smoothening of the objects made of ABS, acetone was put into a jar standing on a heated stove above the boiling point of acetone ($T \sim$ 90 °C). After several minutes, acetone condensate emerges at the (relatively cool) glass jar. Then, the 3D-printed light trap is inserted into the jar for several minutes and exposed to the acetone vapor. This process is repeated several times. The initial temperature of the printed object is critical, as the warm and saturated vapor condenses quickly on cool surfaces. An ice pack was used to reduce the ABS temperature before inserting the model into the jar. The main smoothening occurs in the first seconds due to heavy condensation of the acetone. The acetone dissolves the ABS surface. The liquidized ABS on the surface lowers its surface energy by

forming a smooth surface. The experimental results are shown on page 58 and 81.

To compare the accuracy of the fabricated traps with that of commercial light traps, we ordered several traps made from different materials from a commercial 3D-print company. The accuracy of the commercial parts was not better than that of our prints. Moreover, as they were not made of ABS, smoothening is relatively difficult and/or dangerous as (even more) toxic solvents have to be used. The lack of a proper smoothening method is a common bottleneck for 3D-printing optical parts. When an un-smoothened print is metalized, it stays dark gray and absorbs severely. Other dominant thermoplastics such as Polylactic acid (PLA) are generally more difficult to smoothen than ABS.

Silver Coating. The edges of the CPC are steep and therefore unidirectional evaporation of metal is less suited. Moreover, the temperature during evaporation can deform the CPC; sputter coating is better suited. Therefore, the light trap was metalized with 400 nm of silver using an EMITECH K575X sputter coater.

2.2 Spectral Response

The opto-electronic response of a solar cell for each wavelength is generally described using the external quantum efficiency (*EQE*). This quantity describes the ratio between the number of collected charge carriers to the number of incident photons of a certain wavelength. The *EQE* is unity if the light is completely absorbed in the active layer and all generated minority carriers are collected.

To measure the *EQE* one uses a monochromatic light source. Monochromatic light can be realized as a broadband light source (Xenon arc lamp or supercontinuum laser) with a monochromator or filterwheel. Alternatively, one can use a series of LEDs with a different wavelength. Typically, the cell is illuminated by a small collimated monochromatic beam, with a diameter of a few millimeter. The intensity of this beam is relatively small and therefore a chopper and a lock-in amplifier is used to improve the signal to background noise ratio. No voltage was applied over the cell during the measurements and there was no bias light.

Illuminated Area. The *EQE* is an area independent quantity. When a diverging beam of light is used, it does (in first order) not matter whether the solar cell is placed somewhere at the beginning of the beam (when the beam spot is relatively small and has a relatively high intensity) or on a place further on the beam path (with larger spot size and lower intensity). In both cases the total number of incident photons on the solar cell is equal.

External Light trap. For the results presented in chapter 4 and 5 several external light traps were fabricated. When a light trap is placed on top of the solar cell the *EQE* of the solar cell itself does not change, as the *EQE* is a property of only the solar cell. However, the *EQE* of the system as a whole changes. The *EQE* of

the solar cell with an external light trap (EQE_{trap}) is defined as the number of the total number of collected charge carriers, divided by the number of incoming photons at the top of the CPC. When a photon travels several times through the solar cell (due to the light trapping) the photon has, instead of just one chance, several chances to be absorbed. Thereby, the absorptance increases resulting in a higher system response (EQE_{trap}) than cell response (EQE). On the other hand, when the concentrator absorbs a fraction of the light EQE_{trap} will be lower than the EQE of the bare cell, this will be illustrated in more detail in chapter 6.

For a proper measurement of EQE_{trap} the size of the beam has to be smaller than the opening of the concentrator, otherwise we would lose photons. At the same time, the response of the solar cell with the external light trap depends on the illumination position of the beam. For example, when a beam is oriented normal to a specular reflective solar cell (so parallel to the concentrator axis), the reflected light is not trapped but escapes directly through the aperture. When the beam is directed on the concentrator, most of the light that reflects is trapped. The beam has a diameter of few millimeter. Therefore, the EQE that was determined is an average system response over the beam area.

***EQE* and Homogeneity.** Solar cells are sensitive to the homogeneity of the irradiance as will be further explained in chapter 6. This sensitivity depends on the type of solar cell, the average intensity and the variance of the intensity. When the average intensity is low, the cell response is not affected. Actually, this is generally the case for EQE measurements as only a small area is illuminated. Inhomogeneously distributed high intensities can negatively impact the cell response.

2.3 Milling of External Light Traps

For chapter 6 we fabricated external light traps by an industrial milling process. The concentrators and light cages are milled out of an aluminum rod by a milling cutter machine (Fehlmann P90). The milling head is shown in figure 2.2a. A cooling liquid (a mixture of water and oil) is used to cool and lubricate the workpiece, see Figure 2.2b. The liquid also helps to reduce the stickiness and to get rid of the aluminum chips that are released during the milling.

The fabrication involves several steps. First a roughing cut is performed to make the rough basic shape of the concentrator and to remove most of the material. Next, a finishing cut is performed using a smaller ball mill. The workpiece (which will become the concentrator) slowly rotates below the fast rotating ball mill, while the ball mill translates radially inward and downwards along the intended surface shape. If the ball mill would move layer-by-layer on circular tracks, there would be some places with a discrete vertical step. This leaves an unwanted artifact in the

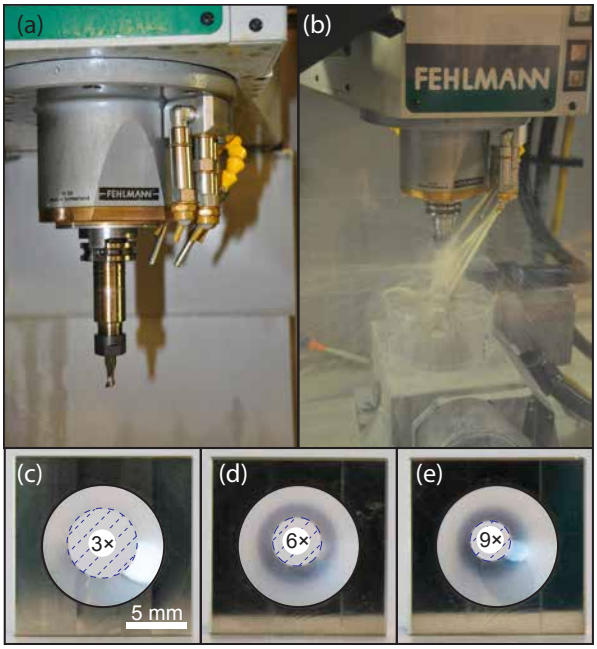

Figure 2.2: (**a**) Close-up of the milling head located inside the milling cutter machine. (**b**) Milling process of the external light trap. The aluminum rod that will become the concentrator is fixed in the setup. Various bits are used for the different fabrication stages of the concentrator. A beam of cooling liquid is used to carry away heat generated during the milling and to remove the released metal chips during the milling. (**c-e**) Top view of the concentrators with different concentration factor (C=3–9×).

workpiece. To prevent these discrete steps, the milling cutter moves along a spiral track, which can be realized by tilting the concentrator by ∼2 degrees.

Bottom-side. For the bottom-side of the concentrator, a center drill is used to make a starting hole in the workpiece in which a larger-sized drill bit fits. Hard metal round bits were used for to achieve a smooth surface. Higher accuracy can be realized by using a diamond drill on a lathe.

Polishing. The milling process leaves small grooves in the surface of the concentrator. These grooves reduce the reflectance and thus the performance of the concentrator. Scratches lead to elevated absorptance of the metal surface and can also reflect or scatter the light in unintended directions. By polishing, the peaks on the surface are flattened by making new (small) scratches. In general, the polishing of hollow objects is much more difficult than convex shapes as one can not use conventional lapping techniques for hollow surfaces. To smoothen the hollow surface, we placed the work piece in a lathe. While the work piece rotated we inserted a cotton swab and polishing abrasives to reduce the surface roughness. To obtain smoother surfaces one could consider the use of an intermediate overcoat

layer to smoothen the surface. Many paints produce a very smooth surface due to surface tension in a similar way as was observed in the smoothening of the 3D-printed parts.

Polishing bottom. The flat bottom of the concentrator was manually polished by lapping on a flat plate. The grain size of the lapping powder was reduced in steps from 5 μm to 0.5 μm.

We could have used the aluminum base material as a reflector. However, the initial reflectance of silver is higher than that of aluminum.[26] A challenge for silver coatings is to prevent the natural tarnishing process. Only a few nanometer of silver sulfide will already severely reduce the reflectance.[27] Therefore, we performed the measurements directly after the deposition of the silver coating. The tarnishing can be overcome by protecting the silver by a transparent dielectric coating, such as half a wavelength of silicon monoxide, also named *protective silver*.[28]

Chapter 3

Plasmonic Scattering Back Reflector for Light Trapping in Flat Nano-Crystalline Silicon Solar Cells

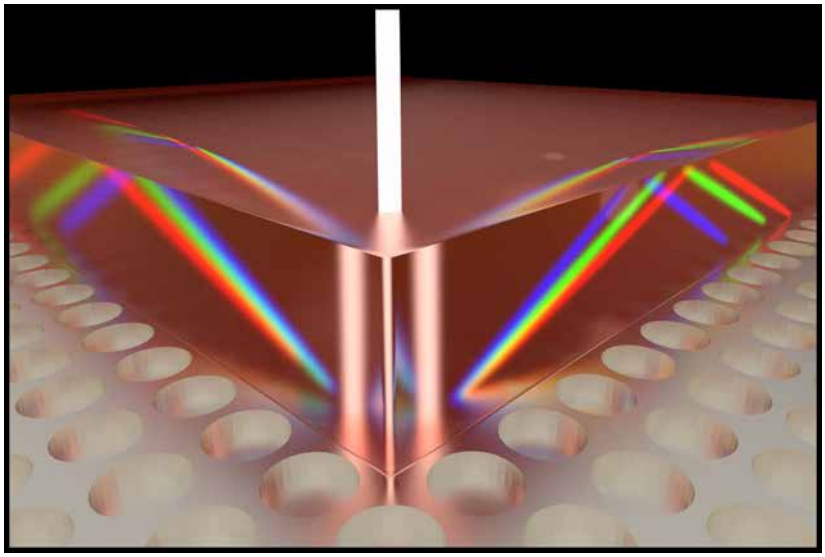

Artistic impression of light scattering by a plasmonic scattering back reflector. The scattered light is trapped in the cell, leading to an enhanced optical absorptance and solar cell performance.

Summary. Most types of thin film solar cells require light management to achieve sufficient light absorptance. This chapter demonstrates a novel scattering back reflector for flat, thin film hydrogenated nano-crystalline silicon (nc-Si) solar cells. This scattering back reflector consists of an array of silica nano-cylinders in a metal sheet. Typically, nc-Si:H solar cells are grown on textured substrates that scatter the incoming light. However, it is challenging to grow defect-free nc-Si:H layers on top of such (nano)-structured substrates. Here, a high-quality nc-Si:H layer is grown on a flat superstrate. On top of this, we apply a plasmonic scattering structure composed of a periodic array of dielectric nano-cylinders, which is overcoated by silver. The use of a flat plasmonic scattering back reflector (PSBR) circumvents silicon growth defects and prevents the associated reduction of the open circuit voltage, while on the other hand the scattering improves the short circuit current. The PSBR is fabricated over a large area using substrate conformal imprint lithography (SCIL). Optical modeling is performed using finite-difference time-domain (FDTD) simulations to determine the absorptance in the active layer of the cell. A particle swarm optimization algorithm is used to optimize the PSBR geometry, such that the photocurrent is maximized. We fabricated a 1 micron thick nc-Si:H cell and experimentally demonstrate a current improvement of 32% compared to a flat reference cell, without affecting the open circuit voltage. The PSBR structure is not only effective for nc-Si solar cells, but can also be applied to other types of thin film superstrate solar cells.

3.1 Introduction

The flexibility and low cost of thin film solar cells makes them attractive for a wide range of applications, such as building integrated photovoltaics,[29] and power generation for mobile devices. However, the design of these cells is challenging, as there is a conflicting interplay between their electrical and optical properties. From the optical perspective a thick solar cell is ideal, while from the electrical and cost perspective a thin cell is beneficial.[30] This dilemma can be solved by improving the diffusion length of the charge carriers, or by improving the absorptance.

Like many thin film solar cells, hydrogenated nanocrystalline silicon (nc-Si) suffers from this opto-electrical dilemma.[31,32] Thick (>2 μm) nc-Si:H solar cells have a relatively low open circuit voltage (V_{oc}), low fill factor (*FF*), and require long fabrication times. Thin cells (∼1 μm) have been shown to have ∼4% higher V_{oc} and ∼7% higher *FF*, but they only absorb a small fraction of the solar spectrum.[33,34] The J_{sc} of the record-efficiency nc-Si:H cell is only 67% of the limiting value given by the Shockley-Queisser model,[35] one of lowest fractions of all major solar cell materials. Therefore, light trapping is required to enhance the optical absorption in thin nc-Si:H solar cells, especially for long wavelengths (λ>600 nm).[36]

Efficient light trapping inside the cell has been demonstrated by depositing the solar cell on textured substrates, like textured aluminum doped zinc oxide[37–39] ZnO nanorods on flat silver,[40] textured Ag films,[41,42] and honeycomb patterns.[39,43] However, growing nc-Si:H on textured substrates commonly results in growth defects, apparent as voids, short-circuiting pinholes and cracks in the nc-Si:H layer which increase the charge carrier recombination rate and can even lead to excessive shunting.[39,44–49] On the contrary, layers grown on flat substrates do not show such defects, but they are hindered by a lack of light trapping. The best of both worlds can be achieved by combining a flat, high quality, nc-Si:H layer and a flat light scattering layer. This combination facilitates both the electrical and optical requirements and can therefore result in high cell performance. Another advantage of the flat architecture is that nc-Si:H can be grown at higher deposition rates on flat substrates than on textured substrates, without inducing excessive material defects.[50,51]

Recently, light trapping in flat substrate solar cells has been demonstrated using the flattened light-scattering substrate (FLiSS) concept.[52,53] For the FLiSS cell, a composite of two dielectric materials (such as ZnO and amorphous Si) is flattened by chemical mechanical polishing, after which a flat nc-Si:H layer is grown on top. However, the FLiSS concept is not suitable for superstrate cells, which are industrially more interesting as the front glass offers high transparency, UV stability, and moisture protection.[54]

Here, we present a plasmonic scattering back reflector (PSBR) that provides efficient light trapping in flat absorber layers, in the superstrate cell configuration. The PSBR is similar to a plasmonic hole array, which is known to support surface plasmon resonances,[55] which can result in strong local electric fields inside the voids,[56] and has a large scattering cross section with a tunable resonance wavelength.[57–59] The benefits of such hole arrays have been successfully demonstrated in substrate solar cells of which the deposition is not significantly hindered by surface textures, for example organic[60–62] and a-Si solar cells.[63,64]

First, a crack-free nc-Si p-i-n solar cell is grown on flat, ZnO-coated glass. Next, a square array of dielectric nano-cylinders is printed on the backside of the flat silicon layer by substrate conformal imprint lithography (SCIL),[63,65–71] which is subsequently overcoated by silver to form the PSBR. The refractive index contrast between the metal and dielectric material gives rise to plasmonic light scattering, while the flat design enables high nc-Si:H material quality.

The generated photocurrent of a thin nc-Si:H PSBR cell is compared to that of two reference cells: a flat reference cell and a reference cell deposited on a textured superstrate. Due to scattering by the PSBR, the J_{sc} improves by 3.7 mA/cm^2 with respect to the flat reference cell. The V_{oc} of the PSBR cell is comparable to that of the flat reference cell, while the textured reference cell shows, as expected, a reduced V_{oc} due to cracks. The results demonstrated here are generic and can be

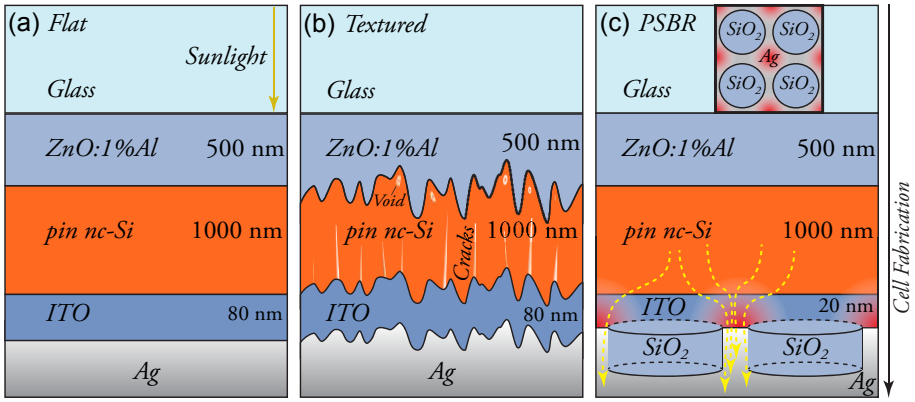

Figure 3.1: Illustration of the fabricated solar cells. (**a**) Flat nc-Si:H solar cell. (**b**) nc-Si:H cell grown on top of textured aluminum-doped ZnO. Voids can occur due to the texture. (**c**) Flat cell with a plasmonic scattering back reflector (PSBR) consisting of a square array of SiO_2 nano-cylinders in a matrix of Ag. The dashed yellow lines sketch the electrical path of the electrons via the conductive Ag. The red circles illustrate the plasmonic scattering by the PSBR. The inset shows a top view of the flat PSBR.

applied to a wide variety of thin film, superstrate solar cells.

3.2 Design and Fabrication of the Solar Cells

We compare three different cell designs as shown in Fig. 3.1. The three designs incorporate nc-Si:H p-i-n layers grown on a glass superstrate. The thickness of the intrinsic nc-Si:H layer is ~1 μm. The cells have an optically thick Ag layer at the backside, which functions both as a back reflector and contact. The fabrication details are provided in Supplemental Section 3.5.

Figure 3.1a shows the flat reference cell in which light travels through the cell without being scattered (except some scattering on the grain boundaries[72]). The flat design allows for high material quality.

The textured reference cell (Fig. 3.1b) is grown on textured aluminum doped zinc oxide (ZnO:Al). The different growing crystal facets approach one another without forming a good physical interconnection, as indicated by the short-circuiting pinholes. Due to the (partially) conformal growth on top of the random front texture, the interfaces between subsequently deposited layers are also textured, and thereby scatter the incident light. An 80 nm thick ITO layer is used as a back dielectric spacer to achieve a high E-field in the Si layer.[73]

Figure 3.1c shows the cell with the PSBR at the backside. The PSBR is applied on a flat nc-Si:H layer. The PSBR is an array of silica (SiO_2) nano-cylinders overcoated with silver. A thin continuous layer of indium tin oxide (ITO) prevents silver dif-

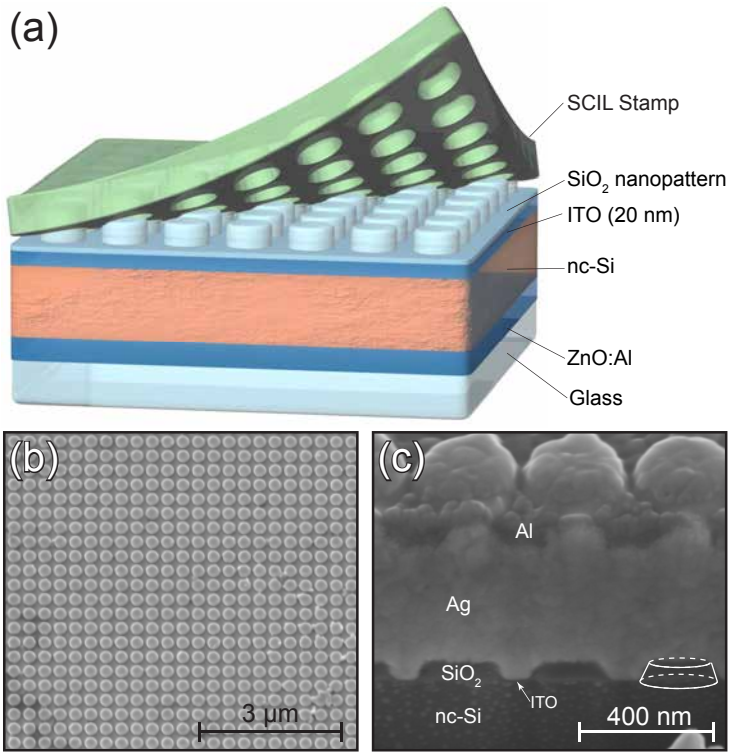

Figure 3.2: (**a**) Illustration of the soft conformal imprint lithography used to fabricate a square array of nano-cylinders. (**b**) Top view SEM image of the imprinted silica nano-cylinders. (**c**) SEM image of a FIB cross section of the PSBR solar cell.

fusion into the silicon and forms an etch barrier between the nc-Si:H layer and the PSBR. The conductive silver in between the silica nano-cylinders is used to contact the cell, similar to the contacting scheme of the 'passivated emitter with rear locally diffused (PERL) cell.[74] The size and geometry of the nano-cylinders array were optimized for maximized scattering into the nc-Si:H layer using numerical simulations.

Figure 3.2a illustrates the SCIL procedure to fabricate the PSBR. First, a master pattern is fabricated on a c-Si wafer using laser interference lithography. This patterned wafer can be used to produce a multitude of stamps. Next, a stamp is fabricated from this master which consists of a bi-layer of two different types of polydimethylsiloxane (PDMS).[75] A layer of liquid silica (sol-gel) is subsequently spin-coated on top of the ITO backside of the solar cell and the SCIL stamp is applied. After 30 minutes of curing at ambient conditions the sol-gel has solidified and the stamp is removed resulting in a silica nano-pattern on the substrate.

A thin residual layer of silica remains in between the silica nano-cylinders,

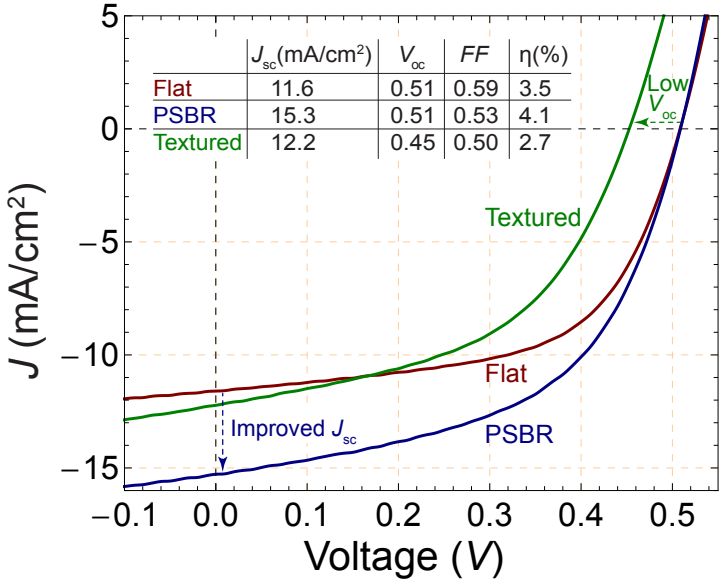

Figure 3.3: Measured current density versus voltage of the flat (red), textured (green), and PSBR(blue) solar cell under AM1.5G illumination. An improvement of 3.7 mA/cm^2 of the short circuit current density of the PSBR cell is observed compared to the flat cell, while the V_{oc} is identical.

which is removed using a CHF_3 based reactive ion etch (RIE). Figure 3.2b shows a scanning electron microscopy (SEM) top view image of the imprinted silica nano-cylinder array. The imprint shows only a few defects, which demonstrates the large-area uniformity of the SCIL process. Figure 3.2c shows a SEM image of a focused-ion beam (FIB) cross section of the PSBR. The nano-cylinders have a diameter of ∼240 nm, a pitch of ∼325 nm, and a height of ∼70 nm. The metal covers ∼57% of the total area. The imprinted nano-cylinders are slightly tapered as a result of the non-perfect anisotropy of the RIE. Due to semi-conformal growth,[49] the shape of the nano-imprinted cylinders propagates through the evaporated Ag layer resulting in half dome like shapes at the surface of the Ag. Finally, a thin layer of aluminum is applied by thermal evaporation to prevent oxidation of the Ag layer.

3.3 Results and Discussion

We determined the performance of the fabricated solar cells by measuring the current density versus voltage *(J-V)* characteristic, *EQE* and optical absorptance. Figure 3.3 shows the measured *J-V* characteristics of the flat, textured, and PSBR solar cell under AM1.5G illumination.

The flat nc-Si:H cell has relatively high *FF*, which indicates high material quality. However, the current is low as light escapes from the cell due to the absence of a proper light trapping scheme. The textured cell shows a slightly higher short circuit current (J_{sc}) than the flat cell due to the light scattering at the textured interfaces. The V_{oc} is significantly lower compared to the flat reference cell as a result of the poor material quality due to growth defects induced by the texture. The strongly increased charge carrier recombination can also reduce the *FF* and J_{sc}. This demonstrates that conventional textures have drawbacks when optimizing light trapping in nc-Si:H cells.

The PSBR solar cell shows the best performance. The J_{sc} improved by 3.7 mA/cm^2 with respect to the flat reference cell, which indicates efficient light scattering into the active layer. The efficiency of the PSBR cell is 4.1%, which is significantly higher than the 3.5% of the flat reference cell. Moreover, these results demonstrate that the current is effectively transported through the narrow conductive silver paths in between the silica nano-cylinders. Although the cell performance is slightly hindered by shunt resistance, it is important to highlight that the shunt resistance of the PSBR cell is similar to that of the flat reference cell, while the shunt resistance of the textured reference cell dropped significantly due to the poor material quality. Finally, the V_{oc} of the PSBR cell equals that of the flat cell, which demonstrates the benefit of flat, high quality nc-Si layers. We note that the overall efficiency of the cells used in this study is relatively low due to the low nc-Si:H quality. However, they serve as a good model system as all cell geometries were made using highly reproducible deposition conditions.

Spectral performance: *EQE* and Absorptance. To investigate the current enhancement of the PSBR cell in more detail we measured the spectral performance of the completed cells. Figure 3.4 shows the absorptance and the external quantum efficiency (*EQE*) of the flat, textured, and PSBR solar cell.

The flat cell shows 80-90% absorptance at short wavelengths (<600 nm). Due to parasitic absorptance in the *p*-type doped nc-Si:H layer, the *EQE* is significantly lower than the absorptance in this spectral range. For longer wavelengths, the absorptance drops to around 30%. Fringes appear due to Fabry-Pérot interference in the front ZnO:Al layer (for wavelengths <∼550 nm) and in the optically thick Si layer (at longer wavelengths).

The textured cell shows a high absorptance of 60-90%, even at the long wavelengths where the nc-Si:H is only weakly absorbing. However, the *EQE* is relatively low compared to the absorptance, especially at short wavelengths. We attribute this to poor internal collection efficiency (*ICE*) of the charge carriers generated at the top of the solar cell. This low *ICE* clearly reflects the difficulty of growing high quality nc-Si:H layers on a texture, inevitably leading to material defects such as cracks.[39,44–49] Moreover, sharp features in the surface of the metal contact layer lead to strong parasitic plasmonic absorption.[76–78] Another loss

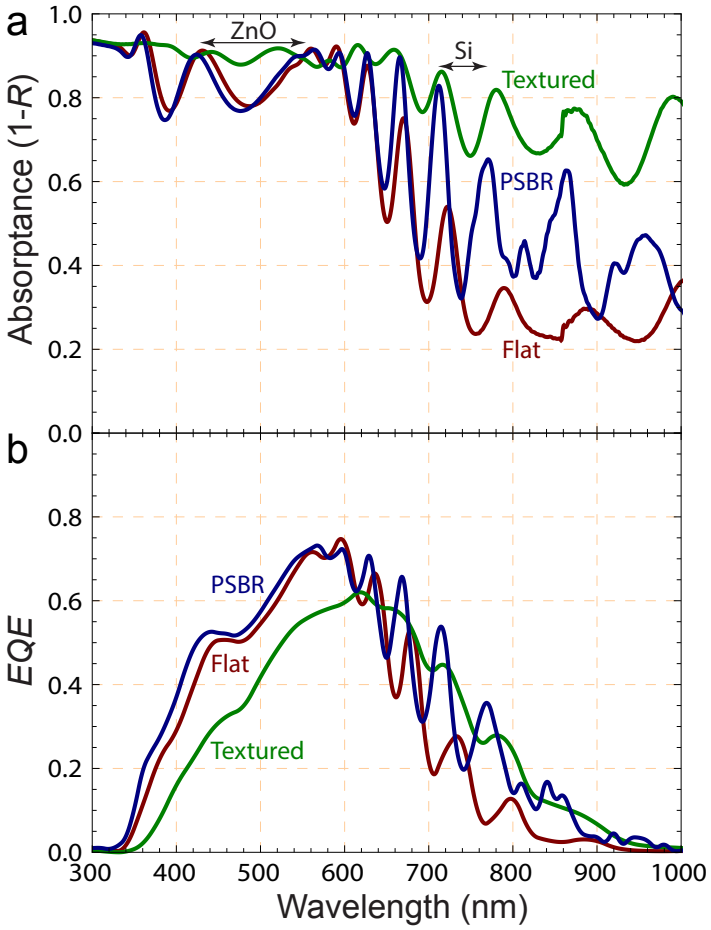

Figure 3.4: (**a**) The absorptance and (**b**) the *EQE* of the flat cell (red), the PSBR cell (blue), and the textured solar cell (green). The *EQE* is measured at 0 V, without bias light.

mechanism that is enhanced by the texture originates from the increased optical path through the parasitically absorbing *p*-layer as a result of the scattering by the front texture. The amplitude of the fringes in the *EQE* is significantly reduced compared to that of the flat cell. This is due to the randomization of the wave vectors inside the cell caused by random scattering at the textured interfaces. Texturing the front ZnO:Al layer induces scattering not only at the front interface, but also at the consecutive nc-Si/ITO/Ag interfaces due to the semi-conformal growth of the subsequent layers. The absorptance of the PSBR cell at long wavelengths is lower than that of the textured cell. This is partly due to improved light incoupling at the ZnO/Si interface and the better light scattering at the three material interfaces of the textured cell. The random interface facilitates scattering over a broad spectral

range. However, even though the absorptance is better, the device performance of the textured cell is worse.

The PSBR cell exhibits the highest overall *EQE*. Due to the light trapping, both the absorptance and the *EQE* are significantly higher than those of the flat cell for wavelengths longer than 700 nm. At wavelengths beyond 800 nm additional sharp peaks are observed, which have been reported before;[79] their origin is discussed in the next section.

Optical Modeling and Simulated Absorptance in Silicon Absorber. We used finite-difference time-domain (FDTD) simulations to obtain a detailed understanding of the optical mechanisms involved in the scattering and the waveguiding in the PSBR cell. The geometry of the PSBR solar cell was optimized using the particle swarm optimization algorithm (PSO), see Supplemental Section 3.5.1. We found the following optimal parameters of the square array of silica nano-cylinders for the PSBR cell: a diameter of 248 nm, a pitch of 339 nm, and a height of 139 nm. Due to experimental constraints the realized PSBR geometry differed from the calculated optimum; the realized height is around 70-90 nm. The PSO algorithm also showed that for optimal absorptance in the intrinsic Si layer, the ITO should be as thin as possible. The light trapping due to scattering by the PSBR is better when the light is scattered in, or close to, a material with a high refractive index such as Si, as this gives rise to larger scattering angles. Also, the PSBR gives rise to strong field intensity in the near-field of the PBSR, and therefore it is beneficial to have the Si layer very close to the PSBR. However, to prevent undesirable Ag diffusion into the Si we used a 20 nm ITO barrier layer in the experiment. The minimum thickness can be further optimized.

We also simulated the absorptance of the PSBR cell with the experimentally realized geometry. Figure 3.5 shows the absorptance in the intrinsic nc-Si layer of the flat and the PSBR solar cell. For long wavelengths, the PSBR cell shows a significant increase in absorptance. Generally, when a rough scattering layer is applied, the light is randomized and thereby these fringes are smoothed. Here, distinct absorptance peaks appear on top of the Fabry-Pérot interference fringes which are strongly correlated to increased absorptance in the Ag nanostructure of the PSBR. These additional sharp peaks are due to a complex interplay between the PSBR and the cell caused by a combination of wave-guiding, interference and scattering, as we discuss in the next section.

Resonances in the PSBR Solar Cell. To obtain a detailed understanding of the absorption in the cell, cross sections of the electric field intensity ($|E^2|$), and separate field components are shown at two distinct absorptance peaks in Figs. 3.6a and 3.6d. The intensity profiles indicate a complex interplay of different resonance mechanisms. Therefore, we also plotted the E_x and E_z component ($E_y = 0$), see Fig. 3.6b, c, and Fig 3.6e, f, respectively. The E_x component at 801 nm reveals a strong E-field within the nano-cylinder, while this is not the case at 895 nm.

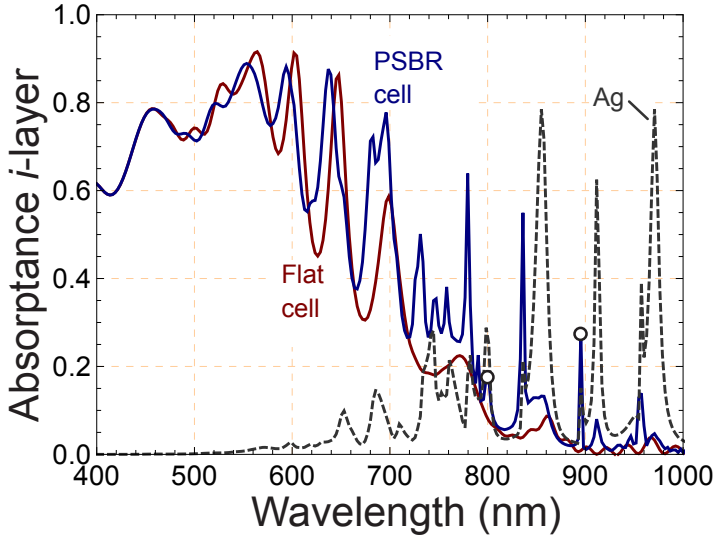

Figure 3.5: Simulated absorptance within the intrinsic layer of both the flat cell (red) and PSBR solar cell (blue). Sharp absorptance peaks are observed in the PSBR cell. The dashed line shows the total absorptance in the structured Ag of the PSBR cell. The black crosses mark some absorptance peaks for which both the i-layer and PSBR structure have a corresponding wavelength.

This has a strong effect on the profile of the E-field within the Si. Interestingly, a "checkerboard" pattern arises in the E_z field plot. The E-field of the incident light is directed along the x-axis, so E_z is zero. Therefore, a strong E_z component indicates lateral propagation through the solar cell which indicates coupling to waveguide modes.

Above each silica nano-cylinder there are two rows of extremes of the electric field. Due to the periodic grating of the PSBR the scattering pattern has a well-defined set of spatial frequencies. As a result, only a subset of the eigenmodes in the cell structure can be occupied, namely those which have an in-plane wave vector (k_x) that matches the periodic pattern of the PSBR. The conservation of the in-plane momentum dictates that these eigenmodes have an integer number of wavelengths in each unit cell of the grating.

Optical Scattering Processes and Interference Phenomena in the PSBR Solar Cell. The interaction of an electromagnetic wave with the PSBR in a nc-Si:H solar cell involves several (wavelength-dependent) interference and scattering phenomena, which form the origin for light trapping. Figure 3.7a shows scattering of light by a single particle. For a periodic array of scatterers, the interference of the scattered light results in a diffraction pattern, see Fig. 3.7b. In the far field, light is diffracted according to the grating equation with several grating constants,

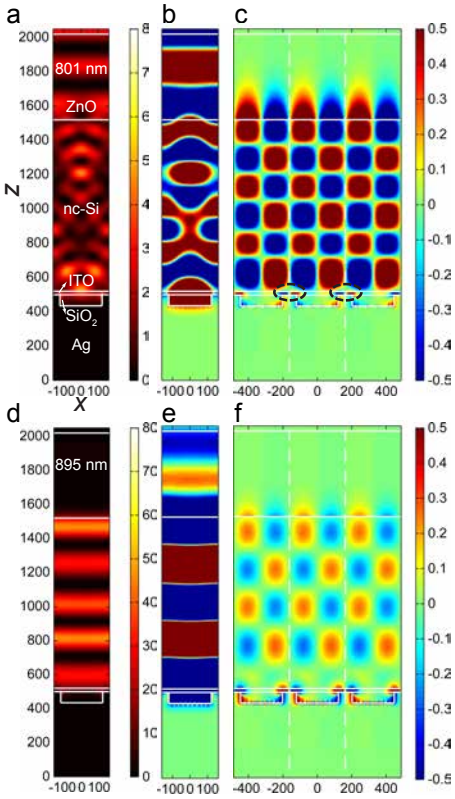

Figure 3.6: Plots of (**a, d**) $|E|^2$ in units of $(\mathrm{V/m})^2$, (**b, e**) real part of E_x, and (**c, f**) real part of E_z in (V/m) at two strong absorbing wavelengths: (**a-c**) λ_0=801 nm and (**d-f**) at λ_0= 895 nm. The interfaces of the different materials in the cell are indicated by white lines. E_z is plotted for three unit cells, a characteristic checkerboard pattern arises due to scattering and wave guiding.

including the pitch (p) and the diagonal pitch ($\sqrt{2}p$). For periodic arrays, the scattering is a superposition of the scattering by both the Ag pattern and the silica nano-cylinders. Figure 3.7c illustrates three phenomena. First, light is attenuated as it propagates through the Si layer, and so the interaction with the PSRB is determined by the fraction of the light that is not absorbed in a single cell pass. Second, the cell is an optical resonator and supports Fabry-Pérot interference modes. These modes are determined by the thickness of the constituent layers and their refractive indices. Third, the electromagnetic field distribution inside the cylinders depends on the wavelength. The electric field at a perfectly flat mirror is zero,[73] however, due to the nano-pattern geometry and losses in the metal, the PSBR behaves as a metamaterial mirror with non-zero E-field at its surface.

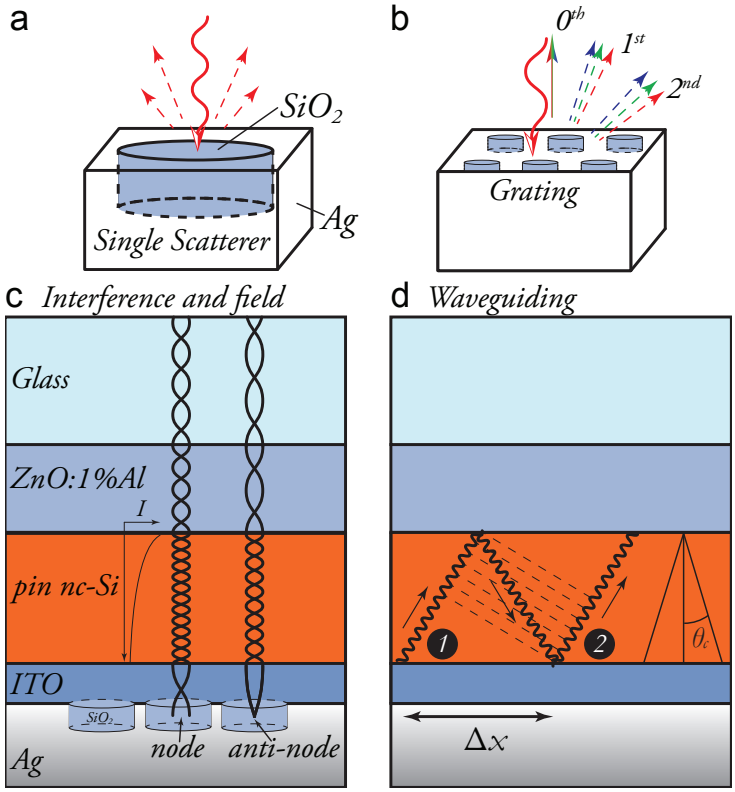

Figure 3.7: Simplified overview of the different scattering and interference mechanisms involved in the solar cell with a PSBR. (**a**) A single particle spatially scatters light to the active layer. (**b**) An array of these scattering particles gives rise to diffraction of light into the active layer. (**c**) The layer structure of the cell supports Fabry-Pérot resonances, leading to fringes in the absorptance spectrum. (**d**) Ray optics representation of waveguiding in the nc Si:H solar cell. Light is totally internally reflected when the angle of incidence exceeds the critical angle θ_c. Waveguiding occurs if the indicated ray ❶ and ❷ interfere constructively. Each waveguide mode propagates at a specific mode angle within the thin Si slab, although only a subset of the available guided modes is populated in the PSBR cell.

Therefore, the optical interaction with the PSBR is wavelength dependent and a non-zero E-field is observed in the ITO, directly above the Ag "ridges" in between the nano-cylinders (see encircled regions in Fig 3.6c). Figure 3.7d illustrates waveguiding in the silicon layer. The supported optical modes are determined by the thickness of the Si layer and the cladding layers.[80,81] When the planar component of the wave-vector of light scattered into a specific mode matches to a grating constant of the PSBR array, light is efficiently coupled into such a mode and strong absorptance occurs in the active layer.

Scattering in a solar cell can originate from for example plasmonic[67,82] and/or Mie scattering.[66] The scattered light propagates towards the top of the cell. Light hitting the Si/ZnO or ZnO/glass interface at an internal angle larger than its associated critical angle is trapped by total internal reflection (TIR). Effectively, the critical angle for TIR of the silicon layer is not affected by the presence of a TCO layer on top of the cell. Light traveling upwards in the Si layer of the cell at an angle larger than the critical angle (of a Si/air interface) will effectively be totally internally reflected: either completely at the Si/TCO interface, or else the light transmitted to the TCO layer is totally reflected at the TCO/air interface. Interestingly, the critical angle a Si/air interface is only around 16°, so only small scattering angles are needed to get total internal reflectance.

Small deviations, in the order tens of nanometers, in cell thickness and refractive index will drastically change the resonance conditions in the cell, thereby the absorptance peaks will shift significantly. This explains the observed difference between the peak width and wavelength between the simulated and experimental data. However, the simulations help to comprehend the complex interplay between the indicated optical phenomena, which results in the sharp absorptance peaks which we observed both in the experimental data and in the simulated absorptance (Fig. 3.5). The resonances of an individual particle are spectrally broad.[66] The amplitude and width of the Fabry -Pérot resonances are determined by the interface reflectivity and cell thickness respectively. In contrast, the width of the modal coupling resonances is determined by constructive interference along the waveguide over the modal absorption length. At long wavelengths, this leads to sharp coupling peaks due to the low absorption in the *i*-layer. In the experiment, local variation in cell parameters (mainly cell thickness) and the use of a light source with a certain spectral bandwidth (∼10−15 nm) result in smoothening of the absorptance peaks, leading to broader observed absorptance maxima as experimentally observed.

Interestingly, it appears that enhanced absorptance in the *i*-layer of the PSBR solar cell coincides with enhanced absorptance in the Ag of the PSBR (e.g. see matching at wavelengths of 800, 838, 895, and 958 nm in Fig. 3.5). This indicates resonant coupling between the PSBR and guided modes, leading to enhanced absorptance in the *i*-layer. Due to the strong resonant interaction with the PSBR, the absorptance in the PSBR also increases (up to 80%). At some wavelengths the resonance in the PSBR is so strong that only a small fraction of light is resonantly scattered into the *i*-layer. Detailed analysis of the field profiles at the absorptance peaks showed that over 85% of the absorptance by the PSBR is absorbed in the Ag due to plasmonic resonances; the ITO and SiO_2 show only weak absorption.

Outlook. The PSBR concept is important for light trapping in many thin film solar cell technologies,[83] such as organics,[60] CIGS,[84] CZTS, perovskite,[85] GaAs,[86] thin c-Si,[87] a-Ge:H,[88] and CdTe. The PSBR approach fulfills the need for light

trapping in flat superstrate cells; other concepts, such as FLiSS, are only suited for flat substrate cells. The integration of a flat PSBR allows the use of minimal contact area between the silver and the ITO, which results into low surface recombination. However, for cells having a high *IQE*, the plasmonic absorptance losses can render the PSBR less effective.[40,68,89] The PSBR structure scatters the light that reaches the backside of the solar cell, but it does not facilitate light incoupling at the front surface of the cell. In this first exploration, we used a periodic pattern of nano-cylinders. Semi-random patterns exhibit a broader range of spatial frequencies, which can broaden the absorptance peaks, resulting in a higher average absorptance[59,70,77,90,91] and reduced angular sensitivity.[92] Additional methods, such as external light trapping[93,94] and/or (smoothened) front textures,[95] can improve the incoupling at the front side of the solar cell.

3.4 Conclusions

A novel method for light trapping in thin film superstrate solar cells was demonstrated. In particular, this method enables the growth of flat nc-Si:H of high material quality. In contrast to conventional structures for light scattering in solar cells, our plasmonic scattering back reflector (PSBR) consisting of silica nano-cylinders in a silver layer does not involve texturization, and thereby prevents growth-induced material defects. The PSBR is fabricated by soft-imprint lithography, which enables large-scale fabrication at low costs. The fabrication process does not involve any mechanical polishing step, and can be applied at the backside of any superstrate cell. The particle swarm optimization algorithm is used to determine the optimal size of the silica nano-cylinder array embedded in Ag. Using simulations, it was identified that the optical scattering mechanisms give rise to the experimentally observed sharp absorptance peaks and the enhanced *EQE*. The PSBR shows an improved absorptance compared to the flat reference cell, without impacting the V_{oc}. This renders the PSBR as an effective candidate for light trapping in superstrate thin film cells.

3.5 Supplementary Information

Cell Fabrication. The nc-Si solar cells are grown on flat Corning glass. The structure of the superstrate solar cell is: ZnO:Al/*p*-type nc-Si:H/intrinsic nc-Si:H/*n*-type a-Si:H/Ag/Al. The ZnO:Al and the tin-doped indium oxide (In_2O_3:Sn, ITO) were sputtered by radio-frequency magnetron sputtering using a target of ZnO:Al_2O_3 (1 wt.%) and In_2O_3:Sn_2O_3 (10 wt.%), respectively. For the textured cell, the ZnO was textured by dipping the sample in a solution of diluted hydrochloric acid (0.5%) for 10 s. Plasma enhanced chemical vapor deposition (PECVD) is used to deposit

the doped layers at a radio frequency of 13.65 MHz. Silane (SiH_4) and hydrogen (H_2) are used as source gases. The 25 nm thick *p*-layer and 27 nm thick *n*-doped μc-Si:H layers were deposited using hydrogen diluted trimethylborane (TMB, 2%) and hydrogen diluted phosphine (2%) as dopant gases, respectively. Hot-wire chemical vapor deposition (HWCVD) using tantalum wires is done to deposit a 1 μm thick *i*-layer in 75 minutes.[96] These two wires have a diameter of 0.3 mm and are spaced by 3.5 cm, at a distance of 4 cm from the substrate. After the ITO deposition, a short descum process is done to make the surface of the ITO layer hydrophyilic using an O_2 -plasma. This improves the adhesion between the liquid silica sol-gel and the ITO surface. The metal back contact was deposited by thermal evaporation of Ag and a finishing thin layer of Al to prevent oxidation. The solar cells have an active area of 4×4 mm^2, which is defined by the mask used for deposition of the metal back contact. Besides the cell area, a manual scribe is done which gives access to the ZnO:Al front contact. Metal is evaporated on top of this scribe, and thereby the front ZnO:Al can be contacted via this metal.

Figure 3.8 shows a sample with 24 flat cells (in front) and another sample with 24 PSBR cells (in back). Due to the periodic pattern of the PSBR the light is diffracted.

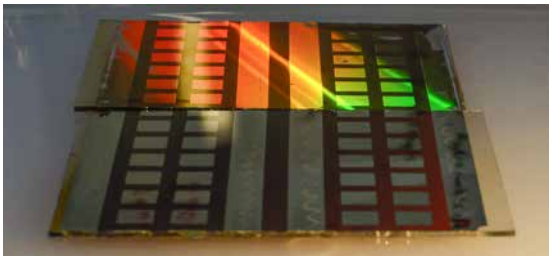

Figure 3.8: Photo of the backside of the flat (in front) and PSBR (in back) solar cell. The light is scattered by PSBR solar cell resulting in the observed diffraction pattern. The 4×4 mm^2 squares define the active cell area. The metal stripes at the sides are used to access the ZnO:Al front contacts of the solar cell.

3.5.1 Optical Modeling: Particle Swarm Optimization Algorithm

In the simulation we calculate the absorptance in each layer. To calculate the electrical current, we assume that only the charge carriers created in the intrinsic silicon layer are collected at the terminals, and thereby contribute to the J_{sc}. The absorption in the doped layers is considered to be lost due to the high defect density and charge carrier recombination.[97,98] By integrating the product of the AM1.5G spectrum and the absorptance in the *i*-layer we calculated the effective photocurrent, which we define as the implied J_{sc}.

A particle swarm optimization (PSO) algorithm[99] is used to determine the optimal height, diameter, and pitch of the square array of silica nanocylinders. The PSO algorithm scans a defined parameter space, in a similar way as a flock of birds explore an area to find food. When one bird finds food, other birds will likely swarm in the direction of this successful bird to search for food in his neighborhood. At the same time, these exploring birds will plan their flight based on their historical success for finding food at previously visited spots.

To apply this search technique to optimize the current in solar cells, the implied J_{sc} was set as the figure of merit (FoM).[100] The PSO algorithm was terminated after 50 generations, with a generation size of 13 individuals. During the last 15 generations the FoM did not change significantly, which indicates that the simulations converged to the optimal geometry. The PSO algorithm saves significant computational power compared to a brute force scan of the parameter space.

Chapter 4

3D-Printed External Light Trap for Solar Cells

Summary. This chapter presents a universally applicable 3D-printed external light trap for enhanced absorption in solar cells. The macroscopic external light trap is placed at the sun-facing surface of the solar cell and retro-reflects a large part of the light that would otherwise escape. The light trap consists of a reflective parabolic concentrator placed on top of a reflective cage. Upon placement of the light trap an improvement of 15% of both the photocurrent and the power conversion efficiency in a thin-film nanocrystalline silicon (nc-Si:H) solar cell is measured. The trapped light traverses the solar cell several times within the reflective cage, resulting in an increase of the total absorption in the solar cell. Consequently, the trap reduces optical losses and enhances the absorption over the entire spectrum. The components of the light trap are 3D-printed and made of smoothened, silver coated thermoplastic. In contrast to conventional light trapping methods external light trapping leaves the material quality and the electrical properties of the solar cell unaffected. To explain the theoretical operation of the external light trap, a model is introduced that predicts the absorption enhancement in the solar cell by the external light trap. The corresponding calculated path length enhancement shows good agreement with the empirically derived value from the optoelectrical data of the solar cell. Moreover, the influence of the angle of incidence on the parasitic absorptance is analyzed to improve the understanding of the trap performance.

4.1 Introduction

Light-management concepts that efficiently couple light into solar cells and enhance the absorption in optically thin absorber layers are essential to achieve high power conversion efficiencies and low production costs.[101–103] To improve the energy conversion efficiency and reduce the material consumption of crystalline silicon (c-Si) cells, a continuation of the trend towards thinner wafers is imperative. However, this reduction in thickness results in a lower absorptance, which can be compensated by light trapping schemes. It is therefore expected that light trapping will become increasingly more important for c-Si cells.[103] Currently, light trapping is important in thin film solar cells like thin film nano-crystalline silicon cells, as they extensively rely on light management to increase the optical path length to realize a competitive efficiency. At the same time, there is considerable interest for anti-reflection coatings for the front surface, for example texturing and structures that resemble nature's solution for reflection as can be found in moth eyes.[104]

One of the reasons why the efficiency of commercial modules is lower than the theoretical efficiency limit is the difficult trade-off between the optical and electrical cell properties. Internal light trapping schemes, like texturing of the surface of the absorber, improve the absorption, but at the same time deteriorate the electrical properties of the solar cell by inducing additional bulk and surface recombination centers.[44, 46, 48, 105] Additionally, nano-textured metallic back reflectors and textured front contacts increase the parasitic absorptance.[68, 106–109] It thus remains a challenge to realize internal light-trapping schemes without affecting the electrical properties of the solar cell.[52, 110, 111]

In this chapter, an external light trap is introduced that is of interest for all solar cell technologies, since the light trap is placed as an add-on on top of the cell and retro-reflects the light that is reflected and radiatively emitted by the solar cell. Although the theoretical concept of external light trapping has been wandering in literature and patents for several decades,[112–118] this is the first report on successful experimental demonstration of the concept. Figure 4.1 illustrates how sunlight can be externally trapped by "squeezing" the light through a small aperture in the light trap. This light trap consists of two parts: a parabolic concentrator and a cage. The cross-sectional area of the aperture is much smaller than that of the solar cell, thereby the light trap retro-reflects a significant fraction of the light that would otherwise escape. Consequently, this external light trap reduces the optical losses and increases the light harvesting over the entire solar spectrum. Most of the photons that are reflected by the front surface of the solar cell and those that passed the cell but were not absorbed are retro-reflected by the external light trap. It should be noted that this method of light trapping differs markedly from conventional light concentration. Instead of focusing light on a small solar cell area, we defocus the light after the concentrator aperture. Thereby, the light can

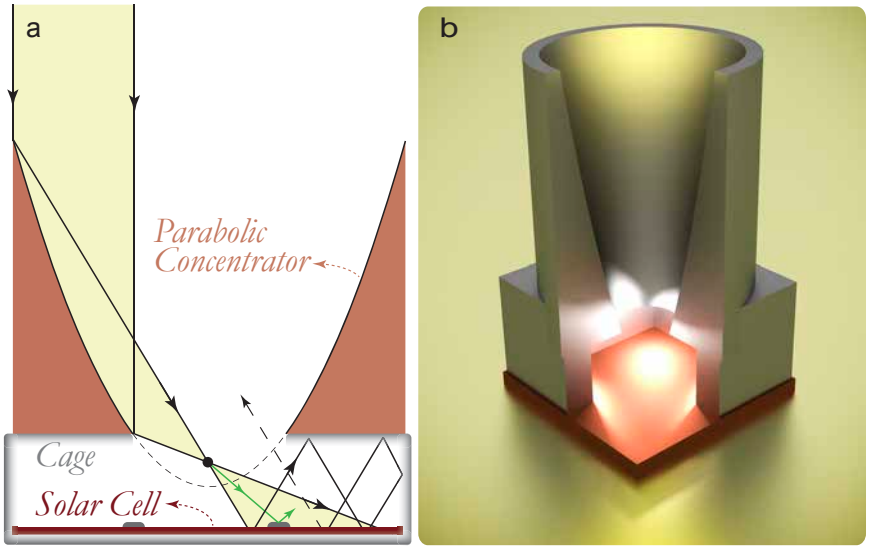

Figure 4.1: (**a**) Schematic illustration of the external light trap. By concentration, light is funneled through a small aperture and is trapped. Also shown in green is the reflection from a metallic reflective front contact. (**b**) A rendered 3D CAD model of the light trap. The front quarter of the light trap is removed for visibility. A concentrator is placed on top of a square cage with the solar cell at the bottom (cell area shown in red). Most of the reflected light from the solar cell is recycled within the cage.

be trapped in between the top of the cage and the solar cell. In the experimental part of this chapter, the external light trap is realized by placing the cage on the solar cell, on top of which a concentrator is positioned.

The external light trap reduces the need for internal light trapping schemes and anti-reflection coatings that interfere with the electrical performance of the cell.[97, 119, 120] The light trap targets three major optical loss mechanisms present in all solar cells: 1. reflection at the cell at its front surface, metal fingers, busbars, and the reflective area between wafer based solar cells; 2. incomplete absorption, mainly at long wavelengths (λ); 3. photons emitted by radiative recombination. For most solar cells, like c-Si, combating the losses due to reflection and poor absorption is most rewarding. Currently, the recycling of radiatively emitted photons is mainly interesting for gallium arsenide (GaAs) cells due to its relative high external radiative efficiency (*ERE*).[121–124] Another benefit of the introduced concept is that it can help concentrated photovoltaics by reducing the heat load of the cell compared to conventional concentrated photovoltaics. A combination of light trapping and concentration can be used to profit from less solar cell material usage and higher open circuit voltage due to high-injection conditions.[112]

Internal light trapping schemes theoretically result in a path length enhance-

ment of maximally $2n^2\times$ the double cell pass.[21] Therefore, low refractive index ($n\sim2$) materials, such as organic and perovskite solar cells can only gain a relatively low path length enhancement. External light trapping is independent of the refractive index and therefore of special interest for these cells.

The top of the external light trap is a compound parabolic concentrator (CPC). CPCs are generally applied for concentrated photovoltaics and solar thermal applications. There are basically three different categories of CPCs: macroscopic, millimeter, and micrometer sized concentrators. Macroscopic CPCs are commonly used in evacuated tube thermal collectors and solar thermal applications.[125–127] Millimeter sized CPCs were proposed to benefit from the relatively low Joule losses of small solar cells[128] and to realize a low-cost, flat plate like concentrated photovoltaic module,[129–131] while others fabricated micro-sized CPCs using two-photon lithography[117, 118] and etching.[132]

We investigate the performance of the external light trap using a millimeter-scaled 3D-printed CPC placed on top of a 1.2 μm thick superstrate hydrogenated nanocrystalline (nc-Si:H) cell. The light trap is applicable to a wide variety cells.

4.2 Optical Model for External Light Trapping

It is a common misconception that one could make a layer on the solar cell that only allows light from the sun to be transmitted towards the solar cell, while it blocks light that travels from the solar cell to the sun. Thermodynamics forbids the concept of such a one-way-mirror that would allow thermal heat (radiation) to radiate unidirectionally from a cold to a hot body, since this violates the second law of thermodynamics.[18] The external light trap seems to violate this law since light can travel unhindered from the hot sun to the cold solar cell, while most radiation originating from the cold solar cell is retro-reflected by the trap. However, the trap also restricts the solid angle of light that is accepted, which enforces an equivalent restriction of the escape area (the aperture in this case) of the light confined in the trap.[133] Therefore, the angular étendue restriction by the CPC enables efficient retro-reflection of the photons that do not escape through the aperture (on their way upwards). Since the étendue restriction of radiatively emitted and accepted photons is identical, the external light trap does not violate the second law of thermodynamics.

For the external light trap, an absorption gain by light trapping is obtained upon placement of a cage between the CPC and the cell. The spacing of the cage enables sufficient divergence of the light beam, such that it does not escape through the aperture after the first reflection. The height of the cage determines the amount of divergence, and thereby the homogeneity of the light distribution on the solar cell.

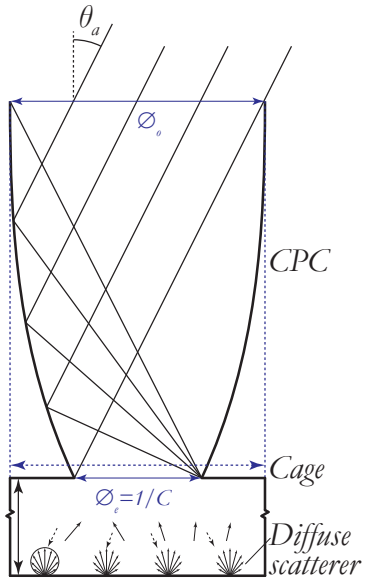

Figure 4.2: Diagram of a CPC and a cage on top of a diffuse scatterer. The CPC has an opening aperture with a diameter $Ø_o$, exit aperture $Ø_e$ and a certain acceptance angle θ_a for the incoming light. The light is scattered at the bottom of the cage. In the limit for a very tall cage, the probability for a photon to escape equals the area ratio $Ø_e/Ø_o$.

Figure 4.2 indicates several important parameters of the external light trap. The trap not only restricts the angular cone of acceptance, but also imposes an equivalent restriction for the trapped light: the light reflected by the solar cell outside this acceptance étendue is retro-reflected. Due to this equivalence, the probability of photons to escape from the trap, $P(\text{escape})$, is in first order inversely proportional to the concentration factor (C):

$$\frac{1}{P(\text{escape})} = C = \frac{1}{\sin(\theta_a)^2}, \tag{4.1}$$

where θ_a is the half angle of the acceptance cone of the concentrator.[133] This reciprocity dictates that the restriction of the escape area within the light trap, is inversely correlated to the angular acceptance restriction outside the trap, which is similar to rugate filters.[122, 134]

The restriction of the escape probability of photons increases the effective absorptance in the solar cell. In general, the intrinsic efficiency limit increases when the cell thickness is reduced while the absorptance stays constant.[112] The improved energy conversion efficiency limit is possible because thin solar cells have effectively less recombination and thereby a relatively high open circuit

voltage. According to literature on c-Si solar cells,[135] the thickness related Auger and Shockley-Read-Hall (SRH) charge carrier recombination restricts the maximum possible efficiency of an ideal thin (3 μm) c-Si cells under maximum angular restriction to 33.4%, which is significantly higher than the ~29.4% of an ideal thick (105 μm) solar cell without angular restriction.[112, 136, 137]

The effectiveness of external light trapping is explained by the following optical model. For simplicity, consider first a hypothetical case in which light is completely diffused and homogenized inside the cage (or cavity). This condition can be realized by integrating a diffuser layer or white paint in the cage. Furthermore, we assume that the solar cell response does not depend on the angle of incidence of the light. When a random set of photons enters a tall cage and is specularly reflected by the cell, the photons are homogeneously distributed in the cage. Thereby, once a photon of this set arrives at the top of the cage its probability to escape via the aperture is given by the following area ratio:[133]

$$P(\text{escape}) = \frac{A_{\text{aperture}}}{A_{\text{cell}}}. \tag{4.2}$$

In the low absorbing limit, the photons thereby traverse the cell statistically C times as much as a bare cell (without light trap on top). The statistically averaged path length enhancement factor due to external light trapping ($\Pi_{\text{ext, low absorbing}}$), is equal to the area ratio:

$$\Pi_{\text{ext, low absorbing}} \sim C = \frac{A_{\text{CPC}}}{A_{\text{aperture}}} \left(= \frac{A_{\text{cell}}}{A_{\text{aperture}}} \right), \tag{4.3}$$

where A_{CPC}, A_{aperture} and A_{cell} are respectively the area of the CPC opening, the CPC bottom aperture and the illuminated cell area.[125, 133] Since in our design A_{CPC} equals A_{cell}, there is effectively no concentration, and we thus only investigate light trapping. In the low absorbing limit, the value of Π_{ext} of an angular restrictor is thus equivalent to C.[133]

The optical model that is used includes the losses originating from the CPC, cage and cell. Initially, a fraction T_{c} is transmitted by the CPC and penetrates into the solar cell with absorptance A_{sc}. A fraction $T_{\text{c}}A_{\text{sc}}$ is absorbed by the cell. Most of the reflected light ($R_{\text{sc}} = T_{\text{c}}(1-A_{\text{cell}})$) does not escape, but is instead retro-reflected by the top of the cage with reflectivity R_{cage}. For homogeneously distributed light a fraction C^{-1} escapes from the trap and $(1-C^{-1})R_{\text{cage}}$ is reflected backwards by the cage. The cage absorbs a small fraction $(1-C^{-1})A_{\text{cage}}$. This process continues infinitely and the absorption accumulates. The total absorptance with trap (A_{trap})

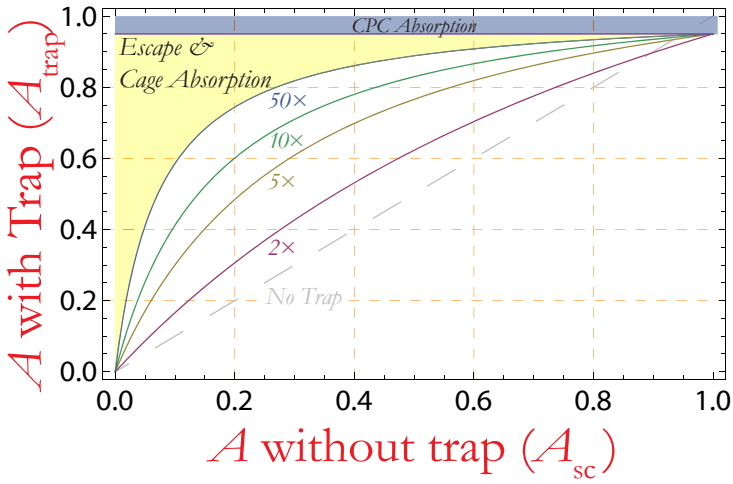

Figure 4.3: Absorptance enhancement by external light trapping. The four path length enhancement cases indicate the cell absorptance with light trap (A_{trap}) as a function of the bare cell absorptance (A_{sc}) at the indicated concentration factors ($C=\frac{1}{P(\text{escape})}$). T_{c} is set to 95% and the R_{cage} to 95%.

is thus given by:

$$A_{\text{trap}} = T_{\text{c}}[\overbrace{A_{\text{sc}}}^{1^{\text{st}}\text{ hit}} + \overbrace{R_{\text{sc}}(1-C^{-1})R_{\text{cage}}A_{\text{sc}}}^{2^{\text{nd}}\text{ hit}} + \sum_{n=2}^{\infty}\overbrace{R_{\text{sc}}^{n}(1-C^{-1})^{n}R_{\text{cage}}^{n}A_{\text{sc}}}^{n^{th}\text{ hit}}] \tag{4.4}$$

The sum of this geometric series is given by:

$$A_{\text{trap}} = T_{\text{c}} \cdot \frac{A_{\text{sc}}}{1-R_{\text{sc}}(1-C^{-1})R_{\text{cage}}}. \tag{4.5}$$

All parameters, except C, are wavelength dependent.

Fig. 4.3 shows the total absorptance for the cell with trap as a function of the bare cell absorptance for four light-trapping cases. For a higher concentration factor the escape probability is lower and thereby the total absorptance is higher. The quality of the CPC is relatively more important for cells with a high absorptance, as the optical loss in the CPC has to be compensated by light trapping. Low values of Π_{ext} ($2-10\times$) do already have a significant impact on the absorptance. For example, for $\Pi_{\text{ext}}=10\times$ a cell with an absorptance of just 20% will be enhanced to 60% by the light trap. When Π_{ext} increases, the total absorptance in the cell converges towards the transmittance of the CPC.

It is of interest to compare internal and (concentrator based) external light trapping to identify the optimal method and to investigate how both trapping mechanisms can be combined. Internal light trapping is realized by scattering and total internal reflection within the cell. At low absorptivity this results in a maximum theoretical path length enhancement factor of $\Pi_{int}=2n^2\times$ with respect to a double cell pass.[21, 138] For silicon cells, this corresponds to a factor of $\sim 2\cdot 3.5^2 = 24.5\times$. However, in practice only broadband path length enhancement factors of at most $\sim 10\times$ are realized.[139]

For a perfect light trap, the external path length enhancement (Π_{ext}) is in the low absorbing limit equal to C (see eq. 4.3). However, as a consequence of the non-zero absorptance values, Π_{ext} ranges from $1\times$ to $6\times$. From the experimental data, the effective path length enhancement factor can be derived using (see next section for the derivation):

$$\Pi_{ext}=\frac{\log(1-A_{trap})}{\log(1-A_{sc})}. \tag{4.6}$$

The external light trap thus results in a path length enhancement of Π_{ext}, which is equivalent to an effective thickness of $z_{eff}=\Pi_{ext}\cdot z$, with z the solar cell thickness. Alternatively, one can consider the net effect of light trapping as an effective enhancement of the absorption coefficient (α) from α to $\Pi_{ext}\cdot\alpha$.

The total path length enhancement (Π_{total}) is determined by the product of the internal and external path length enhancement factor: $\Pi_{total}=\Pi_{int}\cdot\Pi_{ext}$, and thus:

$$\Pi_{total}=\frac{2\,n^2}{\sin^2(\theta_a)}, \tag{4.7}$$

where θ_a is the half angle of the acceptance cone.[112] The sun covers only a very small part of the sky. The required half angle θ_{sun} of only $\sim 0.266°$ translates to a remarkable maximum path length enhancement factor in the order of $2n^2\cdot 46.000\approx 10^6\times$ for direct sunlight! For direct sunlight, the theoretically maximum contribution to the total path length enhancement from external light trapping, is thus considerably higher than that of internal light trapping.

4.2.1 Determination of the Path Length Enhancement Factor

This section describes the experimental determination of Π_{ext} using the implied absorptance derived from the external quantum efficiency (*EQE)* and internal quantum efficiency (*IQE*). The *EQE* of a cell with external light trap (EQE_{trap}) is defined as the total number of collected charge carriers, divided by the number of incoming photons (at the top of the CPC). The *IQE* is defined as total number of collected charge carriers, divided by the number of absorbed photons. The *IQE* describes the internal quality of the solar cell; ideally its value equals 1. The

conditions at which the solar cell operate (such as the internal voltage) only change slightly upon placement of the external light trap. Therefore, we can, in first order, assume that the *IQE* of the cell without and with light trap (IQE_{bare} and IQE_{trap}) are equal.

The path length enhancement can be calculated from the bare cell absorptance (A_{bare}) and the total absorptance by the cell with the external light trap (A_{trap}). However, it is experimentally difficult to measure A_{trap} in a direct manner. The total absorptance is the sum of the absorptance by the cell and the parasitic absorptance by the CPC and the cage. Thereby, the absorptance by the cell (A_{trap}) is in an experiment optically indistinguishable from the parasitic absorptance by the CPC and the cage. However, A_{trap} can be indirectly estimated from the EQE_{trap} using the IQE_{bare}:

$$A_{\text{trap}} = EQE_{\text{trap}} / IQE_{\text{bare}}. \tag{4.8}$$

After determining the absorptance, the path length enhancement factor can be calculated. In first order, the absorptance is described by the Beer-Lambert law. For light that passes the solar cell Π_{ext} times, the net reflectance R_{trap} as observed outside the trap, is thus given by $(R_{\text{sc}})^{\Pi_{\text{ext}}}$. For an idealized light trap Π_{ext} can be estimated from the measured EQE_{trap} and A_{sc} according to:

$$R_{\text{trap}} = (R_{\text{sc}})^{\Pi_{\text{ext}}} \tag{4.9}$$

$$1 - A_{\text{trap}} = (1 - A_{\text{sc}})^{\Pi_{\text{ext}}} \tag{4.10}$$

$$1 - \frac{EQE_{\text{trap}}}{IQE} = (1 - A_{\text{sc}})^{\Pi_{\text{ext}}} \tag{4.11}$$

$$\therefore \Pi_{\text{ext}} = \frac{\log(1 - \frac{EQE_{\text{trap}}}{IQE})}{\log(1 - A_{\text{sc}})}. \tag{4.12}$$

Parasitic Losses. The *EQE* of the cell with external trap (EQE_{trap}) is related to the absorptance according to:

$$EQE_{\text{trap}} = IQE \cdot A_{\text{trap}} = (1 - IPL) \cdot A_{\text{trap}}, \tag{4.13}$$

with *IPL* the internal (optical and electrical) parasitic losses. These parasitic losses are ascribed to both the absorption in the non-active layers and the non-collected (recombined) charge carriers. Notice that the *IQE* is indeed the upper limit for EQE_{trap} (when A_{trap}=1). A_{trap} converges to 1 at moderate (5−10×) trapping factors, see Fig. 4.3.

The *IQE* is related to the carrier collection efficiency (f_{c}) and to the absorption

in the active layer (A_{active}):

$$IQE = \frac{f_c \cdot A_{\text{active}}}{A_{\text{sc}}} = \frac{f_c \cdot A_{\text{active}}}{A_{\text{active}} + A_p}, \tag{4.14}$$

with A_p the parasitic absorption in non-active layers. A high value of f_c and a low A_p are therefore essential for a high IQE. The parasitic absorptance in textured solar cells is generally higher than in flat cells.

Path Length Enhancement as Function of the Absorptance. The achievable path length enhancement factor depends on the cell reflectance. From eq. 4.5 and eq. 4.6 the expected theoretical maximum of Π_{ext} was calculated for the used geometric concentration factor of C=6. Figure 4.4 illustrates that the path length enhancement factor is inversely related to the absorptance. It can be seen that in the low absorbing limit (A_{sc}=0) the path length enhancement factor is equal to the concentration factor. For the case A_{sc}=1, the light is completely absorbed in a one-cell pass (back and forth), and therefore no path length enhancement can be realized.

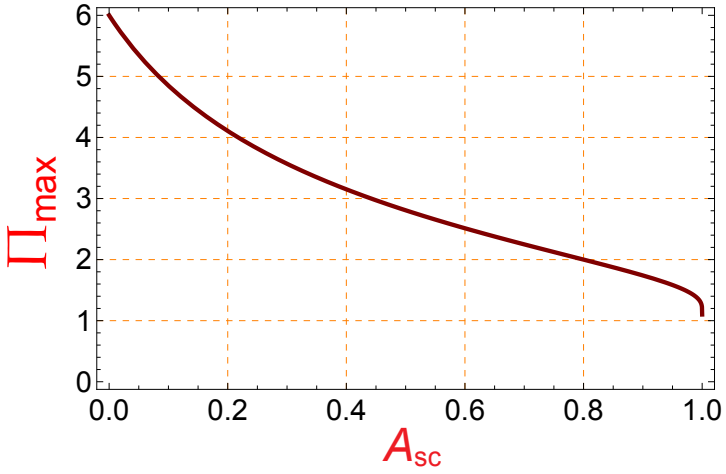

Figure 4.4: Plot of the simulated maximum achievable path length enhancement factor Π_{max} for a perfect external light trap, with a concentrator with C=6, as a function of the absorptance of the bare solar cell (without a light trap).

4.3 Design and Fabrication of the External Light Trap

After introducing this theoretical framework of the efficiency enhancing potential of the external light trap, we address its design and fabrication. A cross section of the fabricated light trap is illustrated in Fig. 4.5a. The CPC is designed in such a way that the angle of incidence at the cell at its front surface is below the Brewster angle of glass. This design prevents undesirably large Fresnel reflectance at large incidence angles (more information on page 56). The optimization of the concentration factor of the light trap is primarily a trade-off between the negative effects of design inaccuracies on the CPC transmission at high C and the improved absorptance due to path length enhancement at high C. It was found that, with the used 3D-print technique and CPC size, it is technically challenging to realize high transmittance for concentration factors with $C>10\times$. This is mainly due to the need for higher accuracy with increase of C. Small deviations from the intended optical path will increasingly result in rejection of the light when the diameter of the exit aperture is reduced. Low concentration factors ($C\sim 2\times - 10\times$) are already sufficient to make a significant absorptance change.

Therefore, in this study a CPC is used with a geometrical concentration factor of $C=6$, which experimentally showed both high transmittance and a descent absorption enhancement.

One can engineer the light trap such that the path length enhancement for specular reflected light in the cage is even higher than the model, which is based on homogeneously distributed light in the cage, predicts. The intensity (I) of light traveling through an absorber drops exponentially according the Beer-Lambert law:

$$I = I_0 \cdot e^{-\alpha \cdot l}, \tag{4.15}$$

with α the absorption coefficient and l the distance traveled through the cell. After one cell pass, the initial intensity dropped to $I = I_0 \cdot A$. Normally this light escapes to the outer world. However, once the trap is applied, the power escaping through the aperture is related to the exponential intensity decay with the number of cell passes: $I_{\text{escape}} = I_0 \cdot A^{\#\text{cell passes}}$. Therefore, the amount of light that comes out of the cell after one cell pass is exponentially higher than after two cell passes. It is thus advantageous to force the light to pass the cell several times without any opportunity to escape, to maximize the absorptance. A cleverly designed external light trap exploits the exponential intensity decay by preventing the specularly reflected light from escaping the trap during the first couple of recycle events. This can be realized by letting the light initially only propagates radially outwards, see Fig. 4.5b. This opportunity to postpone the first escape occurrence is an advantage over internal trapping schemes. This escape postponement cannot be obtained when the cell reflects the light diffusely. The largest path length

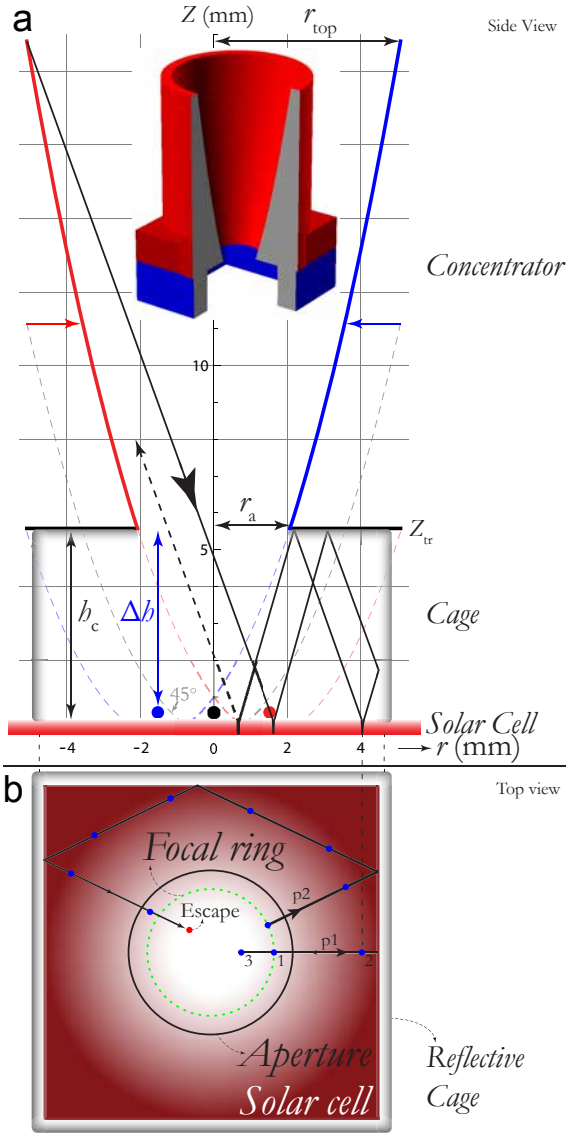

Figure 4.5: (**a**) A vertical cross section through the symmetry axis of the light trap. The CPC is rotationally symmetric, the cage is a cuboid. The light incident on the left side (red) of the CPC is focused on the right focal point (red) and vice versa for the right side(blue). The inset shows a 3D-model of the design: a circular CPC is placed directly on top of the square cage. (**b**) Top view of the square cage. Due to the rotational symmetry of the CPC the focal points form a focal ring (indicated in green). Two horizontal projections of different light paths are shown. The blue dots indicate the spots where the light is reflected by the solar cell. Path p1 corresponds with that shown in Fig. 4.5a. Light following path p2 travels a longer distance and thus hits the cell more often compared to p1. The distance between the spots depends on the polar angle with the z axis. This in turn, depends on the radial location where the initial beam hits the paraboloid.

enhancement is therefore expected for a flat, specular reflective cell, combined with a specular reflective cage. An additional advantage of a flat cell design is the superior electrical quality.[52] Inhomogeneous cell illumination should be prevented as this generally negatively affects the cell performance, see also section 6.4.2.

4.3.1 Design Parameters of the Light Trap

Shifted Compound Parabolic Concentrator. The concentration factor is enhanced further by shifting the paraboloid sides radially inwards by Δr, as shown in Fig. 4.5a. The focal point is shifted Δr outward in the radial direction and a non-imaging focal ring emerges. A shift of $\Delta r = r_{\text{aperture}}/2$ relocates the focal point of each CPC side exactly below the edge of the opposite side. Accordingly, A_{aperture} $(=\pi \cdot \frac{r_{\text{aperture}}^2}{2^2})$ is reduced by a factor $\chi_{\text{shift}}=4$. Thereby, the concentration factor is multiplied by χ_{shift} (eq. 4.3). To prevent severe optical loss by inaccuracies in the printed design χ_{shift} is set to 3. Combining this χ with a 2× parabolic shape yields a trapping factor $C=2\cdot3=6\times$. The corresponding angle of incidence at the cell ranges from 20° to 37°.

Shifted Parabolic Concentrator & Acceptance Angle. Please note that Eq. 4.7 cannot be directly applied to the shifted CPC, because a shifted CPC does not have a well-defined θ_a: for a certain range of angles of incidence the light is only partially transmitted to the solar cell. However, this equation gives a useful estimation of the potential path length enhancement. The inversely proportional relationship between the acceptance angle (or acceptance chance) and the maximum path length enhancement holds for all concentrators: it is a fundamental requirement imposed by entropy considerations.

Choice of Concentration Factor of the CPC. Besides the previously noticed parasitic absorptance by the metal coating on the CPC there can be more optical losses. Fabrication defects (such as deformations and scratches) in the CPC translate to escape losses in the CPC, as the light does not follow the intended optical path. This production related problem becomes more pronounced when the distance between the point at which the light reflects at the CPC and the aperture increases. Conventional CPCs become rather tall for high concentration factors[125] and thereby the achievable transmission is thus reduced. Low concentration factors are therefore advantageous. The optimization of the concentration factor of the light trap is thus primarily a trade-off between the negative effects of design inaccuracies on the CPC transmission with increase of C and on the other hand the improved absorption due to path length enhancement with increase of C.

Cage. The inner dimensions of the square cage are 9×9 mm^2 to enable proper alignment on top of the 10×10 mm^2 solar cell that was used in this study. For the measurements of the bare solar cell the cage is used as a mask with an inner area

of 9×9 mm^2. Thereby, the illuminated active solar cell area is 9×9 mm^2, both for the measurement with and without the external light trap.

If the cell area would be smaller than the concentrator opening area, there would be an effect on the cell performance due to concentration. However, in this research we do not want to investigate an effect of concentration, instead, we only want to determine light trapping. Therefore, the circular opening area of the concentrator (A_{CPC}) and the (horizontal) inner area of the square cage (A_{cage}) are both set to 81 mm^2. The effective illuminated area is thus unchanged upon the placement of the external light trap. By doing so, only the contribution of light trapping is determined. The CPC radius (r_{cpc}, in millimeters) is therefore set to:

$$r_{\mathrm{cpc}}=\sqrt{\frac{A_{\mathrm{cage}}}{\pi}}\left(=\sqrt{\frac{81\,\mathrm{mm}^2}{\pi}}\right). \tag{4.16}$$

The area and the corresponding incident photon flux is thus equal for the bare cell (with the cage used as a mask) and the light trap on top (the cage and the CPC).

Cage Height. Suppose a case in which the (upper surface of the) solar cell is located directly below the exit aperture of the concentrator. In that case the incident light reflected by the cell propagates to the opposite side of the CPC and escapes without being trapped. To prevent this direct escape, a certain cage height (h_c) is needed between the aperture of the CPC and the solar cell. This condition is relaxed in the case of a shifted compound parabolic concentrator, as there the focal ring is shifted radially outwards with respect to the central axis which prevents a direct escape of the light. The cage height is set to 5 mm which enables the beam to expand to an area larger than $A_{aperture}$ at the solar cell. In this way, the reflected light will hit the reflective cage wall, instead of escaping through the aperture. To prevent this direct escape the cage height has to be sufficiently larger than the focal length of the parabola.

CPC Design Parameters. Here, we discuss several design considerations of the light trap. The formula for the height (z) of a parabola is:

$$z(r)=\frac{1}{4f}r^2, \tag{4.17}$$

with r the radius, and f the focal distance with respect to $z=r=0$. So, a parallel beam of light will be focused at $(x,z)=(0,f)$.

In case $z_{\mathrm{tr}}=f$ the paraboloid will make a 45° angle with the horizontal at the truncated paraboloid bottom side (see bottom of Fig. 4.5a) and the light is thus reflected horizontally. The large angle of incidence at the cell results in higher reflectance on the cell interface according to the Fresnel equations (see Fig. 4.7). Thereby, the light that escapes via the aperture increases, so more light is lost. A similar problem is known in image sensors as pixel vignetting. This reflection

problem can be mitigated by truncating the paraboloid higher, at $z_{tr}=f+\Delta z$. Moreover, Δz is set such that the distribution of the angle of incidence shifts towards the surface normal at which the cell has a relative low reflectance. To find a proper f and z_{tr} we use the following equation:

$$(z_{tr}=)\frac{1}{4f}(\frac{r_{top}}{\sqrt{C}})^2 = f+\Delta z. \tag{4.18}$$

Solving this equation for f gives two solutions: a positive and a negative f. The positive solution is:

$$\therefore f = \frac{\sqrt{C^2\cdot\Delta z^2+C\cdot r_{top}^2}-C\cdot\Delta z}{2\cdot C} \tag{4.19}$$

Error Propagation in the Focal Point due to Deformations. During the production of the CPC, several design deformations can arise compared to the intended design. For example, a temperature change can deform the CPC. For the proper functioning of the CPC it is important to examine the effect of deformations from the intended shape (see Eq. 4.17) on the optical properties. Here, the effect of two deformations on the focal point is analyzed.

A linear deformation of the parabolic concentrator in the z-direction results in $z_{deformed}=z_{original}\cdot\circledast$, with $\circledast$ the deformation factor. The focus shifts accordingly:

$$z_{\text{vertically deformed}} = \frac{1}{4f_{original}}r^2\cdot\circledast \tag{4.20}$$

$$\therefore z_{\text{vertically deformed}} = \frac{1}{4(f_{original}/\circledast)}r^2 \tag{4.21}$$

For a deformation $\circledast>1$ the new shape of the deformed CPC corresponds to a CPC with a *downward* shifted focal point ($f_{new}=f_{original}/\circledast$).

Now, consider a linear expansion of a factor $\circledast$ in the *radial* direction. This transforms the radial coordinate according to $r_{new}=r_{original}\cdot\circledast$. The original radial coordinate is thus given by: $r_{original}=r_{new}/\circledast$. We can substitute this relation in Eq. 4.17 and determine the new position of the focal point:

$$z_{\text{radially deformed}} = \frac{1}{4f_{original}}(r_{new}/\circledast)^2 \tag{4.22}$$

$$\therefore z_{\text{radially deformed}} = \frac{1}{4(f_{original}\cdot\circledast^2)}r_{new}^2 \tag{4.23}$$

By comparing this equation and Eq. 4.17 it can be seen that a radial deformation $\circledast>1$ corresponds to a parabola with an *upwards* shifted focal point: $f_{new}=f_{original}\cdot\circledast^2$.

It can be concluded that a deformation in the z direction propagates

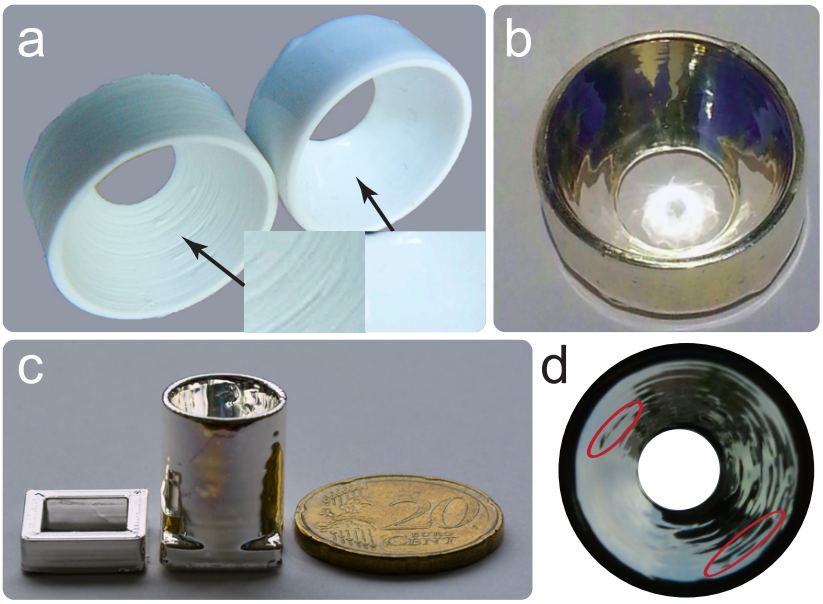

Figure 4.6: (**a**) A 3D-printed CPC before and after chemical smoothening, the insets show a zoom-in of surface. (**b**) The silver coated CPC with a focal ring of sunlight at the center. (**c**) The separated cage and CPC that can be combined to an external light trap. (**d**) View of the CPC from the entrance side, showing the reflection in the parabolic curve. Two wrinkles in the concentrator are encircled in red.

as $f_{\text{original}}/\circledast$ to the height of the focal point, while this is $f_{\text{original}} \cdot \circledast^2$ for radial expansion. For the 3D-printed CPC the deformation is expected to be a few percent at maximum. This error propagates inversely proportionally to vertical deformation. From a Taylor series it can be seen that this error roughly doubles for a radial expansion, which is well acceptable.

4.3.2 Fabrication: 3D-Printing & Silver Coating

Chemical Smoothening. The solubility of ABS thus allows the printed objects to be vapor smoothened according to the procedure described on page 21, the results are shown in Fig. 4.6a. After smoothening, the cage and the CPC were silver coated, which results in focusing of sunlight, as can be seen in Fig. 4.6b. Figure 4.6c shows the square cage and the circular concentrator that are stacked to form the light trap. The opening area of both the CPC and the cage is 81 mm^2. We used a square cage to match the usual shape of the solar cell. Moreover, the square cage design is an interesting candidate for large area module integration: by arranging multiple square cages into a square array, a large area can be efficiently covered by light traps as will be discussed in chapter 5.

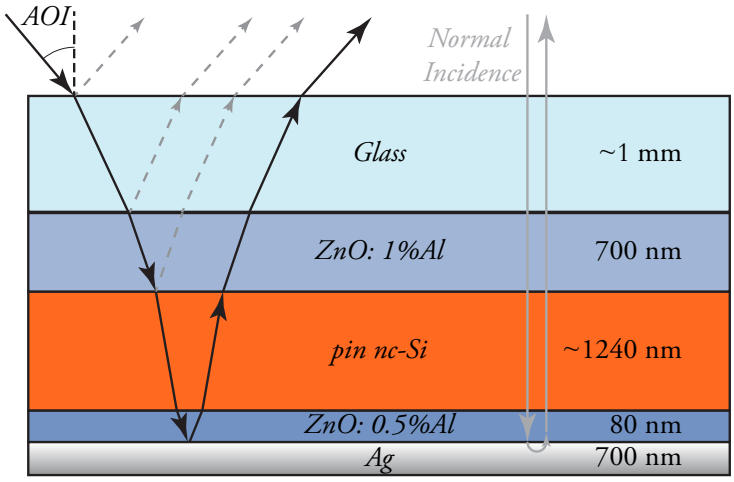

Figure 4.7: Illustration of the design of the hydrogenated nanocrystalline solar cell. The arrows indicate a light trace. Some interface reflections are shown in gray.

Some undesired unevenness of the parabolic shape can be observed by eye from the small distortion in the projected image inside of the CPC, see Fig. 4.6d. The formation of wrinkles might be prevented by using a more accurate fused deposition modeling (FDM) printer and by improving the acetone treatment. As an alternative, one could use a different 3D-printer, such as a stereo-lithography printer (based on optical curing of a resin).

The finished light trap was placed on top of a flat square thin-film nc-Si:H solar cell prepared in superstrate configuration, see Fig. 4.7. The light trap changes the angle of incidence to non-normal angles. According to Snell's law, the path length thereby increases (relatively) more in the low refractive index ZnO than in the high index Si. This results in a relative increase of the parasitic losses.

Irradiance Distribution and External Light Trapping. Depending on the exact geometry of the light trap, the illumination distribution at the solar cell can become inhomogeneous, which negatively affects the cell performance.[140, 141] Thereby, the current generation in the cell also becomes inhomogeneous, which leads to an elevated impact of the series resistance. The impact of this problem can be reduced by using an optimized trap design. When a tall cage is used, the light diverges significantly and illuminates a larger cell area (when it reaches the solar cell for the first time). Another solution that enables uniform and near normal illumination has been described earlier.[121] Here, two CPCs are directly connected at their short aperture; the bottom CPC has its small aperture on top, directly connected to the small aperture of the top CPC. The upper CPC focuses the light and the bottom CPC forms a cage that redistributes the light evenly on the solar cell. This design can be beneficial due to the more normal incidence at the cell

level. A disadvantage is that the light generally is reflected more often at the cage compared to other designs,[133, 142] thereby the parasitic absorptance in the cage increases.

4.3.3 Cell Design: Considerations & Fabrication

For solar cells made in a substrate configuration, the placement of the electrical probes at the sun-facing side of the cell interferes with the placement of the external light trap. The external light trap is tested on a 1.2 μm thick superstrate (p-i-n) nc-Si:H solar cell (see Fig. 4.7). The 10×10 mm^2 cell is electrically contacted from the back side, such that it does not conflict with the placement of the light trap.

For cells that do have reflective front contacts the shadow loss is reduced as a consequence of the optical recycling of the light trap. Thereby, an additional energy conversion efficiency enhancement (typically around 5 to 10%) can be expected. As a superstrate cell configuration is used, without any metal fingers on top of the cell, no reduction of the shadow loss could be demonstrated.

The cell is deposited on a Corning-glass (Corning Eagle 2000) superstrate. A 700 nm thick ZnO:1%Al layer is sputtered at $\sim$430 °C by a radio-frequency magnetron sputtering. The silicon material is deposited at a radio-frequency of 13.56 MHz using PECVD: *p*-layer ($\sim$20 nm); *i*-layer ($\sim$1200 nm); *n*-layer ($\sim$20 nm).[143] The back contact consists a 80 nm RF-sputtered ZnO:0.5%Al and 700 nm of thermally evaporated Ag. The cell area is defined by $10\,\text{mm}\times10\,\text{mm}$ deposited silver back contact. The light trap was placed on top of the unprocessed side of the glass while the cell was contacted from the backside of the glass.

4.4 Results and Discussion

The square cage was placed on top of the square solar cell and used as a mask to determine the current density versus voltage (*J-V*) characteristics of the bare solar cell. The illuminated cell area was thus 81 mm^2 (see page 56). Subsequently, the CPC (with equal opening area) is placed on top of the cage to determine the opto-electrical improvement by the external light trapping. Figure 4.8 shows the *J-V* characteristics at AM1.5G illumination of the bare (masked) solar cell and the cell with the external light trap (cage and concentrator). Due to the light trapping, the short circuit current density (J_{sc}) and the current at the maximum power point (J_{mpp}) improved by 14% and 15% respectively. No significant change in the fill factor (*FF*) and open circuit voltage (V_{oc}) was measured. To understand the origin of this enhancement the *IQE*, the absorptance, and the *EQE* were determined.

The internal quantum efficiency ($IQE=\frac{EQE}{A_{sc}}$) of the bare cell was determined by measuring the absorptance ($A_{sc}=1-R_{sc}$) and the *EQE*, see Fig. 4.9. For short

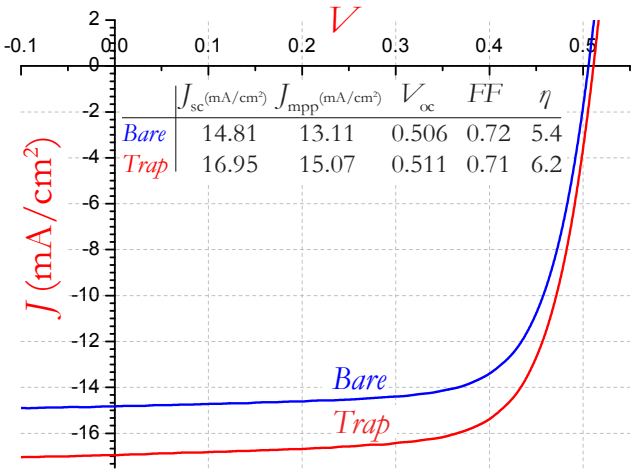

Figure 4.8: *JV*-characteristic of the bare (blue) solar cell (with the cage used as a mask) and the solar cell with the external light trap (red).

wavelengths (λ<400 nm), the absorptance of the bare cell is high (∼80−90%). The relative high parasitic absorptance in the ZnO front contact and the (not photovoltaically active) *p*-layer results in a low *EQE* and *IQE*. This implies that there is only small potential for improvement (∼10 to 20%$_{\text{relative}}$) in this short wavelength regime. For wavelengths around 600 nm the reflectance is 10 to 40%, while at the same time the *IQE* is high. This provides significant room for improvement by external light trapping. For longer wavelengths (λ>700 nm) there is 40-60% reflection. With further increase of the wavelength, the absorptance in the nc-Si reduces compared to the parasitic absorptance and therefore the *IQE* drops to zero. In first order, the achievable *EQE* improvement is given by $EQE_{\uparrow}=R_{sc}\cdot IQE$. Thus, the light trap mainly improves the response when both R_{sc} and *IQE* are high, this is the case for ∼400<λ<∼900 nm. The observed optical interference patterns are mainly due to the Fabry-Pérot modes in the 1.2 μm thick Si layer.

Figure 4.10 shows the *EQE* of the bare cell (*EQE*), the *EQE* of the cell with trap (EQE_{trap}) and the *EQE* as calculated using the model (EQE_{model}). There is a significant external quantum efficiency improvement from EQE_{bare} to EQE_{trap} over the full spectrum. At short wavelengths, the improvement is mostly due to retro-reflection of light that is reflected at the front interface of the cell. For long wavelengths, there is also retro-reflection of light that passed the solar cell but was not absorbed. The enhancement demonstrates that indeed the external light trap effectively prolongs the optical path length in the cell.

The curve of EQE_{trap} is smoother than that of EQE_{bare}, which can be explained by two effects. First, in the extreme limit of external light trapping the light is

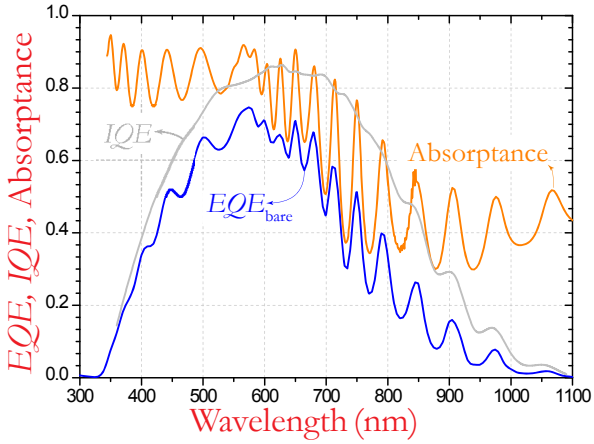

Figure 4.9: Plot of the total absorptance (orange), the *EQE* (blue) and the derived *IQE* (gray) of the bare solar cell.

completely absorbed (A_{sc}=1). In this case the corresponding *EQE* is given by: $EQE = IQE \cdot A_{sc} = IQE$. Because EQE_{trap} converges towards the smooth *IQE* the interference fringes are reduced. Or, to state it differently, for some wavelengths at which the *EQE* has a dip there is relatively a high reflectance. By external light trapping, these *EQE* dips are improved more than the maxima, which smoothens the curve.

Secondly, the trap offers a range of non-normal angles of incidence resulting in a range of different overlapping Fabry-Pérot resonances with a more continuous average; the interference conditions disappear. A distribution of the path length in the cell with a small dispersion of just a few per cent significantly smoothens the absorptance and *EQE*.

From the introduced model (eq. 4.5) the achievable *EQE* was calculated using EQE_{bare} and the *IQE*, see EQE_{model} in Fig. 4.10. The following parameter values were used: T_c=0.95, C=6, R_{cage}=0.93. The overall trend of EQE_{model} corresponds well with the measured EQE_{trap}. There is excellent agreement at short wavelengths between the model and the experimental data. The observed decrease of the interference fringes of EQE_{trap} corresponds with the trend of the model. Although the EQE_{trap} approaches EQE_{model}, there is a discrepancy which is attributed to several losses that were not included in the model: ❶ The glass between the light trap and the solar cell enables some light to escape sideways. ❷ The printed cage and the CPC are not perfectly smooth, resulting in unwanted parasitic absorption and reflection in unintended directions. ❸ Imperfect interconnection of the cell, the 3D-printed cage and the CPC causes small cavities (around a few hundred μm) that gives rise to a small escape loss (estimated to be a few percent). ❹ The wavelength dependence of some of the parameters (T_c and R_{cage}) was not taken into

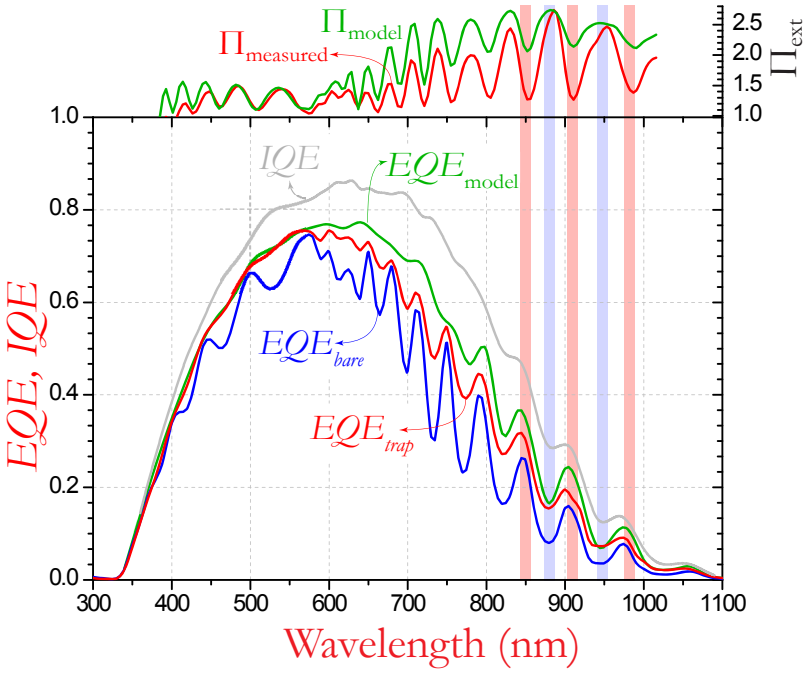

Figure 4.10: Plot of the EQE_{bare} and *IQE* of the bare solar cell (without light trap). Also shown is the *EQE* of the solar cell with external light trap (EQE_{trap}) and the expected *EQE* of the cell with light trap based on the optical model (EQE_{model}). The external path length enhancement factor (top of figure) shows that there is an improved optical path length for all wavelengths. As expected, there is an anti-correlation of Π_{ext} with the interference pattern as indicated by the red and blue bars.

account. ❺ Because IQE_{trap} cannot be determined experimentally, we assumed for the model that IQE_{bare} equals IQE_{trap} . Based on the model, the J_{sc} of the cell with light trap could be ideally 19.9 mA/cm^2. Therefore, by reducing the indicated loss mechanisms one could gain another 2.9 mA/cm^2.

External path length enhancement. The realized and expected external path length enhancement ($\Pi_{\text{experimental}}$ and Π_{model}) were calculated by evaluating eq. 4.6 on the implied absorptivity as described in section 4.2.1, see top of Fig. 4.10. The external path length enhancement ranges from 1.5—2.5× in the long wavelength regime, where light trapping is mostly needed. The pattern of $\Pi_{\text{experimental}}$ agrees with the expected Π_{model}.

The path length enhancement is anti-correlated to the *EQE*, as can be seen from the vertical red and blue background bars in Fig. 4.10. This agrees with the optical model which indicates that the achievable path length enhancement is roughly inversely related to the bare cell absorptance (see Fig. 4.4). Besides that,

the before mentioned smoothening of EQE_{trap} also results in an anti-correlation of the Π_{ext} and EQE data as the interference minima of the EQE_{trap} relatively increase, while the maxima relatively decrease.

A high quality external light trap with a moderate (e.g. $\sim$10×) path length enhancement factor and low parasitic absorption losses results in an EQE_{trap} just below the IQE. In the design process of solar cells that are to be combined with a light trap, one has to optimize the IQE. This can be done by preventing undesirable parasitic absorption, for example in the back reflector.[89]

Concentrated photovoltaics vs. External light trapping. The question now arises how external light trapping differs from conventional light concentration. Concentrators are commonly used to concentrate light directly on a solar cell to benefit from reduced, relatively expensive, cell usage and the higher open circuit voltage. For a cell under concentrated light (without internal light trapping) light traverses the cell just back and forth, after which the non-absorbed light escapes through the front surface. However, for a cell with an external light trap the light is forced to traverse the cell many times which allows the use of thinner and untextured cells, resulting in less bulk and surface recombination.

Improvements. Several improvements for external light trapping can be envisaged. The (individual) external light trap can be scaled to a larger area by designing a CPC array. Large trapping arrays can be made from ABS plastic by injection molding at low cost. The material costs of ABS are in the order of 1€/dm^3. Depending on the exact design parameters such as the height of array, the fabrication cost can be as low as several €/m^2. It has been shown that the thickness of CPC arrays can be scaled down to the micrometer range, which benefits module integration.[117, 118] The need of sun-tracking can be eliminated by matching the acceptance cone of the CPC to the path of the sun. Finally, the positive effects of an enhanced V_{oc} due to light concentration can be combined with light trapping. For example, when a CPC with a concentration factor of 6× is combined with a solar cell with a smaller area of $A_{cell}=A_{CPC}/2$ there is both concentration (effectively 2×) and light trapping ($\Pi_{ext}=3\times$). This also enables mitigation of the high shading losses of the metal grid in concentrator cells of 10-20%.[139] Moreover, the reduced flux will help to mitigate heat problems at cell level compared to full concentration.

The design of the cage is another aspect of the light trap that can be improved. It has been shown that an oblate hemi-ellipsoidal cavity with a specular reflective coating would be an interesting candidate.[123, 133, 142, 144, 145] In this design the solar cell is located in between the focal circle of the ellipsoid and thereby all the light reflecting from the solar cell is reflected backwards to the cell in just one reflection. This enables efficient recycling as it keeps the parasitic absorptance by the cage low.

Sensitivity for diffuse light. For isotropically distributed incident diffuse light a fraction $1/C$ is transmitted by the parabolic concentrator.[126] Therefore, the

use of low concentration factors ($C \sim 2-10\times$) enables transmitting ~10-50% of the diffuse light. There is an inevitable trade-off between loss of diffuse light and reduced escape probability (within the light trap) with increase of C. The geographic location of the solar module determines the fraction of diffusely incoming photons. Geographic regions with a high time-average of clear sky conditions are in favor of external light trapping. Also, it is advantageous to have a short optical path length through the atmosphere to reduce Rayleigh scattering. This implies that the local "AirMass" (AM) spectrum is AM$x.x$, with $x.x$, close to 1. Geographic locations at a high elevation, that are close to the equator, and having only few clouds are therefore best suited for external light trapping.

Further research should be performed to determine an optimal concentration factor. Alternatively, it is worthwhile to model and realize an earlier proposed concept in which both the diffuse and direct component of the sunlight are harvested by geometric separation.[146]

4.5 Conclusions

A combination of a 3D-printed parabolic concentrator and a light cage is used to demonstrate external light trapping for a thin film nc-Si:H solar cell. A 15% enhancement of the energy conversion efficiency in this cell was measured with respect to the same cell without an external light trap. The external light trap recycled both the unwanted reflection from the front side of the cell and enhanced the poor absorptance in the long wavelength regime. The measured absorptance enhancement at short wavelengths demonstrated the anti-reflection effect of the trap. An absorptance model for external light trapping was introduced, which showed good correspondence with the experimental data. As a result of light trapping a path length enhancement factor up to 2.5× was observed. Several optical loss mechanisms were found and described that can be targeted in future research to obtain better trapping than this initial result. For further research, we recommend to focus on the accuracy and the related transmittance of the CPC.

The parasitic absorption losses of this first prototype of the compound parabolic concentrator are more than compensated by the gain in the cell absorptance. The efficiency improvement is caused by an unprecedented broadband absorption enhancement by the external light trap,[147–149] which is universally applicable to all solar cell technologies. Higher gains can be expected upon further optimization of the reflections in the trapping system. Reducing the cell thickness combined with the external light trap is a promising way for further efficiency improvement.

The trap enables decoupling of the optical and electric optimization which yields new perspectives for the design of solar cells. In the current solar cell market, revolutionary light trapping architectures are needed to obtain higher efficiencies.

The demonstrated 3D-printed external light trap is an attractive candidate to accomplish this target.

Chapter 5

3D-Printed Concentrator Arrays for External Light Trapping on Thin-Film Solar Cells

Summary. In the previous chapter, a 3D-printed external light trap on a small solar cell was demonstrated. In this chapter, the potential of this trap for large scale solar panels is analyzed. The light trap is tested on organic solar cells, which have a major need for proper light trapping and could therefore significantly benefit from external light trapping. An external light trap consists of a parabolic concentrator and a spacer that redirects the photons that are reflected by the solar cell, back towards the solar cell. These retro-reflections enable higher absorptance and improved power conversion efficiency. Scaling a single external light trap such that it covers a large solar panel has disadvantages in terms of the height and cost. These disadvantages can be overcome by deploying an array of concentrators as the top part of the external light trap. In this chapter, we present an optimization study of concentrator arrays for external light trapping. We fabricated 3D-printed external light traps with a square, hexagonal, and circular compound parabolic concentrator in order to test their suitability for concentrator arrays. The 3D-printed traps were placed on top of an organic solar cell, which significantly enhanced the external quantum efficiency. The required transmittance of these concentrator arrays is calculated as a function of the parameters of both the concentrator and the solar cell. We compare the theoretical and experimentally determined optical

performance of the different concentrators. Finally, we analyze the prospects of external light trapping and offer guidelines for improving the external light trap design.

5.1 Introduction

Thin solar cells benefit from low bulk recombination of excited charge carriers. Hence the performance of a thick solar cell generally improves by reducing its thickness provided that the absorptance stays constant. Therefore, significant efforts have been conducted to obtain high absorptance in thin solar cells by modifications of the solar cell surface to obtain internal light trapping.[150, 151] However, these internal cell modifications often have a negative impact on the material quality and the electrical performance of the solar cell. For example, by texturing the surface of crystalline silicon (c-Si) solar cells the surface recombination velocity increases due to the enlarged surface area.[152, 153] For other cells like nanocrystalline silicon (nc-Si) the growth of a high quality solar cell on top of a textured scattering surfaces is difficult[36, 44, 46] while for organic solar cells texturing is less effective.[154] Generally, it is thus challenging to realize the full theoretical potential of internal light trapping for solar cells, so there is a need for supplemental light trapping methods.[102] We demonstrate an external light trapping method that can complement or even replace internal light trapping. Conveniently, it can be directly applied on all solar cells.

Fig. 5.1 illustrates the concept of an external light trap: a concentrator focuses the sunlight through a small aperture before the light reaches the photovoltaic device. Most of the reflected (and radiatively emitted) light by the solar cell is reflected back to the solar cell by the reflective coating of the cage. Therefore, there is a higher probability for a photon to be absorbed. This photon recycling enables higher power conversion efficiency.[94, 122, 123, 134, 135] Moreover, external light trapping enables new photovoltaic devices that, for example, can facilitate spectrum splitting.[115, 155]

By external light trapping one can realize a smaller escape probability than the internal escape probability determined by the internal escape angle (which is determined by the refractive index of the active absorber layer). Thereby, the theoretical energy conversion efficiency limit of external light trapping surpasses that of conventional internal light trapping.[112, 121, 135] This is mainly due to the improved electrical quality of thin solar cells and the potential recycling of radiative emission. In chapter 4, we demonstrated a broadband absorption enhancement by applying one external light trap on a $\sim$1 cm^2 nanocrystalline silicon solar cell. A light trap that covers a larger solar cell area can be made of a single tall concentrator, but this translates to high material costs and weight, and moreover it is esthet-

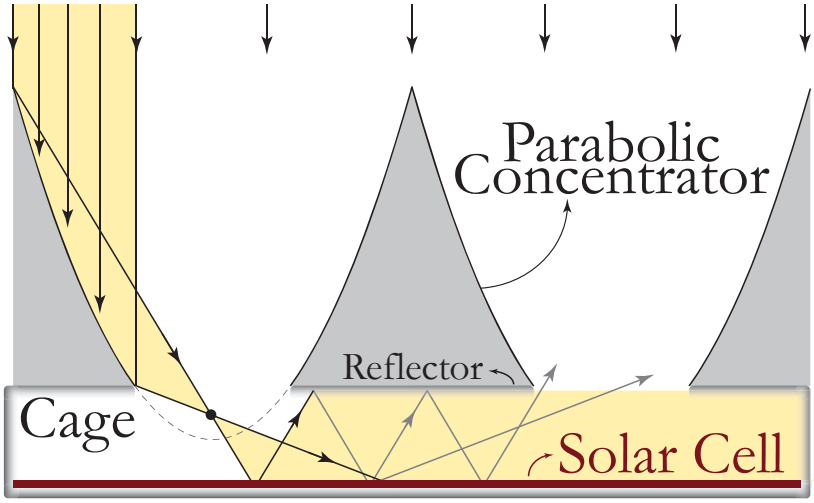

Figure 5.1: Schematic illustration of a parabolic concentrator array for external light trapping. Light is focused through a small aperture. The spacing between the concentrator and the solar cell allows the light beam to expand. Most of the light that is reflected by the solar cell is reflected back to the solar cell. A small fraction (determined by the aperture area) of the light can escape out of the cage.

ically unattractive. The use of an array of small concentrators overcomes these disadvantages. We present an optimization study of the design of concentrator arrays suited for external light trapping. Furthermore, we compare the theoretical and experimental transmittance of a square, hexagonal and circular 3D-printed parabolic concentrator. Previously, a light trap incorporating a micro-lens array has been shown to be successful on an organic solar cell.[147, 156] Here, a low cost fabrication method is presented that requires less fabrication steps and is industrially scalable.

To test the performance of the external light traps we use an organic solar cell (OSC), because these cells strongly require light management to realize sufficient absorptance. For organic solar cells there are currently no adequate light trapping methods. The absorptance of thin organic solar cells is relatively low. Although a thick cell has high absorptance, a thick cell design is not desirable as it exhibits a high bulk recombination loss.[157, 158]

Internal light trapping schemes based on Lambertian scattering can realize a significant path length enhancement factor for high refractive index (n) solar cells as the escape probability scales as[139] $P_{\text{escape}} = \frac{1}{n^2}$. However, they are less effective for low refractive index solar cells like organic solar cell materials (with $n \sim 2$).[21, 138, 154, 159]

Moreover, it is difficult to scatter the broadband sunlight effectively in OSCs.

Macroscopic surface textures efficiently scatter the light in relative thick crystalline silicon solar cells. However, this method cannot be directly applied to thin OSCs as scattering by geometric features smaller than the wavelength of light is not effective.[160]

Due to the lack of a sufficient light trapping method there has been interest for alternative light trapping methods like arranging solar cells in a macroscopic V-shape in which incoming light hits both flanks of a V-shaped solar cell several times.[149, 158, 161] This is an effective method to enhance the total absorption, but it complicates the fabrication considerably. Due to the enlarged area the light is effectively diluted which reduces the injection level and the corresponding open circuit voltage of the solar cell. Moreover, the enlarged surface area will increase surface recombination and deteriorate the dark current. These disadvantages are absent for external light trapping where the optical path is prolonged without using more solar cell material.

5.2 Experimental

Design of the Concentrators. Metallic parabolic concentrators with a square and a hexagonal top shape can be arranged in an array. Figure 5.2a and 5.2d show a square concentrator that is composed of four parabolic segments. These square concentrators can be arranged in a square array as shown in Fig. 5.2g. In a similar way a hexagonal array can be made as shown in Fig. 5.2b, 5.2e and 5.2h. Circular concentrators cannot completely fill a plane. To overcome this filling problem the circular concentrators can be truncated at four sides to enable the formation of a square array as illustrated in Fig. 5.2c, 5.2f and 5.2i. In a similar way a hexagonal array of circular concentrators can be made. In between the neighboring concentrators there are sharp peaks which are fragile and challenging to fabricate.

The transmittance of the concentrator is a key parameter for the performance of the external light trap. Incoming light that travels in a straight line towards the aperture of the concentrator is transmitted without being reflected by the concentrator. The main part of the light is reflected one or more times at the reflective concentrator surface before going through the aperture to enter the cage. The exact number of reflections depends on the geometry of the parabolic concentrator. At each reflection a small fraction of the light is absorbed by parasitic losses at the reflective surface of the concentrator. The averaged transmittance of a concentrator therefore decreases with increasing geometric concentration factor (C), where C is defined as the following area ratio:

$$C = \frac{A_{\text{cell}}}{A_{\text{aperture}}}. \tag{5.1}$$

To determine the optimal concentrator geometry we calculated the average transmittance of incoming light propagating parallel to the central axis of the concentrator. The transmittance of light originating from other angles depends on the parabolic shape of the concentrator.[125] Diffuse light is only partly transmitted by the concentrator as rays with a large angle of incidence are reflected out of the concentrator. The maximum transmitted power (P_{trans}) of isotropically distributed diffused light (P_{diff}) is $P_{\text{trans}} = \frac{1}{C} \cdot P_{\text{diff}}$.[162] Sun tracking will yield the best averaged transmittance of the concentrator as all rays of the direct sunlight will be transmitted through the aperture. However, external light trapping can be more cost effective without diurnal sun tracking which is possible: at low concentration factors ($C < 10\times$) a static concentrator can still accept the direct sunlight for around 8 hours per day.[113]

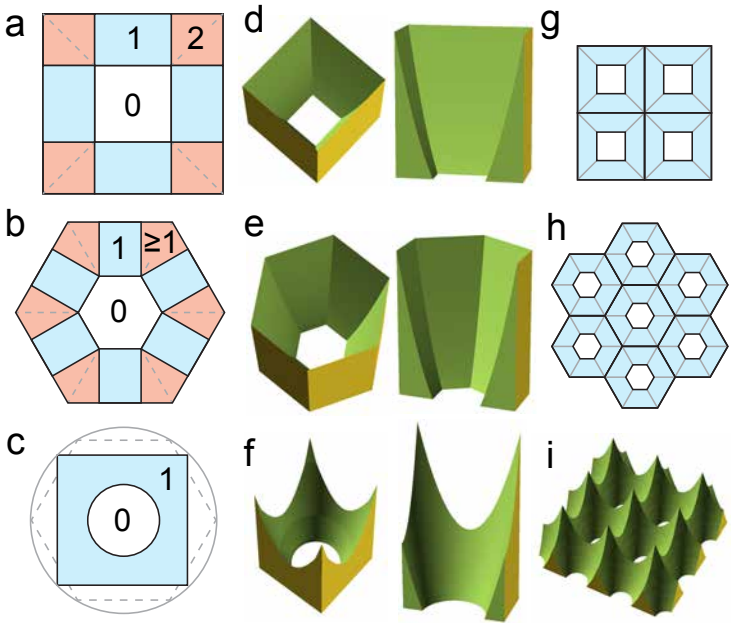

Figure 5.2: Illustrations of several concentrators and their corresponding arrays. **Left**. Top view of **(a)** a square, **(b)** a hexagonal and **(c)** a vertically truncated circular parabolic concentrator. The white areas in the middle represent the bottom aperture of the concentrator. The hexagonal concentrator has six kite-shaped red colored corners. At paraxial light incidence, a photon that hits a blue area is reflected once before being transmitted through the aperture; for the red areas light is reflected at least once. **Middle.** Perspective and side view of **(d)** a square (4 parabola segments), **(e)** a hexagonal (6 segments) and **(f)** a truncated circular (rotational symmetric) concentrator. **Right.** Top view of **(g)** a square array and **(h)** a hexagonal array. **(i)** Perspective view of a square array made of truncated circular concentrators.

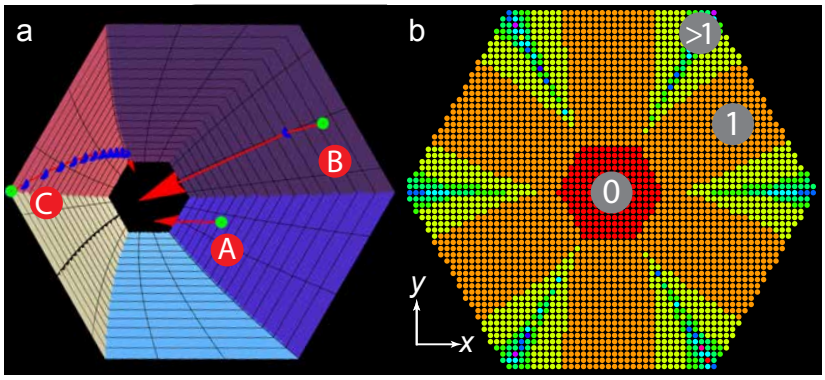

Figure 5.3: **(a)** Propagation of three paraxial rays through a hexagonal concentrator (C=15×). The green dots mark the starting position of the rays; the blue dots represent a reflection at the parabolic surface. Ray A and B are transmitted with zero and one reflection respectively. Ray C shows an extreme example of a ray that is reflected 13 times before it is transmitted. **(b)** Number of reflections per ray before transmittance for 3000 rays of the hexagonal concentrator. The position of each dot corresponds to the initial position (x,y) of each ray. The hue of the dots indicates the number of reflections (ranging from 0-13×): the orange dots hit the concentrator once and the yellow dots twice. The figure is not exactly symmetric due to the meshing of the incoming rays.

It is difficult to determine the transmittance of a hexagonal concentrator analytically and therefore we performed ray tracing. Figure 5.3a shows three different rays at paraxial incidence with a different number of reflections at the concentrator surface. Depending on the origin, a ray hits the hexagonal concentrator a certain number of times. Figure 5.3b indicates the number of reflections for a large number of rays. The average number of reflections for this concentrator with C=15× is 1.43. From this ray tracing the transmittance is approximated by the average transmittance of all rays assuming a wavelength and angle-independent reflection coefficient of 95%.

Fig. 5.4 shows the calculated transmittance of the concentrators as a function of the concentration factor and a fixed reflectance (R). The right inset depicts the average number of reflections at the concentrators before a ray is transmitted. For the circular and square concentrator this average converges to 1 and 2 reflections(s) respectively. Therefore, the transmittance of these concentrators converges to R and R^2 respectively. There is no convergence for the hexagonal concentrator.

Rounded ridges in between neighboring concentrators will inevitably form during fabrication due to e.g. limited fabrication accuracy and limited material strength. We assume that these limitations translate to ridges having a width Δ. The fraction of the total area covered by ridges (f_{ridge}) is shown in Fig. 5.5. Light hitting a rounded ridge is not transmitted to the solar cell but is instead reflected

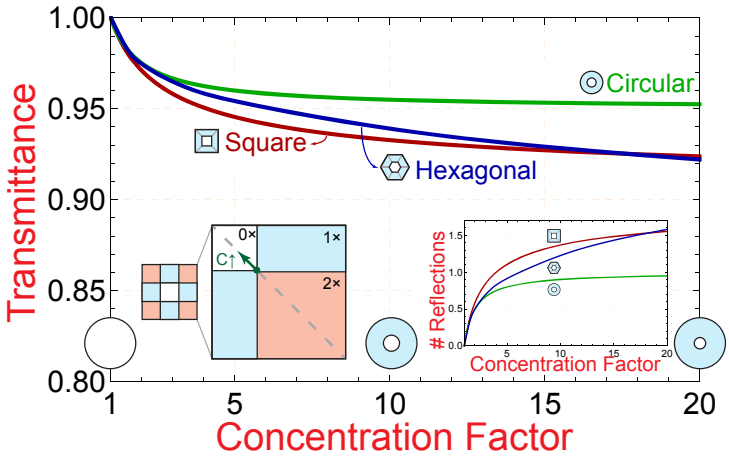

Figure 5.4: Plot of the transmittance of a circular, square and hexagonal concentrator as a function of the concentration factor (C) at a reflectance (R) of the concentrator surface set to 95%. The average number of reflections at the concentrators increases with C. At the bottom of the figure some top views of the circular concentrator are illustrated. The left inset of the square concentrator illustrates how the different areas (of 0×, 1× and 2× reflections) change with C: with increase of C the green joined corner of the four different segments moves towards the left top along the dashed diagonal. The right inset shows the average number of reflections at the concentrator as a function of the concentration factor.

to another direction which limits the transmittance to $1-f_{\text{ridge}}$. It can be seen that a hexagonal array has the lowest ridge fraction. The horizontal dimensions of an individual concentrator in an array should be roughly 200 times larger than the smallest ridge width that can be fabricated to realize a ridge loss below 1%. For the fabrication of a concentrator array, a trade-off has to be made between the ridge area fraction, the material consumption, the height of the array, and the transmittance.

To optimize the performance of the external light trap we use an optical statistical model to determine the key parameters for the performance. We consider a bare solar cell with an absorptance A_{sc} and a concentrator transmittance T_{c}. We assume the light to be scattered such that it is uniformly distributed and the escape probability is given by the area fraction of the aperture. According to the model, the total absorptance in the cell with an external light trap (A_{trap}) is given by:

$$A_{\text{trap}} = T_{\text{c}} \cdot \frac{A_{\text{sc}}}{1-R_{\text{sc}}(1-C^{-1})R_{\text{cage}}}, \tag{5.2}$$

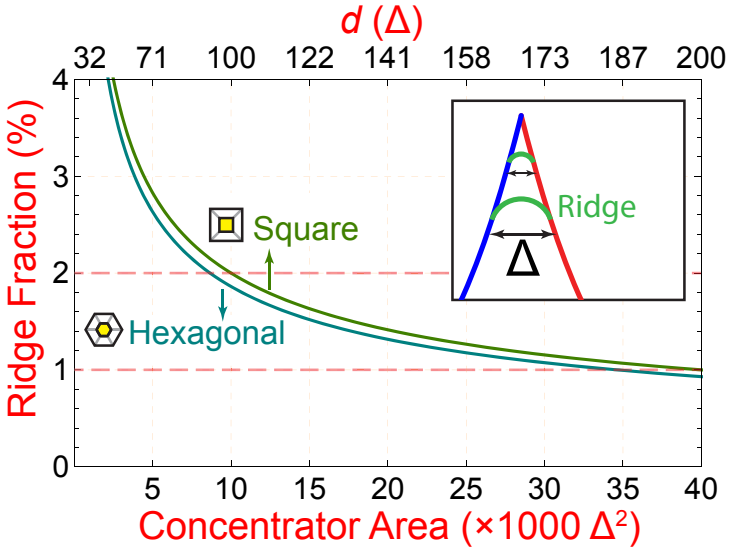

Figure 5.5: The ridge area fraction (f_{ridge}) is plotted as a function of the cross-sectional area of different single concentrators. The inset illustrates a ridge having a width (Δ). At the top of the graph the length of the sides of the square concentrator is shown. For comparison, the area and the dimension ($d=\sqrt{\text{concentrator area}}$) are expressed in units of Δ.

where R_{sc} and R_{cage} are respectively the reflectance of the bare solar cell and the cage. The external quantum efficiency (EQE) of the cell with light trap EQE_{trap} is given by:

$$EQE_{\text{trap}}=A_{\text{trap}}\cdot IQE, \tag{5.3}$$

with IQE the internal quantum efficiency of the cell.

With this statistical model we can derive the equivalent optical thickness of a solar cell with an external light trap. Therefore, we introduce the optical path length enhancement factor (Π_{ext}) which indicates how many times a photon statistically passes the solar cell. In other words, the effective optical thickness is given by Π_{ext} multiplied by the thickness of the cell. From absorption measurement with and without the external light trap applied we can calculate the effective external path length enhancement factor according to (see eq. 4.12 for derivation):

$$\Pi_{\text{ext}}=\frac{\log(1-A_{\text{trap}})}{\log(1-A_{\text{sc}})}=\frac{\log(1-A_{\text{trap}})}{\log(R_{\text{sc}})}. \tag{5.4}$$

In the low absorbing limit ($T_{\text{c}}=R_{\text{cage}}=R_{\text{sc}}=1$) the value of Π_{ext} interestingly equals C. By substituting A_{trap} (from eq. 5.2) into eq. 5.4 it is found that Π_{ext} gradually drops to 1 with decrease of cell reflectance, see also Section 4.2.1.

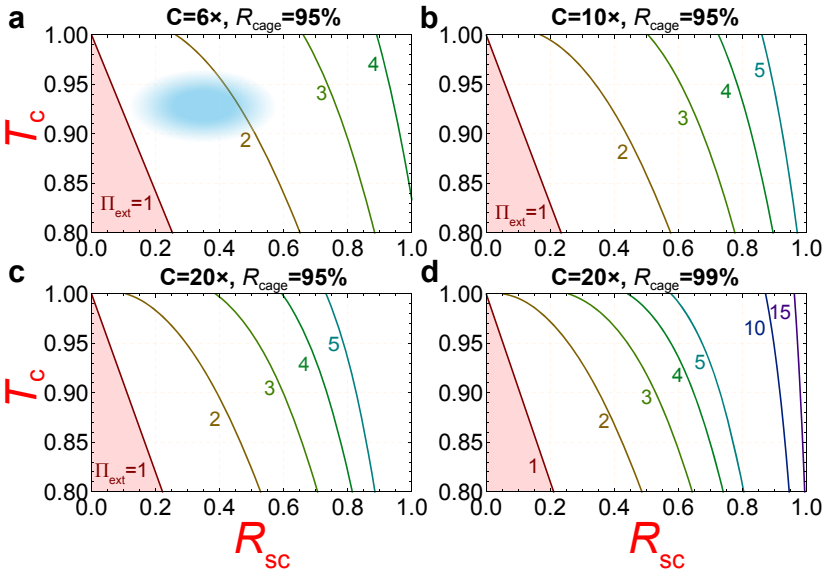

Figure 5.6: Overview of the relation between the path length enhancement factor of an external light trap, the concentrator transmittance (T_c), and the solar cell reflectance (R_{sc}) at several concentration factors. **(a-d)** The solid lines depict the T_c required to obtain the indicated path length enhancement (Π_{ext}) as a function of R_{sc} at different concentration values (C) and cage reflectance (R_{cage}). In the light red area the cell performance is reduced in the presence of the light trap. The blue shaded area in (a) indicates the range in which our experiment is performed.

This theoretical framework enables us to determine the critical design parameters of the external light trap. A reduction of the aperture diameter (which is equivalent to an increase of the concentration factor) results in significantly enhanced light trapping as the escape probability becomes more restricted. However, at a certain aperture diameter, the device performance does not improve any further as its performance will become most significantly limited by other device parameters such as the reflectivity of the cage, see eq. 5.2.

We calculated the achievable path length enhancement factor from the concentrator transmittance, the reflectance of the solar cell and the concentration factor of the external light trap. By reversing this procedure, we determined the concentrator transmittance required for a desired path length enhancement factor.

Fig. 5.6a illustrates the concentrator transmittance at C=6× and R_{cage}=0.95 required to obtain an effective path length enhancement factor of 1× to 4× as a function of the cell reflectance. When $\Pi_{ext}=1$, the gain due to light trapping equals the transmittance losses. The net absorptance is reduced by the light trap when $\Pi_{ext}<1$ as indicated by the light red zone in the parameter space.

For solar cells with a high reflectance the external trap enables the highest degree of light trapping and efficiency improvement, even at a relatively low concentrator transmittance. On the other hand, for solar cells with a low reflectivity a relatively high concentrator transmittance is required for a significant performance boost.

External light trapping is thus of less direct interest for highly absorbing solar cells. In the end, however, external light trapping can enable more efficient solar cell designs. For example, the combination of a thin, non-textured solar cell of high electrical quality and a high optical quality external light trap that has the potential to outperform conventional light trapping methods.[112, 135]

Figure 5.6b and 5.6c show the same scan of the parameter space at C=10× and C=20× which improves the light trapping. At a concentration factor of 20× and a cage reflectance of R_{cage}=0.95 the escape loss via the aperture and the absorptance in the cage are both 5% per cycle. Interestingly, the loss at the concentrator is a one-time event, while the loss at the reflective cage accumulates for each recycle event. The absolute optical loss at the cage depends on the intensity of the (multiple times) reflected beam and is thus related to the reflectivity of the solar cell. The net optical absorptance loss is mainly determined by the dominant loss mechanism. Therefore, only diminishing returns are obtained upon a further increase of the concentration factor: the loss by the cage becomes dominant. For a further improvement it is rewarding to improve the reflectance of the cage as shown for R_{cage}=0.99 in Fig. 5.6d. This reduction of the parasitic cage absorption can be realized by using a highly reflective white paint.[163, 164]

Absolute Absorptance Gain. The path length enhancement factor is a useful and wavelength independent parameter. However, it does not quantify the total absorption enhancement. The Π_{ext} values plotted in Fig. 5.6 are calculated by substituting Eq. 5.2 into Eq. 5.4, which is solved to $T_c(R_{\text{sc}}, C, \Pi_{\text{ext}}, R_{\text{cage}})$. Figure 5.7 shows the corresponding absolute absorptance gain as a function of the cell absorptance for a concentration factor of C=6× and a transmittance and cage reflectivity of both 95%. At very high absorptance values the absolute gain can be negative as the loss in the concentrator is larger than the gain due to light trapping.

5.2.1 Transmittance of the Concentrators

For a circular parabolic concentrator with a concentration factor of C, a fraction $\frac{1}{c}$ of the light is transmitted without being reflected. The remaining part $(1-\frac{1}{c})$ of the light is reflected just once. The average transmittance of the circular concentrator thereby converges to the reflectivity of the concentrator area (R).

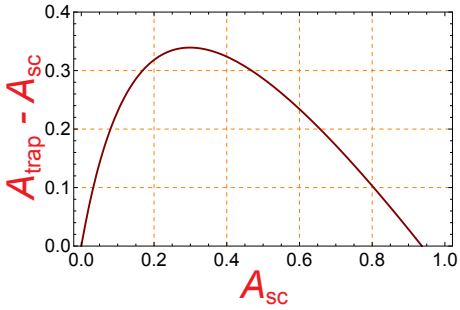

Figure 5.7: Plot of the absolute absorptance gain ($A_{trap}-A_{sc}$) as a function of the cell absorptance for a C=6× concentrator assuming $T_C=R_{sc}$=0.95. The absolute gain is highest when the cell absorptance is roughly 10-60% (equivalent to a reflectance of 40-90%).

The average transmittance of a square concentrator is:

$$T_{square}(C,R)=\overbrace{\frac{1}{C}}^{\text{Aperture}}+\overbrace{R\cdot 2(\sqrt{\frac{1}{C}}\cdot(1-\sqrt{\frac{1}{C}}))}^{\text{4 side segments}}+\overbrace{R^2\cdot(1-\sqrt{\frac{1}{C}})^2}^{\text{4 corner segments}}, \tag{5.5}$$

where $\frac{1}{C}$ is the area fraction of the aperture. The last term increases with increase of C and thereby T_{square} converges to R^2.

The average transmittance of a hexagonal concentrator depends on several design parameters like the truncation height. Figure 5.8 shows the transmittance of four hexagonal concentrators with a different concentration factor. As seen from top, there are six areas at which light is reflected only once. In the six intermediate corners segments the light is reflected at least twice depending on the incidence spot, concentration factor and the parabolic shape. For each image around 3000 rays were traced to obtain a reasonably low numerical error. With increase of the concentration factor the number of reflections at the concentrator increases as well resulting in a lower averaged transmittance.

5.2.2 Ridge Fraction of an Array

The ridge area scales linearly with both the ridge width and the characteristic concentrator dimension e.g. the diameter or the length (l). The total concentrator area scales as l^2. The ridge area fraction (f_{ridge}) does not depend on the concentration factor and decreases with the ridge width Δ according to:

$$f_{ridge}=\frac{A_{ridge}}{A_{concentrator}}\propto\frac{\Delta}{l}. \tag{5.6}$$

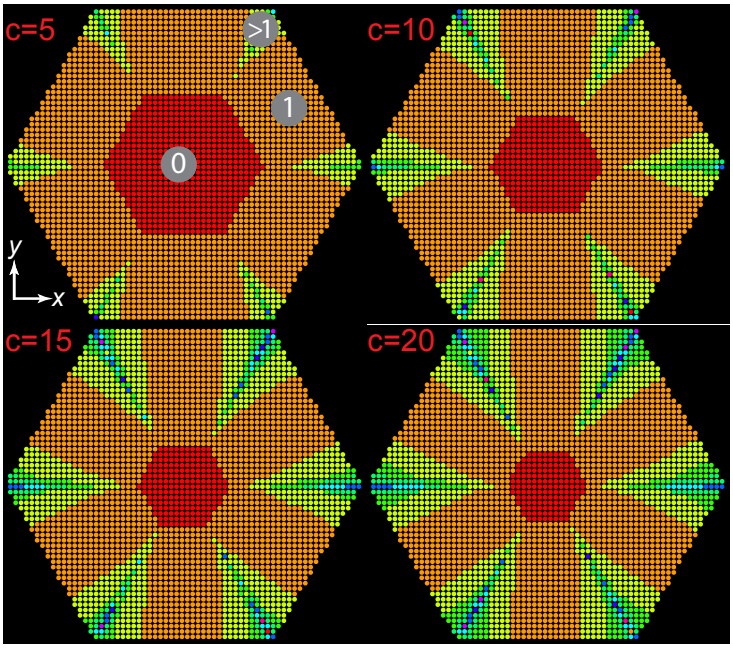

Figure 5.8: Illustration of the number of reflections for different areas of the hexagonal concentrator as seen from top. The position of each dot corresponds to the initial position (x,y) of each ray. In the middle light travels unhindered through the hexagonal aperture. At the six orange marked areas light hits the concentrator once. For the more or less kite-shaped intermediate corners a photon hits the concentrator at least twice. For a very small number of rays that hit the concentrator very close to a boundary of two segments the number of reflections can be up to 15× (for C=20×).

In order to enhance the transmittance, it is thus rewarding to make l relatively large compared to Δ. (See Fig. 5.5 for the calculated ridge fraction of a trough-shaped, square and hexagonal infinitely large array.)

The ridge width of the 3D-printed concentrator arrays is around 0.4 mm. A ridge fraction below 1% requires horizontal concentrator dimensions of at least 80 mm. Other fabrication techniques, like injection molding, can achieve much higher accuracy which enables smaller designs with less optical losses.

The sharp edge at the bottom of the concentrator will also become rounded in most fabrication processes. This will slightly affect the transmittance of the concentrator, but this effect is expected to be much smaller than that of the ridge between the concentrators.

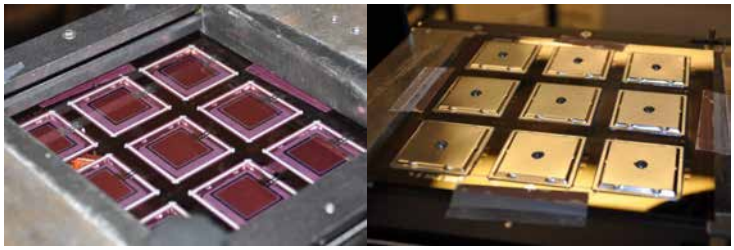

Figure 5.9: Photo of **(a)** the front and **(b)** the back of nine organic solar cells.

5.2.3 Fabrication Details of the Organic Solar Cell

Soda-lime glass substrates (152×152 mm^2) pre-patterned with nine ITO (22×23 mm^2) pixels were cleaned as described elsewhere.[165] PEDOT:PSS (Clevios^{TM} P VP AI4083) was purchased (from Heraeus Clevios GmbH, Leverkusen, Germany) and filtered before use. P3HT (Plexcore® OS 2100) was purchased from Sigma-Aldrich and used as received. PCBM was purchased from Solenne B.V., the Netherlands and also used as received. P3HT:PCBM blends were prepared by dissolving P3HT and PCBM in 1,2-dichlorobenzene at a 1:1 ratio by weight at 80 °C. P3HT:PCBM solutions were filtered and allowed to cool down to room temperature prior to use.

The organic solar cells with an active area of 19×20.4 mm^2 were prepared as follows. A thin layer of PEDOT:PSS (100 nm) was spin-coated on the substrates and annealed for 6 minutes at 130 °C. P3HT:PCBM was spin-coated on the PEDOT:PSS-covered substrates and dried at room temperature, resulting in thin layers with an average thickness of 90 nm. The substrates were transferred to a nitrogen atmosphere, and subsequently annealed for 10 minutes at 130 °C. Cathodes (LiF/Al) were applied by thermal evaporation of 1 nm lithium fluoride followed by 100 nm aluminum under vacuum conditions ($P < 5\times10^{-7}$ mbar). The separate cells were encapsulated with a metal lid to prevent degradation of the cathode, see Fig. 5.9.

5.2.4 Design Specifications of the Light Trap

Cage. A square cage, shown in Fig. 5.10, was fabricated in the same way as the concentrators. For the measurements with a light trap, the cage is first aligned on top of the solar cell. Subsequently one of the concentrators is aligned on top of the cage. The cross-sectional area of the cage is equal to that of the top of the concentrator. The height of the cage is 4 mm. Due to the vertical spacing of the cage the light diverges away from the central axis before it penetrates into the solar cell. After its first reflection the non-absorbed (specular reflected) light is reflected back to the solar cell. It is trapped in the cage until it is being absorbed in the solar cell, cage or escapes via the aperture.

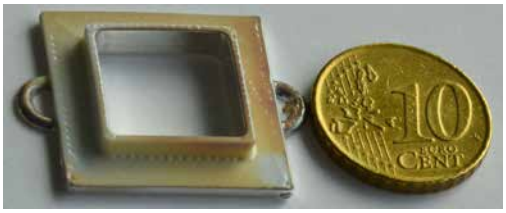

Figure 5.10: Photo of 3D-printed cage with a 10 eurocent coin for reference.

Concentrator. The fabricated concentrators have a concentration factor of C=6×. Light would thereby travel effectively 6× through the solar cell in the low absorbing limit. The sides of the parabola are shifted inwards by 0.35 mm to enhance the concentration factor and limit the height of the concentrator, see also page 53. The parabolic shapes have a focal distance of 0.7 mm.

5.3 Results and Discussion

Figure 5.11 shows the fabricated concentrators with a concentration factor of C=6×, which experimentally showed both high transmittance and thereby a decent absorptance enhancement. They were 3D-printed, chemically polished with acetone vapor and metalized. The cage and concentrators were coated with silver, which is also used in optical telescopes because of its high reflectance.[166] The flat, reflective bottom side of the concentrator forms the top of the cage which reflects the light back to the solar cell. The light traps were placed on top of an organic solar cell which is illustrated in Fig. 5.12a.

The effectiveness of the light trap is largely determined by the concentrator transmittance, which in our experiment is limited by the reflectance of the sputter coated silver. Figure 5.12b shows the reflectance of silver (R_{silver}) measured at normal incidence. Also shown is R^2_{silver} which represents the two reflection at the corner areas of the square concentrator. Close to the plasma wavelength (λ∼310 nm) the parasitic absorptance in the silver is extremely high, resulting in a low concentrator transmittance.[167] Because of the higher average number of reflections at the square concentrator compared to the circular concentrator, a significant transmittance difference is expected between both concentrators for wavelengths shorter than ∼500 nm. At longer wavelengths the silver reflectance gradually improves to 95%.

In addition to the transmittance of the concentrator the reflectance of the solar cell affects the light trap performance. Figure 5.12c shows the reflectance, absorptance, *EQE* and *IQE* of the organic solar cell. Most of the light is absorbed in the poly(3-hexylthiophene-2,5-diyl) (P3HT):phenyl-C61-butyric acid methyl ester (PCBM) blended layer. At wavelengths of ∼300 nm PCBM absorbs strongly,

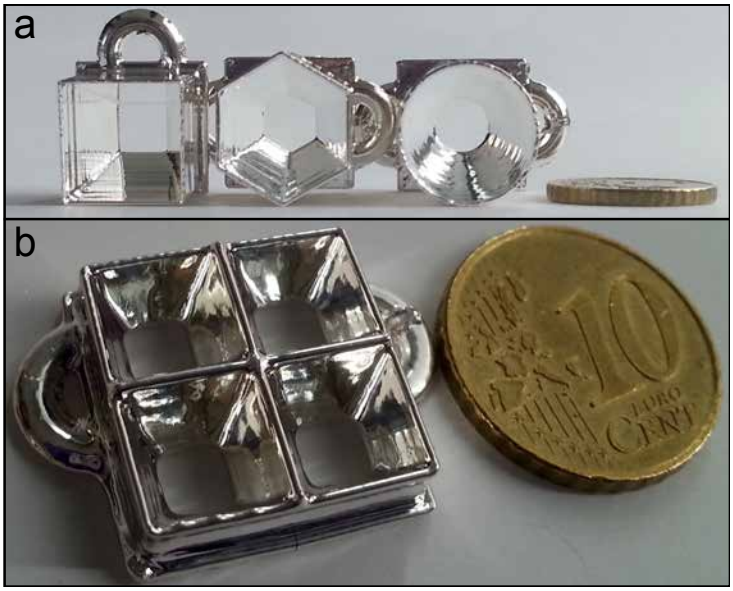

Figure 5.11: **(a)** Silver coated square, hexagonal and circular parabolic concentrator. For reference a 10 eurocent coin is shown on the right. **(b)** A 3D-printed 2×2 square array of concentrators that can be used as a top part of an external light trap. The coin is shown as reference.

while P3HT peaks at around 500 nm.[168] In the wavelength range of 300-600 nm there is significant potential for recycling as the reflectance varies from 5 to 55%.

The *EQE* curves of the solar cell with the external light traps on top are shown in Fig. 5.13a-d. For each concentrator three *EQE* measurements were performed, their spread is indicated by the colored areas. The light trap was re-aligned for each measurement which translates to this spread of a few percent. For the hexagonal and the circular concentrators an improvement at almost all wavelengths > 380 nm is observed. The *IQE* and R_{sc} are relatively high at wavelengths around 400 and 620 nm, this combination translates to a high absolute gain of the *EQE* at these wavelengths. The *EQE* of the hexagonal light trap improved by $9\%_{abs}$ at 620 nm and by $69\%_{rel}$ at 660 nm. The circular concentrator shows the best performance below ∼500 nm because the absorptance loss in the silver of this concentrator is relatively small as there is only 1 reflection. The hexagonal and circular concentrator show the best performance: the implied short circuit current improved from 6.5 to 7.3 mA/cm^2.

From the difference in *EQE* of the cell with and without light trap the external path length enhancement factor was calculated using eq. 5.4, see Fig. 5.13e. At short wavelengths (λ<400 nm) the external path length enhancement is less than 1 due to the relative low concentrator transmittance. At 400 nm the transmittance

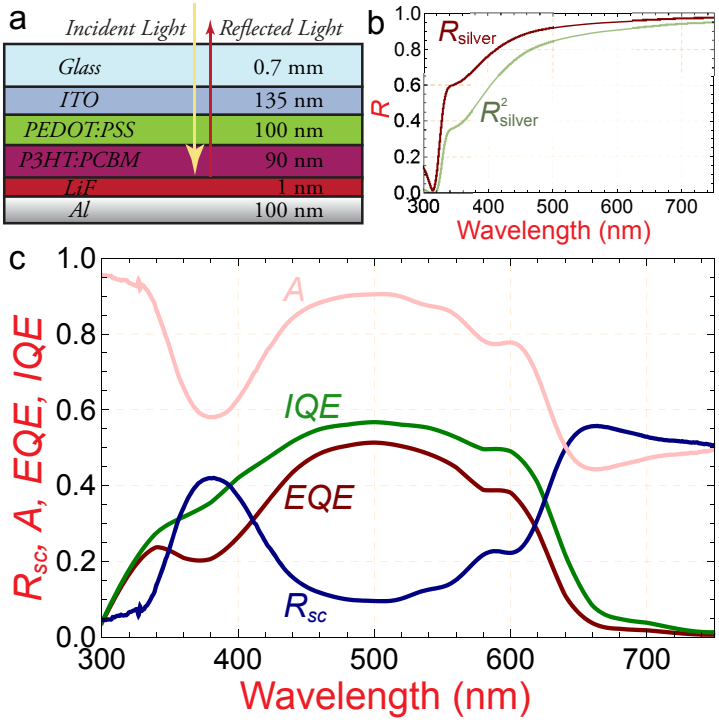

Figure 5.12: **(a)** Illustration of the layer stack of the organic solar cell. **(b)** Reflectance of silver at normal incidence for one and two consecutive reflections (R_{silver} and R^2_{silver}). **(c)** Plot of the experimentally determined absorptance (A), the reflectance (R_{sc}), the external quantum efficiency (*EQE*), and the internal quantum efficiency ($IQE=\frac{EQE}{A}$) of the organic solar cell without external light trap.

losses are roughly compensated by the gain due to light trapping. At 500 nm the cell reflectance is low, which slightly reduces the gain of light trapping and therefore Π_{ext} is ∼1. In the long wavelength regime (λ>600 nm) the optical path length is effectively doubled.

The path length enhancements caused by the different concentrators do not all follow the exact same trend. This is partly caused by the different optical paths of the light within the cage due to the different concentrator shapes. Furthermore, there are small variations in the smoothness and the reflectance of the bottom side of the concentrator (which forms the top reflector of the cage). Light is reflected only once in the circular concentrator, therefore it has a higher transmittance and a higher Π_{ext} at short wavelengths than the square and hexagonal concentrator.

We made a fit to the experimental *EQE* data by inserting the parameters of the solar cell and the concentrator into our optical model (see dashed black lines in Fig. 5.13a-d). The formula for the fit is obtained by substituting eq. 5.2 into eq. 5.3

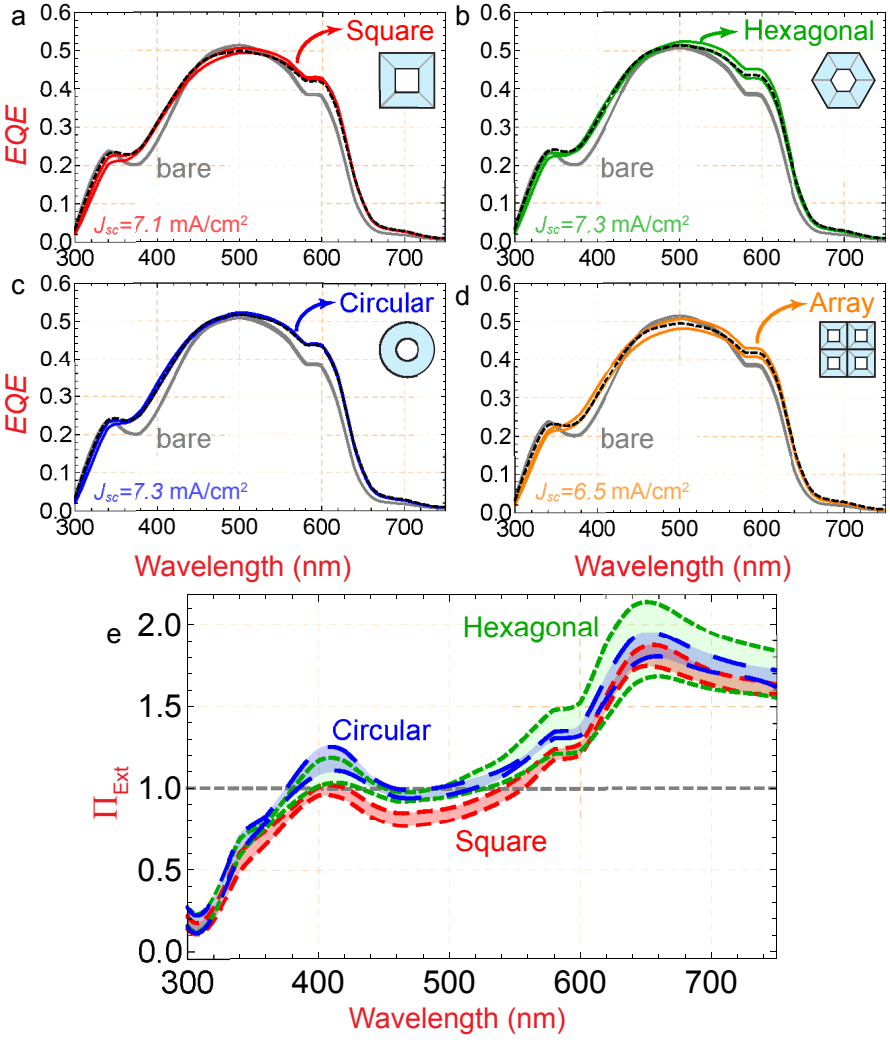

Figure 5.13: The external quantum efficiency of the bare solar cell and the cell combined with an external light trap with **(a)** the square concentrator, **(b)** hexagonal concentrator, **(c)** circular concentrator and **(d)** an individual concentrator in the 2x2 square array. The gray line shows the solar cell response for the cell without a light trap (bare). For each concentrator a best fit to the averaged experimental data is shown (black dashed line). The *EQE* of the bare cell corresponds to an implied short circuit current (J_{sc}) of 6.5 mA/cm^2. **(e)** Illustrates the corresponding path length enhancement factor for the external light traps. The vertical line at Π_{Ext}=1 is shown as reference.

from which $EQE_{\text{External light trap}}(T_C, R_{sc}, C, R_{cage}, IQE, \lambda)$ is derived. The concentrator transmittance (T_C) was set variable. There is an excellent agreement between the fitted curves and the experimental *EQE* data.

When the light trap is applied, there is a range of angles of incidence (*AOI*) at the solar cell, while without the light trap the light comes in at normal incidence. In order to keep the optical model universal the *IQE* is assumed to be independent of the *AOI* and to be the same for the cell with and without external light trap. However, depending on the type of solar cell, this non-normal *AOI* can have several effects on the cell performance: an increased *AOI* can reduce the *IQE* especially at short wavelengths due to the relative high absorption in electrically dead top layers[149, 169] as was also observed in chapter 4. For this reason we presume that the experimental data at short wavelengths (λ<350 nm) is a few percent lower than the fit.

The theoretical and measured average transmittance of the fabricated concentrators (C=6×) are listed in Table 5.1. At least 4% of the light is lost due to the absorptance in the concentrator. The theoretical transmittance of the concentrator is calculated at a reflectance of 95% at the concentrator surface. The transmittance of the square array is significantly lower than the single square concentrator due to the ridge fraction.

	Theoretical T_C	Fitted T_C
Square	94%	89-91%
Hexagonal	94%	92-95%
Circular	96%	93-94%
Square Array	86%	80-84%

Table 5.1: Theoretical and fitted concentrator transmittance (T_C) for several concentrators

The theoretical and experimental values of T_C differ by a few percent for which we can indicate several causes. First, the 3D-printing process results in small contour errors with respect to the intended 3D-model. Secondly, the vapor smoothing of the concentrator does not lead to a perfectly smooth surface. These errors are expected to be most severe at the sharp corners of the square and hexagonal concentrators.

5.4 Conclusions

We demonstrated that external light trapping is of interest for all solar cells as its effectiveness does not depend on the refractive index or texture of the solar cell and it is easy to apply. As the device is an add-on, it guarantees that there is no negative impact on the electrical properties of the solar cell. We proposed several

possible designs for an array of concentrators that can be integrated in an external light trap that covers a large solar cell area. The use of 3D-printed light traps with a square, hexagonal, or circular parabolic concentrator resulted in a significantly improved *EQE* of an organic solar cell. Excellent agreement was found between the fit based on our model and the experimental data, which shows the predictive power of the model. Moreover, an effective path length enhancement factor larger than 2 is observed while the *EQE* improved by up to 69%$_{\text{rel}}$, corresponding to an increase of the short circuit current of 13%. This indicates that external light trapping is an interesting alternative or supplement for internal light trapping.

To determine the critical design parameters of the light trap we calculated the achievable path length enhancement as a function of several parameters of the light trap and the solar cell. The transmittance loss in the concentrator has to be fully compensated by light trapping, and therefore a high concentrator transmittance is essential for a high device performance. For further optimization we indicated how the achievable concentrator transmittance depends on the concentration factor, fabrication accuracy, cage reflectivity, concentrator shape and concentrator size. Our theoretical analysis shows that a hexagonal array of circular concentrators has the best optical performance.

High fabrication accuracy is essential to realize a high transmittance and performance. Once a sufficiently high concentrator transmittance has been realized the concentration factor and the cage reflectance become more critical. We thus demonstrated how an external light trap made from an array of concentrators can effective improve the efficiency of solar cells and we showed a clear pathway for further optimization.

Chapter 6

Universal External Light Trap for Photovoltaic Modules

Summary. The reflection of incident sunlight by photovoltaic modules prevents them from reaching their full energy conversion potential. In this chapter, we present a universal external light trap that tackles this reflection loss. A unique feature of external light traps is their capability to simultaneously recycle various broadband sources of reflection on the module level, such as the reflection from the metal front grid, the front interfaces, the reflective backside of the cell, and the white back sheet in between the cells. The reflected light is recycled in a cage between the solar cell and a mirror above the solar cell. A concentrator funnels the light into this cage through a small aperture in the mirror. A 64% reflectance reduction of a bare crystalline silicon (c-Si) solar cell is demonstrated. In contrast to conventional light trapping methods, external light trapping does not induce any damage to the active cell material. Moreover, this is a universally applicable technology that enables the use of thin and planar solar cells of superior electrical quality that were so far hindered by limited optical absorption. We milled a series of prototype millimeter-scale external metal light traps and applied these on a c-Si solar cell. We determined the concentrator transmittance and analyzed the effect of both the concentration factor and cage height on the absorptance and spatial intensity distribution on the surface of the solar cell. This relatively simple and comprehensive light management solution is a promising candidate for highly efficient solar modules.

6.1 Introduction

All solar cell technologies exhibit optical reflection losses that limit the power conversion efficiency. For example, industrial crystalline silicon (c-Si) based solar modules are hindered by reflection from the metal front grid (fingers and busbars), front interfaces, and incomplete fill factor of the module area ("optically dead area"). Long wavelengths are reflected out of the module due imperfect absorption. Highly efficient solar modules thus require a general solution that simultaneously recycles the light from these four broadband reflection sources on the module level.

The surface coverage by the grid of industrial modules is typically 5-10%.[97, 170, 171] The optical absorption of c-Si modules is generally enhanced by texturing the cell surface, which results in both improved light incoupling and internal light trapping. However, even for textured cells, the reflection at normal incidence from the front interfaces (air-glass-ethylene-vinyl acetate (EVA)-cell) ranges from 5.5%-6% for encapsulated textured mono-c-Si (mono-Si) modules;[172] ∼6-13% for multi-c-Si (multi-Si) modules;[153, 173] and less than 6% for heterojunction (HIT^{TM}) cells.[170] For larger angles of incidence, the reflectance is significantly larger.[173, 174] Around 2-6% percent of the light escapes the cell due to imperfect absorption,[112, 170] mainly caused by wavelengths near the band-edge. Finally, ∼2-10% of the total module area is covered by an inactive back-sheet.[171, 175] For white back-sheets, around 80% of the reflected light escapes from the module.[176] Although the sum of these four reflection losses varies by manufacturer, typically more than 13% of the potential short circuit current is lost due to reflection.[177]

Generally, the optical absorptance of a cell is enhanced by increasing the cell thickness and by texturization of the front surface.[111] However, increasing the thickness results in an increase of Auger and Shockley-Read-Hall recombination.[178] Texturing results in a larger surface area and thereby higher surface recombination.[152, 179, 180] The probability for charge carriers to recombine can therefore be reduced by using a thin and planar c-Si solar cell that benefit from a high V_{oc}. Theoretically, it has been shown that thin c-Si cells with angular restriction can have a V_{oc} close to 800 mV.[135, 181] Over the past decades, the thickness of commercial c-Si solar cells has been reduced from roughly 300 μm to 175 μm. It is expected that the average wafer thickness will drop further to 100 μm in 2024.[11] This trend is driven by significant advantages of thin cells, such as their low material cost, weight, and low bulk recombination. Moreover, once the cell thickness drops below 50 μm, texturing cannot easily be applied as the texture dimensions become similar to the cell thickness. Several companies are already producing such thin wafers by kerfless methods.[182, 183] Due to their thin absorber, these cells require even more efficient light trapping methods than today's available options.

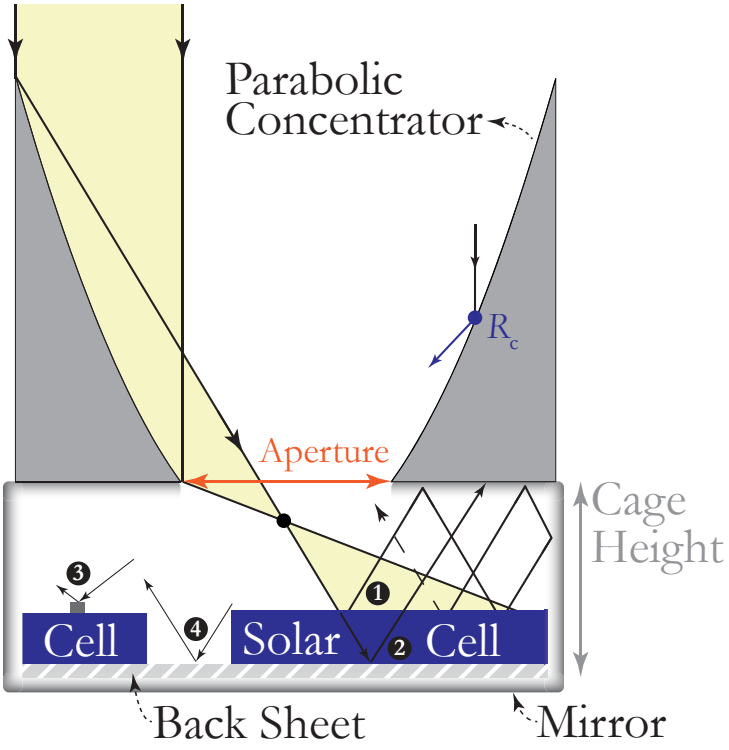

Figure 6.1: Illustration of a cross section of an external light trap on top of a specularly reflective solar cell. Light is focused through an aperture and is trapped within a cage. The reflectivity of the concentrator (R_c) and that of the cage are important parameters of the light trap. The cage height determines the optical path within the cage and the intensity distribution on the solar cell. Light reflecting from the front interfaces (❶), back interfaces (❷), metal grid (❸), and white back sheet (❹) is recycled.

There exist many light trapping solutions that resolve one of the four aforementioned reflection losses. For example, prismatic covers, SmartWire,[184] contact cloaking,[185] and interdigitated back contact technologies[186] have been used to reduce or eliminate reflection loss from the front contacts. One can improve the absorption within the c-Si by limiting the escape probability of photons inside the cell using angular restriction. This restriction can be realized by multilayer stacks and Rugate filters.[122, 134, 187, 188] However, these solutions have in common that they only resolve one of the four indicated reflection sources and/or are limited to narrowband improvements as a result of their resonant nature. Moreover, many of these solutions suffer from significant parasitic absorptance.

Here, we demonstrate the effectiveness of a universal external light trap for c-Si solar modules. The key concept of external light trapping is illustrated in figure 6.1.

Incident sunlight is focused through a small aperture by a parabolic mirror. The light enters a cage and diverges before it reaches the cell. Most of the light that reflects from the solar module is retro-reflected and recycled in this optical cavity. External light trapping addresses the four indicated reflection losses at once. At the same time, the trap enables the use of thinner cells with higher power conversion efficiency[112, 133, 141, 189] and can supplement or take over the anti-reflection role of the front texture and enable planar front textures. Most internal light trapping solutions behave antagonistic: while they improve the optical properties they deteriorate the electrical properties. Interestingly, the external light trapping concept decouples the optical properties from the electronic properties. Thereby, it is able to improve the absorptance without inducing any damage to the active cell material.

The conceptual idea of external light trapping recently draws significant attention due to its advantages.[93, 94, 123, 141, 142] As the trap is universally applicable, it is of special interest for multi-Si, because multi-Si cannot be textured as effectively as mono-Si.[97] The external light trap works over the full solar spectrum and can be integrated industrially at low costs. Moreover, by external light trapping one can surpass the $4n^2$ path length enhancement limit as the trap acts as a multiplier of the internal path length enhancement (see eq. 4.7). External light trapping is based on relatively simple reflective geometric optics and thereby virtually wavelength independent. Furthermore, external light trapping could be of interest for a wide variety of other solar applications, such as luminescent solar concentrators,[190] concentrated solar and up-conversion.[191]

We stress that the use of a concentrator in an external light trap differs from its use in concentrated photovoltaics (CPV). In CPV the photon flux is increased to allow a reduction of the cell area, while for external light trapping the goal is to improve the cell absorptance. Interestingly, CPV and external light trapping light can be combined by making the cell area larger than the aperture area but smaller than the concentrator opening to realize both concentration and light trapping (see also page 64).

In the previous chapters we demonstrated the effectiveness of 3D-printed external light traps for thin film nanocrystalline Si and organic solar cells. In this chapter, we fabricated several millimeter-scale concentrators using an industrial milling process. This method offers higher contour accuracy and the strong metal parts can be used as a mold for cheap, large area fabrication of thermoplastic concentrators. Similar designs have been fabricated on micro-scale,[117] but for commercial application a millimeter scale design is expected to have lower fabrication costs and to yield higher performance as shown in chapter 5. We analyze several fabrication aspects that determine the transmittance of the concentrator of the external light trap.

We demonstrate a 64% reflectance reduction of a bare c-Si solar cell due to an

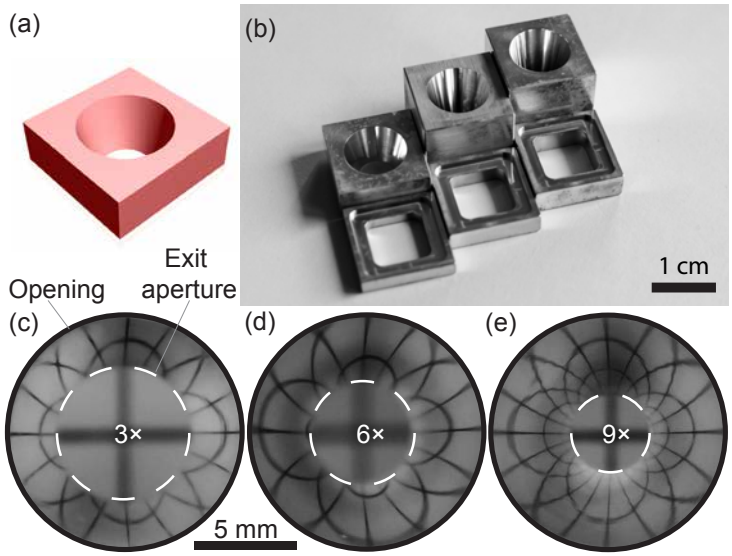

Figure 6.2: **(a)** Design of the 3× concentrator. **(b)** Photo of the milled concentrators and the cages. The milled concentrators have a concentration factor of 3×, 6×, and 9×. The cages make a vertical spacing between the cell and the reflective bottom of the concentrator of 2, 3, and 4 mm. (**c-e**) Photos of the top view of the concentrators with different concentration factor: **(c)** C=3×, **(d)** C=6×, and **(e)** C=9×. The concentrators are placed ∼3 cm from a sheet of squared graph paper. The camera is focused on the concentrator surface. The center (white dashed ring) shows a direct view of the squared graph paper (out of focus) through the aperture. Outside the center, a distorted image is formed of the straight lines of the graph paper due to the curvature of the concentrator.

external light trap. The performance of the concentrator is analyzed by comparing the theoretical and experimental polarization dependent transmittance maps. Previous optical analytic external light trapping models where based on complete randomization of light within the cage.[94, 189, 192] We demonstrate the accuracy of this analytic model for our external light trap by ray tracing. Also, we determine the effect of both the geometric concentration factor and cage height on the total cell absorptance and spatial intensity distribution on the cell. We show that the use of a tall cage results in sufficiently homogeneous cell illumination.

6.2 Materials and Methods

Fabricated Light Traps. We fabricated concentrators with different concentration factors (3–9×) and cages with different heights (1–4 mm) out of aluminum using an industrial milling machine. To improve the reflectivity, the parts were thoroughly

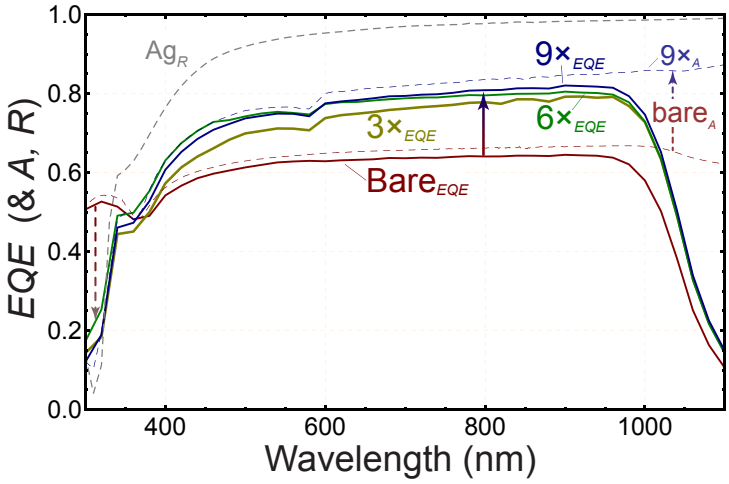

Figure 6.3: Plot of the *EQE* for various trap configurations. The red solid line shows the *EQE* of the bare, flat, and untextured c-Si solar cell. The yellow, green, and blue solid line are the best measured *EQE* of the c-Si cell with a cage height of 4 mm external light traps with respectively C=3, 6, and 9×. The red dashed line shows the measured absorptance of the bare cell (bare$_A$). The blue dashed line shows the calculated absorptance of the cell with the 9× concentrator applied. The gray dashed line is the measured reflectance of polished silver coated aluminum.

cleaned and sputter-coated with a 400 nm thick layer of silver. Figure 6.2 shows three milled concentrators with different geometric concentration factor (C) and three cages with a different height.

Solar Cell Specifications. We use a 1 cm^2 c-Si Hamamatsu photodiode as a model system to study the effect of concentration factor and cage height. The surface of the diode is untextured and does not have an anti-reflection coating (ARC). The reflection of this c-Si photodiode is higher than that of solar modules, but in the near-infrared it resembles that of a thin c-Si cell with an ARC. As the external light trap is indifferent with respect to the origin of the reflected light, this photodiode is a reasonable model for a module with thin c-Si solar cells; we refer to it as the solar cell. See Supplementary Section 6.6.3 for more background information.

6.3 Results and Discussion

6.3.1 *EQE* for Several Concentration Factors

The spectral response of the cell was measured for different trap configurations. Figure 6.3 shows the absorptance (A=1−R, dashed) and the external quantum

efficiency (*EQE*, solid) of the bare solar cell and of the cell with light traps with different concentration factors (3–9×).

Overall, the bare cell has an *EQE* (bare$_{EQE}$) of ∼58-64%, and an absorptance (bare$_A$) of ∼60-66%. The dip in the absorptance of the bare cell around ∼380 nm is a result of strong reflection from the c-Si front interface. For wavelengths longer than 950 nm, bare$_{EQE}$ drops significantly as there is only little absorption in the c-Si close to the band gap (λ∼1120 nm). Due to the parasitically absorbing back contact, most of the light that goes into the cell is absorbed. Therefore, bare$_A$ reduces only slightly in this wavelength range.

To measure the spectral response of the cell in the presence of a light trap, a 4 mm tall cage was placed on top of the solar cell, onto which a concentrator with different concentration factors (C=3×, 6×, or 9×) was mounted. It was found that the optical transmittance of each concentrator varies significantly with the location of the incident (collimated) beam (diameter ∼2.5 mm), as we show later. The reported *EQE* are the best measured data of the same cell (with and without light trap). A significant broadband enhancement of the *EQE* is observed for all configurations of the light trap. The trap with a 6× and 9× concentrator show higher improvement than the trap with a 3× concentrator due to enhanced external light trapping. The analytical model and the simulations explain how the concentration factor affects the *EQE* and absorptance.

The absorptance of a solar cell with an external light trap on top (A_t) cannot be easily measured. However, it can be extracted from the *EQE* and the internal quantum efficiency (IQE=$\frac{EQE_\mathrm{bare}}{A_\mathrm{bare}}$) according to:

$$A_\mathrm{t} = \frac{EQE_\mathrm{trap}}{IQE} = \frac{EQE_\mathrm{trap}}{EQE_\mathrm{bare}} \cdot A_\mathrm{bare}. \tag{6.1}$$

Using this formula we calculated the absorptance of the 9× concentrator (9×$_A$, dashed blue line). It can be seen that the overall absorptance improved by almost 20%$_\mathrm{abs}$.

The transmittance of a concentrator is linearly related to the performance of the cell in the presence of the external light trap and is determined by the reflectivity of the silver surface (Ag$_R$). The gray dashed curve shows the measured reflectivity of a flat, polished part of silver over-coated aluminum. The strong decrease in the *EQE* around ∼310 nm (see arrow) is due to parasitic absorptance in the silver and this absorption loss gradually decreases towards longer wavelengths. This corresponds to our observations in Section 5.3 and does not represent a large absolute loss since there is only a small number of photons in this range of the solar spectrum.

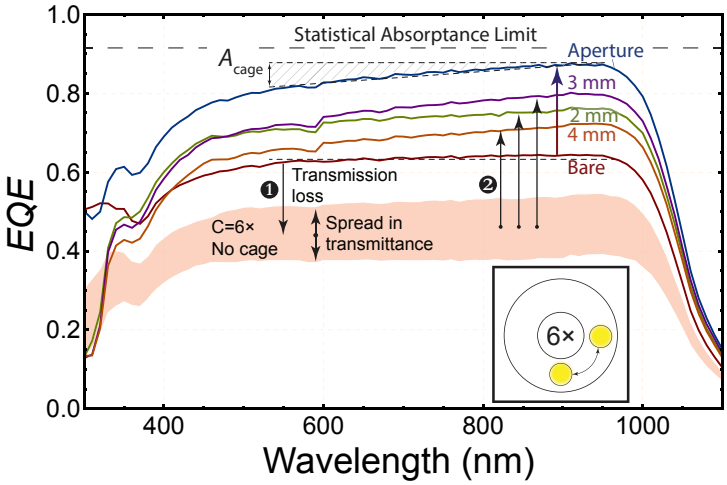

Figure 6.4: Plot of the *EQE* for different cage heights measured using the C=6× concentrator. The red line shows the *EQE* of the bare solar cell. The light-red shaded area indicates the drop in *EQE* when the concentrator is placed directly on top of the cell due to parasitic absorption in the concentrator (see ❶). Integration of a cage below the concentrator results in external light trapping. Thereby, the *EQE* of cell with external light trap exceeds the *EQE* of the bare cell (see ❷). The upper blue line (EQE_{aperture}) shows the *EQE* for a slightly tilted beam of light that passed the aperture without hitting the concentrator, for a cage height of 4 mm. EQE_{aperture} closely approximates the black dashed statistical absorptance limit. The inset shows the top view of the concentrator and roughly indicates the size of the monochromatic beam in yellow.

6.3.2 *EQE* for Several Cage Heights

In the external light trap a fraction of the reflected photons is reflected back to the solar cell by the reflective bottom of the concentrator. The size of this fraction is partly determined by the cage height. When the concentrator is placed directly on top of the concentrator (so there is no cage) there is no light trapping. Due to the parasitic absorptance by the concentrator the absorptance in the cell drops. Upon insertion of a (sufficiently tall) cage, a fraction of the reflected light is recycled. Therefore, by changing the cage height, the optical recycling efficiency is altered. We measured the cell performance for several trap configurations with different cage height (Fig. 6.4).

First, a concentrator with C=6× is placed directly above the solar cell. The *EQE* drops due to the non-unity transmittance of the concentrator as a result of parasitic absorptance in the silver. There is a spread in the data due to the spatial variation in the transmittance of the concentrator.

Light Trapping Gain. The *EQE* improves significantly when a cage is inserted between the concentrator and the solar cell. The best measured *EQE* for a 2, 3,

and 4 mm high cage are shown in green, purple, and orange respectively. A broadband *EQE* enhancement over the entire spectral range is observed. The *EQE* decreased for wavelengths shorter than ∼350 nm (as was also observed in Fig 6.3). Due to the strong variations in the transmittance of the concentrator for different positions of the illumination spot, we cannot determine a clear relation between the *EQE* and the cage height.

Potential. To indicate the potential improvement of the *EQE* when the concentrator has unity transmittance, we positioned the beam under a small angle, directly through the aperture without the light hitting the concentrator. The corresponding *EQE* is shown as the blue curve. This illustrates the potential for an ultimate external light trap. The *EQE* improved from ∼64% to ∼88% (=+23%$_{abs}$), see Fig. 6.4. The reflectance of the cell was reduced from ∼36% to 12%. The observed reflectance reduction is very close to the statistical absorptance limit of 8.6% as was calculated using our statistical model (eq. 6.3). A similar reduction in reflectance can be expected for a thin, planar cell with an anti-reflection coating.

Comparing EQE_{bare} and $EQE_{aperture}$, it is notable that EQE_{bare} has a horizontal plateau, while $EQE_{aperture}$ has a slope (see both dashed lines). For a perfect light trap (in which all wavelengths are retro-reflected with equal reflectivity) the *EQE* improvement should not be wavelength dependent. The small improvement from ∼600 nm onwards is due to *decreasing* parasitic absorptance (with increase of wavelength) in the silver coating of the cage (indicated A_{cage}).

6.3.3 The Transmittance of the Parabolic Concentrators

The performance of an external light trap is proportional to the transmittance of the concentrator.[94] We measured the transmittance of the concentrators and compared it to the theoretical transmittance calculated from the optical constants of silver. The optical constants (n and κ) of a freshly sputtered silver layer on a flat glass plate were determined by spectroscopic ellipsometry. We calculated the spectral reflectance using the Fresnel equations with the measured n and κ. Figure 6.5a shows the calculated reflectance at a wavelength of 532 nm as a function the angle of incidence (θ_i) for different polarizations. The reflectance of such a flat layer is ∼96-100%, and is highest for *s*-polarized light. Based on these reflectance values and the curvature of the concentrator we calculated the transmittance of each position of the concentrator.

Besides this calculated transmittance, we measured the spatially resolved transmittance of the concentrators by raster scanning the illumination position of a collimated laser beam over the surface of the concentrator. An optical single mode polarization-maintaining optical fiber is connected to the laser and is fixed to a 2D-automated stage. The concentrator is mounted in front of an integrating sphere with a photodiode. The integrating sphere collects the total transmittance

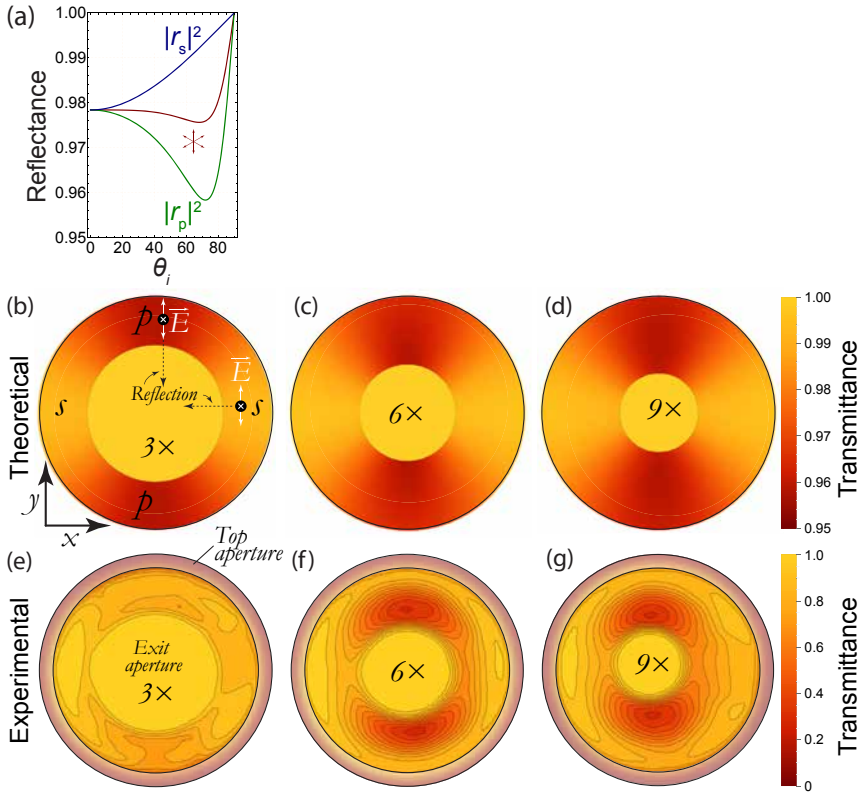

Figure 6.5: Comparison of the theoretical and experimental transmittance of the concentrators. **(a)** Reflectance as a function of the angle of incidence (θ_i) of a smooth silver surface, for *s*-, *p*-, and un-polarized (∗) light, at a wavelength of 532 nm. This data is used to calculate the following transmittance maps. (**b-d**) Calculated transmittance maps according to the Fresnel equations based on the polarization and incidence angle of the three silver coated concentrators (C=3×, 6×, and 9×) for incoming light (532 nm), traveling parallel to the concentrator axis. The maps (top view of concentrator) show the transmittance as a function of the incidence (x, y) position. Due to the geometry of the concentrator, the light can be *p*-polarized and *s*-polarized with respect to the plane of incidence depending on the incident spot. (**e-g**) Experimental transmittance maps for light with a wavelength of 532 nm. Note that the color bars of the theoretical and experimental maps differ. The measured transmittance at the outer edge is faded out, to indicate that the laser beam slightly overlaps with the rim of the concentrator.

such that the photodetector is homogeneously illuminated, without collecting any direct reflection. The spot size of the 532 nm diode laser is less than 1 mm and the beam is vertically polarized, and propagates parallel to the central concentrator axis, see Supplemental Section 6.6.2 for the experimental setup.

Figure 6.5 shows the calculated (b-d) and measured (e-g) transmittance maps

of the concentrators for vertically polarized light. Light traveling through the center of the concentrator is fully transmitted. Light hitting the concentrator is reflected once before it reaches the bottom aperture. The transmittance was calculated using the calculated Fresnel reflection coefficients (Fig. 6.5a). A notable difference between the reflections of the two polarization directions is observed. For a vertically polarized source, the light at the top and bottom of the concentrator is *p*-polarized, while at the left and right side it is *s*-polarized, which gives rise to a lower transmittance for light incident on the top and bottom part of the concentrator.

Figure 6.5 e-g show the measured transmittance of the parabolic mirrors, which is significantly lower than the values based on theoretical Fresnel reflection (note the different colorbar range). The 3× concentrator has higher transmittance (74-93%) than the 6×, and 9× concentrator (31-93%). Especially the transmittance of *p*-polarized light is significantly lower than expected. We will analyze the origin of this reduced transmittance in the next section.

6.3.4 Surface Quality of the Concentrators: Reduced Transmittance due to Roughness

The track of the milling cutter leaves small grooves on the surface of the concentrator. Figure 6.6a shows a schematic top view of the 6× concentrator and it illustrates the milling tracks. The size of these scratches is determined by the material hardness and several settings of the milling machine, like the overlap between consecutive drill paths and the shape and size of the milling cutter. The surface was polished using abrasives to improve its smoothness. To remove all residuals of the milling process, we did extensive cleaning with soap followed by ultrasonic cleaning in anisole (8 min) and ethanol (60 min).

The reflectivity and surface quality of the concentrator surface affects its transmittance. By visual inspection of the concentrator surface some haze is observed, which indicates scattering due to surface imperfections. Due to the strong curvature of the surface it is not possible to scan the surface by conventional AFM and surface profilers. However, we can get an indication of the surface roughness from SEM images.

The figures 6.6b-d show several SEM images of the surface. Figure 6.6b shows a milled concentrator directly after fabrication. The milling lines can be clearly observed. The deposition of silver slightly improves the surface quality, but still some artifacts remain, as shown in Fig. 6.6b. The visible metal blobs have a feature size in the order of microns. After silver deposition on these rough blobs, small silver grains are observed. There are thus several origins of surface roughness with each a typical feature size. Although the surface roughness cannot be quantified based on this images, we do observe that typical feature sizes in the order of

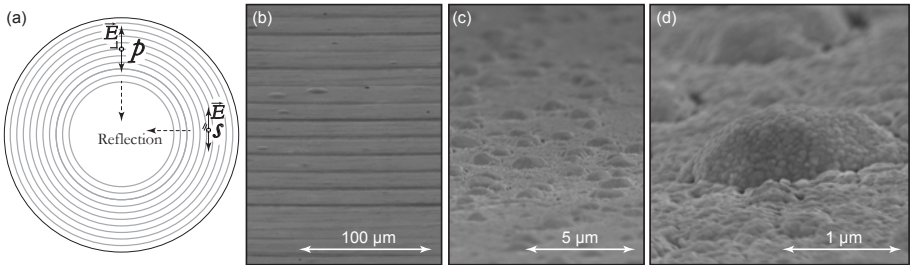

Figure 6.6: **(a)** Schematic top view of a concentrator. The concentric circles illustrate a few milling lines. Polarized light hitting the concentrator induces oscillating electrical currents on the surface of the concentrator. At the top and bottom these currents are orthogonal to the milled circles, while at the left and right side these currents are parallel to the milled lines. This difference in orientation has a major impact on the observed reflectance. **(b-d)** SEM images of the concentrator surface. (**b**) A 3× aluminum concentrator before deposition of silver. The regular stripes are caused by the milling process. **(c)** A 6× concentrator after polishing and evaporation of Ag. **(d)** Zoom-in of a metal blob on which different metal grains can be seen.

hundred nanometers. This is the origin of the observed reduced transmittance. Smoother surfaces can be produced by diamond turning on a lathe.

6.4 Modeling & Theory of External Light Trapping

To obtain a detailed understanding of the effect of the concentration factor and cage height on the absorptance by the solar cell, we introduce a generic analytic model based on statistical ray optics. We compare the results of this statistical model with the results obtained by ray tracing. The ray tracing also gives detailed understanding of the effect of the cage height and concentration factor on the cell illumination.

6.4.1 Statistical Model with Lambertian Scattering

In this statistical model we first determine the probability for a photon that is inside the reflective cage to escape via the aperture. After determining this escape probability we can calculate a well-defined statistically averaged absorptance for the large ensemble of photons in the solar spectrum. An upwards moving photon in the cage with an arbitrary position and orientation has an escape probability (P_{escape}) which is given by the following area ratio:

$$P_{\text{escape}} = \frac{A_{\text{aperture}}}{A_{\text{concentrator}}} \left(= \frac{1}{C}\right). \tag{6.2}$$

This statistical average is valid for isotropically distributed (randomized) light in an integrating sphere, but is not necessarily true for other trap geometries such as our trap.[192] For eq. 6.2 to be true it has to be proven that there is a well-defined statistical escape probability for an ensemble of upward moving photons. Although the light is not randomized in our external light trap, eq. 6.2 can still be valid . For example, when the light intensity is homogenized when it reaches the aperture plane after being reflected by the solar cell. As will become clear from the ray tracing, this condition is approximately fulfilled for several geometries of the light trap. The cage height is one of the parameters that determines the degree of this homogeneity and thereby the accuracy of the following analytical model.

If the statistic condition for eq. (6.2) is fulfilled then the (integrated) absorptance (A_{trap}) of the solar cell with a light trap is given by (for derivation see eq. 4.5):

$$A_{\text{trap}} = T_{\text{c}} \cdot \frac{A_{\text{sc}}}{1 - R_{\text{sc}}(1 - C^{-1})R_{\text{cage}}}, \tag{6.3}$$

with T_c the transmittance of the parabolic mirror, A_{sc} the absorptance of the solar cell and R_{cage} the reflectance of the top of the cage (the reflectance of the four sides is assumed to be 1).

This model is valid for incoming light within the acceptance angle. The acceptance angle determines the amount of diffuse light that can enter the cage. The optimal value for C is therefore a trade-off between the degree of light trapping and the acceptance of light. From this statistical model we can determine the following two limits.

Limits. In the limit of high cell absorptance ($A_{\text{sc}} \sim 0.8-1$) it can be seen (e.g. by making a Taylor series) that the reflectance of the cell with trap (R_{t}) reduces according to $R_{\text{t}} \sim \frac{R_{\text{sc}}}{C}$. As a rule of thumb, the effective reflectance of a cell with trap is thus reduced by a factor C.

In the limit of infinite light trapping ($C \to \infty$, $T_{\text{c}}=1$) the absorptance (Eq. 6.3) becomes $A_{\text{t}} = \frac{A_{\text{sc}}}{1 - R_{\text{sc}} \cdot R_{\text{cage}}}$. So, A_{t} is given by the ratio of light absorbed in the cell ($A_{\text{sc}}=1-R_{\text{sc}}$) and the total light absorbed per double pass ($1-R_{\text{sc}} \cdot R_{\text{cage}}$). The ratio between the parasitic cage absorptance and cell absorptance is thus of even greater importance.

For specular reflection of light, the entropy is preserved. Interestingly, it has been shown that the escape probability can be reduced below the statistical escape probability of randomized light by deterministic light trapping,[103] thereby the $4n^2$ internal path length enhancement limit can be surpassed. Due to the conservation of etendue and entropy upon specular reflection in the external light trap there are certain cases in which the statistical absorptance limit is exceeded.

From a thermodynamic point of view, the effective emitting area of a cage with a small aperture is reduced to only the aperture area. The radiation coming from the aperture equals that of a (perfect) black body with an emissivity of 1 as shown

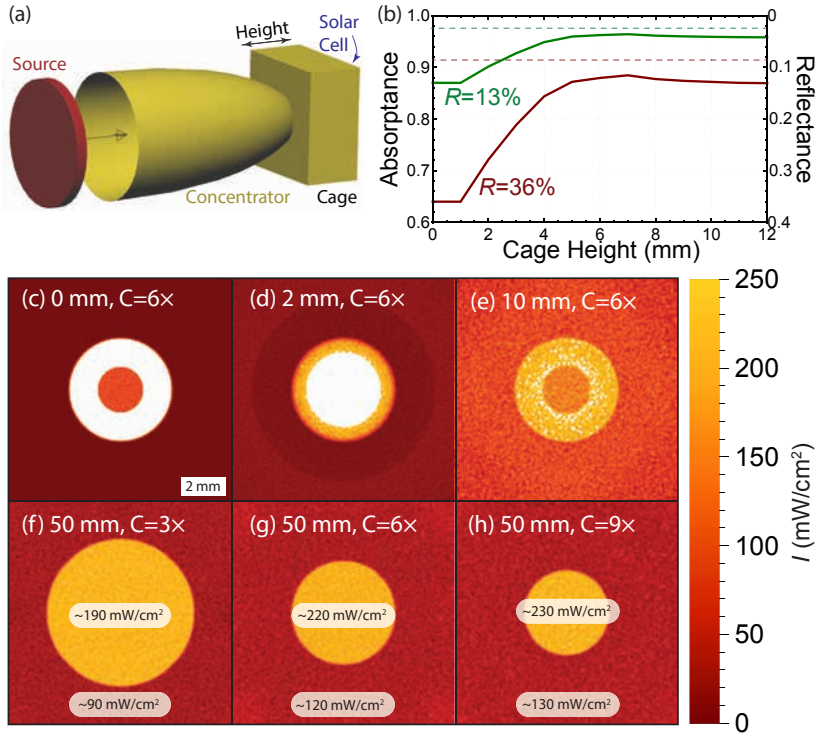

Figure 6.7: (**a**) Illustration of the setup used for the ray tracing. A light source with a collimated beam (I=100 mW/cm^2) is aimed at the C=6× concentrator with a cage and solar cell behind. A series of simulations was performed with different cage height. The simulations are performed at normal incidence. **(b)** Effective absorptance by a cell within an external light trap with C=6×. The reflectivity represents that of our cell (36%) and that of a typical solar module (13%). For a short cage the light is not trapped. The absorptance increases initially, and levels off at ∼6 mm. The dashed lines show the statistical absorptance limit. (**c-e**) Simulated intensity distribution on the solar cell with increase of cage height (0-10 mm) for R= 36%, and C=6×. The absorptance becomes more homogeneous with increase of the cage height. For pixels with a white color the absorptance exceeds 250 mW/cm^2. (**f-h**) Intensity maps for h_{cage}=50 mm, R=36% at C=3×, 6×, and 9×. The central ring is illuminated stronger due to direct and reflected illumination.

by Planck.[193] Here, it is assumed that the walls do not transmit any radiation to the exterior. Due to reciprocity, the effective absorptivity of light entering the cage via aperture is thus 1. Thereby, the thermodynamic energy conversion efficiency limit of this system is higher than that of bare solar cells.[18] For a cell in an external light trap this elevated efficiency limit is caused by a net reduction of the radiative recombination current due to recycling which results in a larger splitting of the quasi Fermi-levels and thus a higher V_{oc}.

6.4.2 Ray Tracing of External Light Trap & Effect of Cage Height

The conditions for the statistical model are not necessarily satisfied for all configurations of the external light trap. To analyze the effect of the cage height and the concentration factor on the cell absorptance and spatial intensity distribution on the cell, we set up a series of light traps with different cage height and performed ray tracing. The setup is illustrated in Fig. 6.7a. A collimated beam of light, consisting of 1 million rays, is directed to a C=6× reflective compound parabolic concentrator (CPC),[125] which funnels the rays through a small aperture, via a perfectly specular reflective cage, towards the solar cell. A non-sequential ray-tracer was used,[194] see Supplementary Section 6.6.5 for the used simulation settings.

Figure 6.7b shows the total absorptance in the solar cell, as a function of the cage height for two reflectance levels. The reflectance of 36% represents the overall reflectance of our cell, and 13% represents that of a typical industrial solar module. For a very short cage (h_{cage}<1 mm), the light is concentrated on a small spot in the center of the cell and the reflected light will escape. Once the cage becomes higher than ∼1 mm there is a sudden increase in the absorptance as an increasing amount of light retro-reflected by the top of the cage just next to the aperture. This fraction steadily increases up to h_{cage}∼6 mm. There is an optimum absorptance around this cage height because the escape probability at this cage height is low (so high recycling efficiency) during the first couple of recycling events. These first recycle events are most important as the intensity is highest.[94, 103]

When a light trap with a 6 mm cage is applied on our solar cell (with R=36%) the reflectance at normal incidence is reduced to 12%; for a typical industrial solar module the reflectance drops from 13% to 4%. At normal incidence the light that reflects from the center of the cell is not trapped; it escapes directly through the aperture. At other angles of incidence, this "central light" can be totally retro-reflected to the cell. Interestingly, the statistical absorptance limit is exceeded in these cases, because the escape probability of photons becomes lower than the statistical escape probability as given by eq. 6.2.

The dashed lines indicate the statistical limit calculated using eq. 6.3 at C=6×. For R=36% and R=13% the reflectance is reduced to 8.6% and 2.4% respectively. The derived reflection reduction of $R_{\mathrm{t}} \sim \frac{R_{\mathrm{sc}}}{C}$ yields R_{t}=2.1 for R=13%, so this is a reasonable approximation. For larger cage heights (h_{cage}>6 mm) and normal incidence, the light distribution becomes more and more homogeneous. Thereby, the absorptance determined by the ray tracing approximates that of the statistical limit (dashed line) within a few percent. The small absorptance difference between the ray tracing and analytical model is caused by the direct escape of the specular reflection of the center of the cell. This fraction ($R_{\mathrm{sc}} \cdot 1/C$) is thus not trapped at normal incidence. At different incoming angles, the direct reflection of the cell can be completely reflected, and thereby the statistical limit is surpassed.

Averaged over all incoming angles (θ_i) within the acceptance angle of the CPC, the escape probability is only defined by the ratio $A_{\text{aperture}}/A_{\text{sc}}$, and A_{t} is therefore given by the statistical limit (see eq.6.3). The statistical model thus gives an excellent approximation of the absorptance of a cell with an external light trap.

Figures 6.7c-e, and g show the intensity distribution on the cell for different cage heights (h_{cage}=0−50 mm) at C=6×. In absence of a cage (h_{cage}=0, Fig. 6.7c), the center is illuminated by ∼6× concentrated light. For a 2 mm cage (Fig. 6.7d) most of the light hits the cell and is reflected without being trapped and the cell illumination is still rather inhomogeneous. The rays enter the cage with a distribution of propagation angles. Therefore, the spread of the beam becomes more and more homogeneous as light travels through the cage. For taller cages (Fig 6.7 e and g), most of the reflected light gets trapped; most of the reflected light hits the top of the cage and is reflected back to the cell. The circular white spot in the center is caused by the light that went straight through the aperture (without being reflected by the CPC). Due to the divergence of the beam after the CPC and the light trapping the illumination of the outer area of the solar cell is very homogeneous.

Spatial Intensity Distribution. Figures 6.7f-h show the intensity distribution for a tall cage at C=3×, 6×, and 9×. The cage height determines the intensity distribution on the cell. The emitted power of the beam is 0.1 W and its area is 1 cm^2, equivalent to AM1.5G irradiance of 1000 W/m^2. The intensity is thus 100 mW/cm^2. Due to the external light trapping, the effective intensity at the cell is higher (130-230 mW/cm^2 in Fig. 6.7h) than the intensity of the beam (above the concentrator). It can be seen that the cell on average operates at a higher irradiance level due to the light trapping. For a tall cage, the light distributes homogeneously over the cell, except on the center. The intensity in the center of the solar cell is roughly twice as high as the outer area, which matches to our expectations based on the statistical model, see Supplementary Section 6.6.6.

Inhomogeneous cell illumination can be detrimental for the cell response because of Ohmic losses and local heating.[140, 141] Mild intensity fluctuations do not impact the performance of most solar cells as long as the maximum-to-average intensity ratio is less than ∼3.[141] The observed intensity difference of a factor ∼2 is therefore acceptable. If improved homogeneity is needed this can be realized by integrating a diffuser in the cage. By downsizing the dimensions of the external light trap to ∼100 μm (order of magnitude of the thickness of the solar cell) the impact of inhomogeneity can be further reduced as the electrical current will redistributed evenly over the cell after a short (∼100 μm) lateral distance.

Considerations regarding diffuse and direct components of solar illumination and the effect of solar tracking versus stationary modules are presented in Supplemental Section 7.2. Due to the cos(θ_i) relation of the incident flux, we presume that there can be a gain in total energy efficiency by designing the trap such that it has a higher degree of light trapping when the sun is at normal incidence (noon)

and lower at other moments.

6.5 Conclusions

We demonstrated that external light trapping is a universal solution for light management on a module level. We showed improved performance of a crystalline silicon solar cell due to optical confinement by an external light trap over the full solar spectrum. The light trap is effective for all types of solar cells, including multi-crystalline Si cells that are difficult to texture. Using our thick prototype c-Si solar cell without an AR coating, our proof-of-principle demonstrator showed an absorptance enhancement from 64 to 87% by external light trapping. A similar improvement can be expected for very thin c-Si solar cells. We compared the results of our statistical model and that of ray tracing for our trap design. It was found that the model gives a good approximation of the total absorptance. Our optical model shows that on module level a reflectance reduction from 13% to 2.4% is feasible. Our simulations show how the absorptance and the cell illumination change with the cage height. We found that there can be a factor two difference in intensity on cell level due to the external light trap. This intensity distribution is acceptable since such a difference does not reduce the cell performance significantly.[140, 141]

It was found that imperfections of the surface of the concentrator result in strong polarization-dependent transmittance. There are many lens fabrication technologies available that offer major improvements to the concentrator transmittance.

Due to external light trapping, the cell thickness can be reduced by a factor of at least 2, without reducing absorptance. The use of an external light trap with thin, planar c-Si cells does not only result in higher short circuit currents, but also in increased V_{oc} due to reduced bulk and surface recombination.

We have shown that external light trapping offers a simple and effective overall light management solution. Therefore, it deserves serious attention as a new candidate for highly-efficient solar modules of the foreseeable future.

6.6 Supplementary Information

Silver reflectance, "Flat" vs. Polished Silver. Figure 6.8 shows the reflectance at normal incidence of Ag deposited on glass and that of a flat, polished surface of aluminum coated by Ag. This piece is expected to be smoother than the surface of the concentrator. The reflectance of Ag on polished Al is significantly lower than the reflectance of Ag on flat glass surface mainly from 340—800 nm. For wavelengths up to ~600 nm there is still >5% absorptance in the silver.

Plasmonic Absorptance. Generally, sharp metal features result in parasitic plasmonic absorptance and scattering of light.[76–78, 195] The reflectance of polished silver steadily improves with wavelength, as shown in Fig. 6.8. This can partly be caused due a thin tarnish layer. A tarnished surface of ~5 nm roughly corresponds to the observed reflectance.[27] Furthermore, the effect of roughness of the film might be less for long wavelengths as surface features become relatively smaller for long wavelengths.

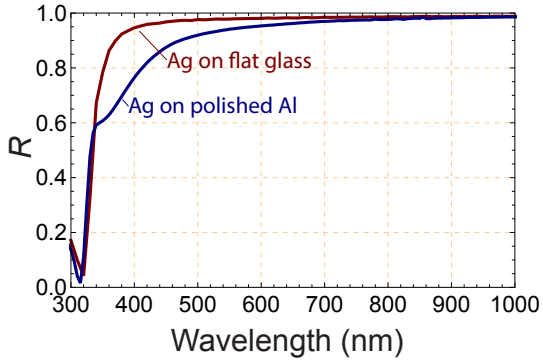

Figure 6.8: Comparison of reflectance by Ag on flat glass and on polished Al. Mainly a drop from 340 to 600 nm.

Surface Requirements. The surface quality plays an important role in the reflectivity of mirrors. The surface quality can be defined in terms of planarity and roughness. Planarity refers to the long range (tens of microns) flatness and should typically be less than $\lambda/10$. Roughness is defined on a smaller area (ten to hundreds of nanometers) and should also be less than $\lambda/10$.[80] Light that hits a rough surface will diverge due to diffraction. With an increase of the surface roughness the angular distribution of the specular lobe becomes wider.[196, 197] External light trapping is part of a less stringent branch of non-imaging optics: a small deviation of the optical path still contributes to light reaching the exit aperture. The relatively low transmittance of the high C concentrators is partially attributed to the tighter cutoff of the diverging reflected beam.

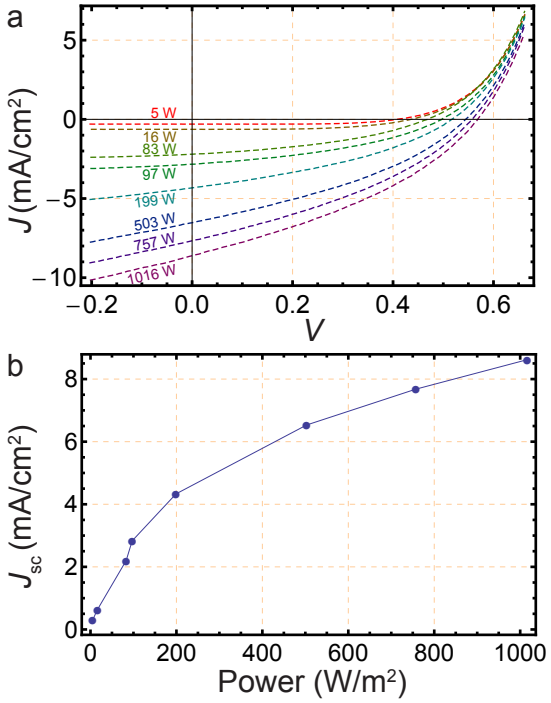

Figure 6.9: (**a**) Plot of the *JV* response of the photodiode at different illumination levels. (**b**) Short circuit current (J_{sc}) of the photodiode at several illumination levels (0-1 sun).

Smoother Surface of 3D-Printed Concentrators. The transmittance values for 3D-printed concentrators that were determined in the previous chapter (Section 5.3) are higher than that of the milled concentrators. Although the form accuracy of these 3D-printed surfaces is worse than that of the milled concentrators, the surface smoothness of these concentrators is better. This is due to the excellent smoothening procedure of the 3D-printed parts, that results in very smooth surfaces. A smoothening procedure or additional smoothening coating can improve the transmittance of the milled concentrators. Smoother concentrator surfaces can also be achieved using a diamond milling cutter without any polishing.

Intensity. The transmittance of the concentrator (T_c) is determined by the direct silver reflectance and the amount of scattered stray light (SL) according to: $T_c(\lambda) = R_{Ag,\,direct} = 1 - A_{Ag} - SL$. Some stray light (i.e. the light not reflected specularly) can still be transmitted by the exit aperture of the concentrator, but this is only a small fraction. Presumably, there is a difference in amount and direction of the stray light for both polarizations.

Intensity of Scattering/Diffraction. Rayleigh criterion for surface smoothness

dictates that $k \cdot \sigma^2 \ll 1$, with $k = \frac{2\pi}{\lambda}$ and σ the rms surface roughness.[197] This indicates that the surface roughness should be much smaller than the wavelength of light. Clearly, this is not the case for our concentrator which limits the transmittance.

6.6.1 *JV*-Measurements

As the photodiode does not have a metal front grid for the electrical current, it is significantly hindered by Ohmic losses at 1 sun illumination. Figure 6.9a shows the *JV* data of the photodiode under different illumination levels. Figure 6.9b shows the short circuit current as a function of the illumination. It can be seen that the short circuit current does not scale linearly with the illumination power, which indicates significant Ohmic losses. Besides, the photodiode is more sensitive to inhomogeneous illumination than solar cells. This cell is therefore not suited for *JV*-measurements, so we limited ourselves to *EQE* measurements in which the generated electric currents are sufficiently low to operate in the linear response regime of the photodiode.

6.6.2 Setup for Transmission Measurements

When a collimated beam of light hits the concentrator, the light exits the concentrator with a certain angular distribution.[198] The transmittance cannot be measured directly from a photodiode placed at the exit aperture of the concentrator, as its response function is angular sensitive.[169] Moreover, the reflection from the photodiode is recycled by the light trap, and therefore there is no (easily) resolvable correlation between the concentrator transmittance and the photodiode signal.

As a solution, we placed the concentrator in front of a port opening in an integrating sphere to collect the transmitted light.[199] At another port opening of the sphere a photodiode is placed to measure the integrated transmittance. This setup enables collection of the transmitted light and is not sensitive to the angle at which the light exits the concentrator. By raster scanning a laser beam over the surface of the concentrator, we measured a spatially resolved transmittance map. The spot size of the 532 nm diode-pumped solid-state laser is less than 1 mm and the beam is vertically polarized, and parallel to the central concentrator axis.

The laser is coupled into a fiber which is connected to a translational stage. A (x, y) raster scan is performed by scanning the glass fiber over the surface of the fixed concentrator. Each pixel takes a few seconds to measure, so measuring an area of 100 by 100 pixels takes a few hours.

The measured transmittance maps represents the average transmittance of the area of the laser beam (diameter less than 1 mm). Therefore, the observed values within 1 mm from the edge of the concentrator gradually drop to zero (as indicated

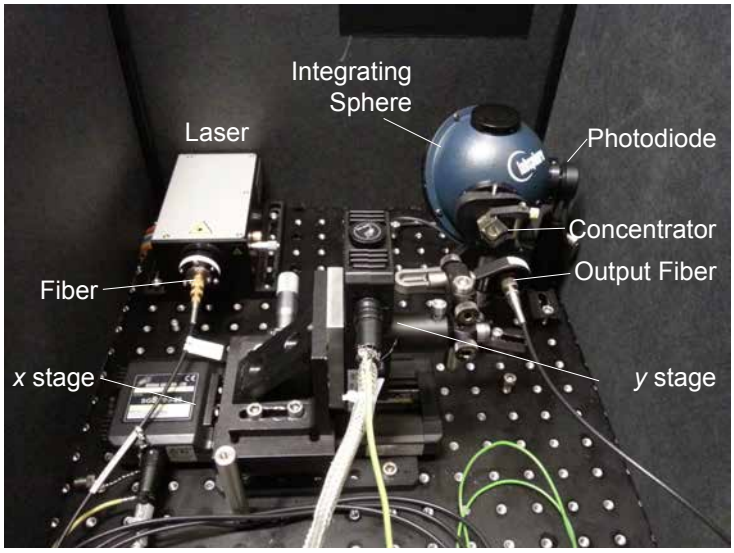

Figure 6.10: xz—translation stage used to determine the transmittance of the concentrators.

by the outer ring) as a part of the beam hits the flat top of the concentrator and is reflected back to the laser.

6.6.3 Solar Cell Specifications

The reflectance of the solar cell comes mostly from its front side. Due to the thickness (300 μm) of the solar cell that was used (Hamamatsu photodiode S1337-1010BQ[200]) the light that goes into the cell is almost completely absorbed. As the external light trap is ignorant about the origin of the reflected light (front or back-side) a demonstration of trapping of light reflecting at the front side of the cell, also shows the potential for recycling of light reflected at the backside of a (thin) solar cell. Indeed, the wavelength-dependent reflectance of a thin cell is different from that of the cell used in this experiment, however, the optics involved is equivalent. The solar cell has a photosensitive area of 10×10 mm^2. The cell does not have an anti-reflection layer nor electrical front grid. The electrical current is collected outside the optically sensitive area.

6.6.4 Advantage of Planar Solar Cells

The textured front surface is the most defective part of the solar cell. Due to the exponentially decaying absorption profile, there is strong generation of charge carriers close to the surface. The surface recombination rate is partly determined by

the distance (and the diffusion velocity) of the generated minority carriers towards the surface. Therefore, it is beneficial to (i) have low surface recombination and (ii) create the electrons and holes not too close to the defective surface. Both aspects are better for a cell with a planar front surface than for a textured front surface; a planar front surface thus reduce the absolute surface recombination rate. As the external light trap facilitates improved in-coupling of light, it becomes interesting to have a planar front surface and only texture the backside of the solar cell to scatter the light for internal light trapping. This enables less surface recombination and thus higher cell efficiency.[201]

6.6.5 Ray Tracing Settings

In each simulation 1 million rays (or photons) are sent towards the concentrator. Each time a ray hits the solar cell, a defined fraction is absorbed. The total absorptance in the cell is obtained by integration over all absorption events of all rays. The simulation of a ray continuous until the ray escapes out of the concentrator or until the energy of the ray dropped to less than 1% of its initial energy. The accuracy of the simulated results is thus within 1%. The reflectance of the cage and the CPC are both set to 100%. The total emitted power by the source is 100 mW.

6.6.6 Intensity Distribution

Intensity Distribution and Cell Performance. When light is concentrated on a small spot of the solar cell, several electrical and optical conditions change. Especially the effect of series resistance becomes more pronounced.[140, 141] At concentration, the current has to be transported laterally by a smaller surface area and less fingers compared to homogeneous illumination. Therefore, the local current (I) is relatively high and thus more energy is dissipated ($P_{\text{dissipated}}$) due to the (effective area) series resistance (R). This Ohmic loss is in first order given by $P_{\text{dissipated}}=I^2 \cdot R$.

The intensity distribution depends on several design parameters such as the cage height and concentration factor. Mild intensity distributions can be tolerated for most cells as long as the maximum-to-average flux ratio is around 3.[141] If needed, the light can be more randomized by using a secondary optical component, such as a prism, or diffuser at the exit of the concentrator.

Wavelength Difference. Long, poorly absorbed wavelengths will propagate longer through the cage. Due to this recycling the effective illumination contains more long-wavelength light than the solar spectrum. A benefit of a tall cage is the light is geometric mixed such that the cell is homogeneously illuminated, also known as the “Kaleidoscope effect”.[202]

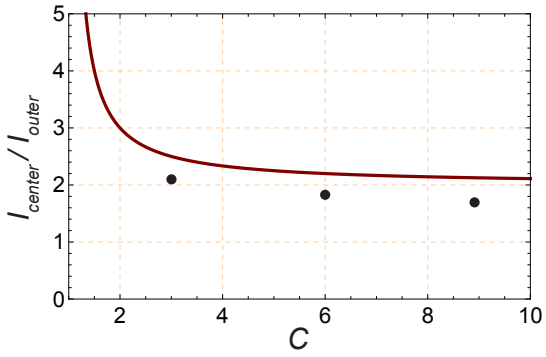

Figure 6.11: Intensity contrast between center and outer area of cell as a function of the concentration factor.

For a conventional compound parabolic concentrator, the light that reaches the exit aperture via a reflection on the concentrator surface makes an angle $\theta_{\text{acceptance}}-90°$ w.r.t. the plane of the exit aperture.[125, 203] This angular spread determines the divergence of light within the cage. As the beam moves downwards, the beam width increases. When the beam diameter is sufficiently larger than the dimensions of the cell, the light becomes homogeneously spread.

The absorptance in the central region of the cell consists of three contributions: (1) direct illumination (light that went directly through the aperture without hitting the concentrator); (2) the (homogenized) light reflected via the concentrator; and (3) retro-reflected light. In the limit of a "tall cage" the intensity of (2) and (3) is homogeneously distributed on the cell. However, the intensity of (1) only illuminates the center at normal incidence. The illumination intensity in the center of the cell is therefore higher by an amount equal to the intensity of the irradiance beam (I_{beam}). If we neglect the recycled light, we can quantify the intensity at the center I_{center} according to: $I_{\text{center}}=I_{\text{beam}}+(1-\frac{1}{C})I_{\text{beam}}$. The second term equals the intensity of the area outside the central ring I_{out}. The ratio between both illumination is now given by:

$$\begin{aligned} I_{\text{contrast}} &= \frac{I_{\text{center}}}{I_{\text{out}}} = \frac{I_{\text{beam}}+(1-\frac{1}{C})I_{\text{beam}}}{(1-\frac{1}{C})I_{\text{beam}}} \\ &= \frac{1+(1-\frac{1}{C})}{1-\frac{1}{C}} \\ &= \frac{2C-1}{C-1} \end{aligned} \tag{6.4}$$

The retro-reflected light also distributes equally on the cell. If we would include this term both the nominator and denominator would increase, and thereby I_{contrast}

decreases depending on the amount of reflection.

Figure 6.11 shows $I_{\text{contrast}}(C)$ based on eq. 6.4. This function move asymptotically to 2. If we neglect the retro-reflected light, the intensity in the center is thus often more than a factor 2 more intense than the outer part of the cell. The three dots in figure 6.11 indicate the observed intensity contrast on the intensity maps (Fig. 6.7). The observed I_{contrast} is slightly lower due to the contribution of retro-reflection (which is not included in eq. 6.4).

Chapter 7

Valorization Approaches for External Light Trapping for Solar Modules

The three previous chapters presented promising results on external light trapping for various solar cells. In this utilization chapter we present a more rigorous technology assessment and address the commercial potential of external light trapping. We introduce a *light trapping module* that can be realized relatively easily. We illustrate several modifications of this light trapping module that lead to some interesting additional features which cannot be realized (or not effectively) using conventional module designs. For example, we will show a design of an arbitrarily colored module that can be integrated into buildings.

In the previous chapters we showed several hollow, metalized parabolic concentrators that guide the light through a small aperture. However, parabolic concentrators cannot be directly sandwiched into a conventional module. For example, the concentrator needs a glass cover sheet for protection. At normal incidence, the air-to-glass and glass-to-air interfaces bring a cumulative reflection loss of ∼8%. In a conventional module the refractive index gradually increases towards that of silicon (n∼3.5). However, when a sheet of glass is placed on top of hollow (air filled) metalized parabola the refractive index decreases. This decrease is unwanted as it brings additional reflection losses, especially at higher angles of incidence. As this significant loss is not acceptable for module integration we have to develop an alternative design. To eliminate the contrast of the refractive indices, one can fill the parabola with e.g. index matching oil. However, this is technically difficult to realize. Texturing the front glass to control the flow of light is expected to be a better option, as shown in the next section. This design keeps the number

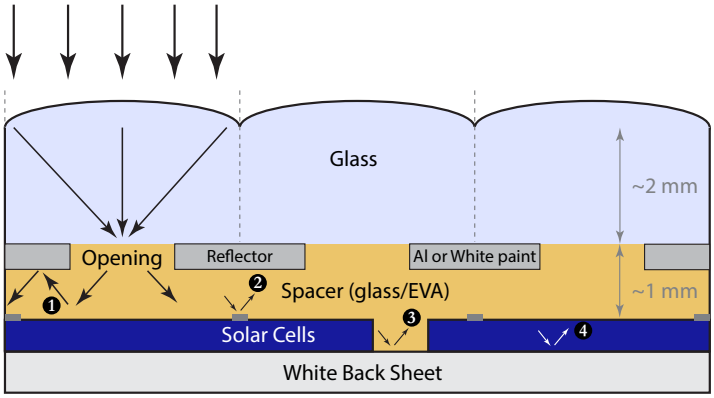

Figure 7.1: Basic concept of a light trapping module. Light is focused by lenses on the front side of the glass through openings in a reflector at the backside of the glass. The reflector can be made of a metal (e.g. Ag or Al) or of white paint. The light gets trapped in the space between the reflector and the white back sheet. Four different sources of reflection can be reflected back to the solar cell.

of additionally required layers to a minimum and tries to stay as closely as possible to the conventional module design.

7.1 The Light Trapping Module

7.1.1 Design 1: The Basic Design for Enhanced Efficiency

Figure 7.1 shows a *light trapping module*, in which an external light trap is integrated into a conventional solar module. An array of lenses is applied on the front side of the glass which generally has a thickness of around 2 to 5 mm. At the inner side of the glass a reflector is applied with openings through which the light is funneled towards the solar cell. The focal distance of the lens should be roughly equal to the thickness of the glass to have the focal point (of a normal incoming parallel beam of light) between the reflective areas to funnel the incoming light through the openings (as indicated at the left side of Fig. 7.1).

Each type of lens has a specific acceptance angle.[204] An ideal lens (e.g. a CPC, see Fig 7.6) gives the maximal theoretically possible concentration factor for light entering within a certain acceptance angle (θ_a). The acceptance angle is measured with respect to the concentrator axis (or normal); the total acceptance angle is thus $2{\cdot}\theta_a$. For an ideal linear concentrator (also known as "parabolic trough" and "2D geometry"), the concentration factor (C) is related to the acceptance semi-angle (θ_{max}) and the refractive index of the glass (n_{glass}) according to the following

equation:[125]

$$C = \frac{n_{\text{glass}}}{\sin(\theta_{\text{a}})}. \tag{7.1}$$

To give an example, when n_{glass}=1.5 and θ_{max}=30° we obtain a concentration factor of 3×. For an ideal 3D concentrator the concentration factor is given according to:

$$C = \left(\frac{n_{\text{glass}}}{\sin(\theta_{\text{a}})} \right)^2. \tag{7.2}$$

In the first part of the chapter we only consider normal incoming parallel beam of light; later we consider the consequences for (sun)light coming from different angles.

The light that falls between the reflective areas is transmitted to the (commonly used) ethylene vinyl acetate (EVA) encapsulation layer. The space between the reflector and the white back sheet forms a cavity (or cage) in which the light is trapped. Due to the light trapping, the efficiency of the module increases. As indicated in Fig. 7.1, four different sources of reflection are recycled. It also enables a different cell design; for example, the series resistance can be reduced using a larger electrical grid at the front side of the cell without effectively increasing the shadow losses.

Design of Lens Array. There are several options for the configuration of the lenses. For example, one can use a square or hexagonal array (similar as shown in chapter 5) or rows of lenses. Incoming sunlight is either accepted or rejected: accepted light reaches the solar cell via the aperture; rejected light reflects on the top side of the reflector out of the module without hitting the solar cell. The shape of the lens determines the geometrical area of the sky from which the sunlight is accepted. The sun moves on a well-defined path through the sky for a fixed geographical location during the year. The lens shape can be tuned to match the daily and yearly path of the sun. In section 7.2 we illustrate how this matching can be realized.

The best shape of the lens has not been fully developed yet. Its optimal shape depends on, among others, the thickness of the glass, the achievable curvature of the glass (without getting problems with dust and high reflectance), and the preferred acceptance angle (which also determines the concentration factor and thus light trapping efficiency). The optimal lateral dimension of the lenses is expected to be in the same order of magnitude as the thickness of the glass (2 to 5 mm). The associated dimension of the openings would be in the order of ∼1 to 2.5 mm

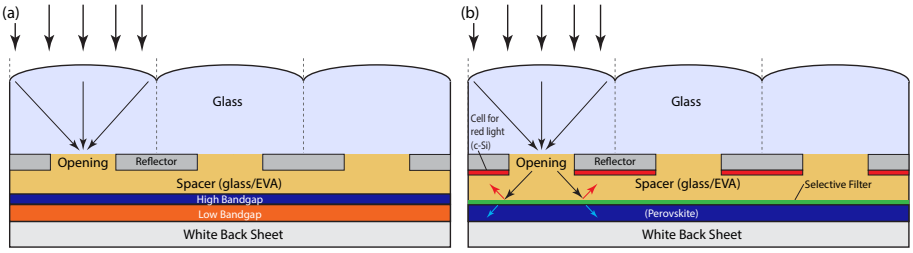

Figure 7.2: Two different integrations of a tandem solar cell. **(a) Design 2A** Illustration of "conventional" 2-terminal tandem cell integration inside an external light trap. **(b) Design 2B** Illustration of two physically separated, independently operating, solar cells (4-terminal) in a light trapping module. The light first propagates through openings in the top cell before it reaches the (high band gap) bottom cell. A large fraction of the reflected light reaches the low band gap cell located directly below the reflector. A shortpass filter can be integrated between both cells for spectrum splitting. This design allows for 4-terminal contacting and the reflective metal layer can be used both as a conductor and a reflector.

7.1.2 Design 2: Tandem Cell Integration

In a conventional tandem solar cell, two cells with a different band gap are stacked on top of each other to use the energy of each photon more efficiently. The integration of two cells with a different band gap in the light trapping module can have several advantages over the conventional design.[205] We present two options to realize tandem cell integration.

DESIGN 2A: Conventional Tandem. A stacked tandem cell can be placed at the bottom of the cage, as shown in Fig. 7.2a. This design has the same light trapping benefits as those of the basic light trapping module of the previous section. The potential gain of this design is in the same order of magnitude as that of the basic light trapping module.

DESIGN 2B: Two Facing (Different-Bandgap) Solar Cells. Figure 7.2b shows an alternative integration design of two solar cells. Here, the physical order of the low and high band gap cell is inverted compared to a normal tandem cell. This design can be realized by placing a low band gap cell (like c-Si) at the top of the cage and a high band gap cell (like a-Si or Perovskite) at the bottom of the cage. In conventional tandem solar cells, the light travels not much more than a single path through the high band gap cell, while in this design with two facing cells the light makes at least a double path through the high band gap cell before it reaches the low band gap cell (or opening).

The reflector and low band gap cell are processed on the inner side of the glass sheet. Openings are made in the reflector to enable the light to enter the cavity. A laser can be used to drill openings in a c-Si solar cell. This drilling process is commonly used for c-Si metal wrap through (MWT) solar cells.[206] Below the top

cell (low band gap) there are the EVA layer and the high band gap cell. Incoming light propagates through the holes in the low band gap cell and reaches the bottom cell. Inside this bottom cell it makes a double pass before it travels towards the low band gap cell. This forms an advantage over normal monolithically interconnected tandem cells in which the light (in first order) makes only a single pass through the high band gap cell.

Separate Cell Fabrication and Contacting. Another advantage of the two facing cells design is the potential to contact the two cells separately by four electrical terminals. Moreover, the two individual cells can be fabricated (and optimized) separately, which thereby circumvents restrictions (such as temperature, lattice matching and chemical compatibility) that occur when one cell is processed on top of another cell. The advantage over two terminal contacted cells is that current matching of the two cells is not required.

Spectrum Splitting. Long wavelength light that travels through a high band gap bottom cell is subject to a certain degree of parasitic absorptance in the active cell material, contacting electrodes, and/or encapsulation layers. This can be prevented by integrating an optical filter (also known as dichroic mirror) that is transparent for short wavelengths, while reflective for long wavelengths. The use of such a shortpass filter can thus split the solar spectrum and send different spectral components to the appropriate cell. This can reduce the overall parasitic absorptance of sub-bandgap wavelengths in the high band gap cell. This is mostly interesting when the high band gap cell exhibits significant sub-bandgap absorptance. Such filters are also used in "cool-beam halogen" light bulbs to retro-reflect the infrared radiation (IR, "heat"), thereby improving their energy efficiency.

Comparison. Other concentrated solar module concepts in which multiple cells are used are often based on one of the following concepts: 1) one of the cells is placed vertically or 2) small stripes of cells of alternating band gap cells are placed next to one another.[207] This complicates the fabrication of a large module as many individual components are involved. An advantage of the two facing cells design is that a large area top cell can be fabricated on a single large surface, thereby lowering the fabrication cost.

7.1.3 Design 3: Diffuse Light Harvesting

An inevitable consequence of external light trapping is the restriction of incoming photons from certain angles. Photons entering the concentrator from an angle larger than the acceptance angle are reflected outwards at the reflective areas. A certain fraction of the diffuse light therefore does not reach the solar cell. This optical loss reduces the power output of the module. However, this problem can be solved by geometrically separating the diffuse and direct light, after which

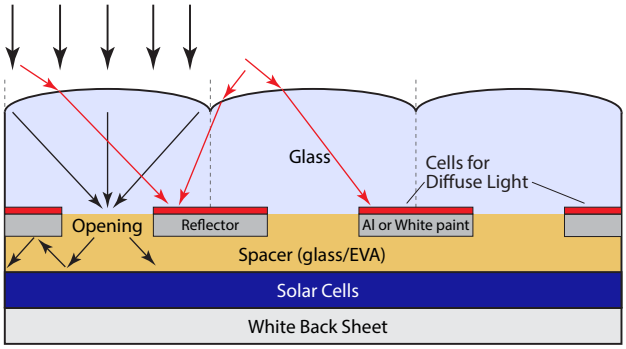

Figure 7.3: Design 3: Diffuse Light Harvesting. By integration of a solar cell on top of the reflector the "rejected" diffuse light can be harvested by the top cell.

both components are sent so a separate cell. A *diffuse light harvesting design* is illustrated in figure 7.3.

In the light trapping module, the path of the light is determined by the position and angle of incidence. When light is incident under a large angle it may not reach the aperture, instead it is reflected out of the module by the reflector. This problem can be resolved by placing a cell on top of the reflector to capture this part of the incoming light. A dedicated cell may be chosen that operates well under low irradiance conditions, e.g. a dye-sensitized solar cell.[208] The cell receives the diffuse light that did not travel through one of the apertures, which has a relative high amount of blue light due to the strong scattering of blue light by the atmosphere.

Market Potential. This diffuse light harvesting design increases the complexity and cost of the light trapping module. It can be an interesting option for geographical areas with a high amount of diffuse irradiance, which in a very rough approximation corresponds to areas with a low GHI as shown in Fig. 1.3. Once the basic light trapping module is developed it can be an interesting feature.

7.1.4 Design 4: Solar Panels with a Color, Logo or Image

Colored Solar Panel. Figure 7.4 shows a module design of a colored module. Here, the top side of the reflector is painted by the desired color. This can be a homogeneous color or a colored drawing. The light that does not pass the aperture reaches the painted area and is reflected out of the module. The simplest form to realize a colored light trapping module is by using a highly reflective white paint for the reflector. This enables a white solar module, while at the same time the design reflects the light coming from the backside of the module (e.g. contacts and back sheet) back to the solar cell. Other colors can be displayed by applying paint on top of the white or metallic reflector.

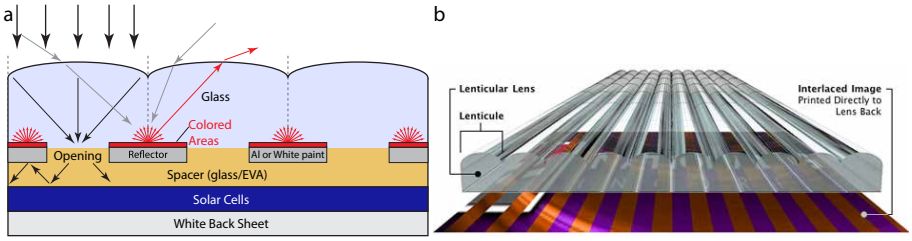

Figure 7.4: (a) **Design 4A.** The top side area of the reflector can be painted. This gives the module a color when it is viewed from a "sufficiently large" angle while it has a dark color as seen from the normal direction. (b) Lenticular lens as is commonly used for lenticular 3D postcards. When the postcard with lenticular lens is viewed from an arbitrary direction, only one of the two colored stripes (orange or purple) can be seen. Light reflecting at one of these two stripes is directed to different angular directions. Different images can be displayed in different directions by replacing the colored stripes by (properly adapted stripes of) images. © Scenix3D

Image Displaying Solar Panel. Instead of painting the module in a single color one can also visualize a colored pattern (e.g. a simple logo) or even a detailed photo/painting by the light trapping solar module.

Lenticular Lenses. Several types of lenses can be used for the light trapping module. The simplest and most well-known lens that can be used is a lenticular lens. An example of this type of lens is shown in Fig. 7.4b. Incoming light is refracted to one of the interlaced images. Thereby, this design shows different images when viewed from different directions. This technique is applied for 'Quasi-holographic' posters and postcards to show different images from different angles, an example is shown in Fig 7.5. These more or less semi-cylindrical lenses have also been used for developing (glasses-free) 3D-displays.[209] This lens design can be adapted such that light coming from the normal direction is guided towards the opening. Light from oblique angles reaches the colored areas and is reflected. When this *image displaying solar panel* is viewed from an oblique angle an image will be visible, while the module will look very black when seen within the acceptance angle (±30° from the normal). The technique to fabricating the lenses for posters, bill boards, and 3D-displays can be easily adapted to be suited for the light trapping module. Alternatively, one can integrate LEDs into the module to convert light to electricity during the day and to give light when desired. Potential applications are the areas besides airstrips for airplanes and (tall) buildings.

Alternatives. Recently, an alternative approach for colored modules was developed by CSEM, and is now further developed by S*olaxess*[210]. Here, the visible light is completely reflected out of the module, resulting in a white solar module. As a consequence of the solar cell receiving a reduced amount of light, its efficiency drops by $\sim 40\%_{\text{rel}}$.[211] Our module concept can also show detailed images and

Figure 7.5: Example of a lenticular lens applied for advertisement posters. © Snapily

can have significantly higher efficiency. SunpartnerTechnologies[212] developed a billboard that produces solar electricity, under the name Wysips® Cameleon. This module has a power rating of 90 W_p/m^2. The non-disclosed technology of this billboard is expected to be similar to the technology presented in this chapter, except that the Cameleon module (presumably) does not include light trapping.

Market Potential. The feature of showing detailed images is unique. As the material and processing costs of the module are low, the fabrication costs are expected to be reasonable. Due to the unique displaying feature, this design is expected to have the best market potential.

Alternative Lens Design. Figure 7.6 shows an alternative module design based on solid glass compound parabolic concentrators (CPCs). An advantage of CPCs is their ideal optical response; they have a very sharp acceptance angle as given by eq. 7.1. These lenses are based on geometrical optics and their size can thus be reduced as long as the artifacts remains sufficiently small, in a similar manner as we discussed in chapter 5.

Additional Option: Integration of Up or Down-converter. To improve the efficiency of the module it can be interesting to integrate an up or down-converter in the module, for example in the reflector. Figure 7.7 shows the use of concentrator combined with an up-converter[191] that can be adapted to fit within the light trapping module. The efficiency of up-converters strongly increases with intensity, so the best option is to place the up-convertor in an area with high intensity.

7.2 Incoupling of Diffuse Light when Using External Light Trapping

In nature, many plants (like sunflowers) orient their flowers or leaves towards the sun to collect more light, this motion is called Heliotropism. In concentrated photovoltaics (CPV) one also tracks the sun by aligning the concentrator axis

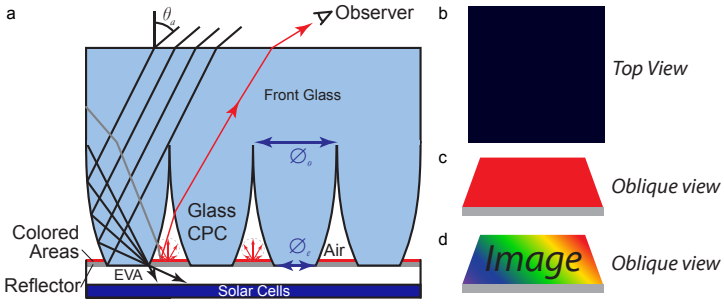

Figure 7.6: Design 4B. (a) Illustration of a colored light trapping module based on compound parabolic concentrators (CPC). Instead of using curved lenses on the front side of the glass, an array of CPCs can be applied at the inner-side of the glass front sheet. Light originating from angles larger than the acceptance angle will illuminate the areas in between the exit apertures. Light is specularly reflected from these painted areas resulting in a seeing a color for an observer that views the module from an angle larger than the acceptance angle. The CPCs can be of arbitrary size as long as ray optics applies (the illustration is not drawn to scale). The gray line illustrates an incoming ray that enters the module at an angle larger than the acceptance angle. This ray can for example originate from diffuse irradiance or reflection from the ground. Also indicated are the acceptance angle θ_a, the diameter of the opening ($\varnothing_o$) and that of the exit ($\varnothing_e$) of the CPC. The images on the right illustrate **(b)** the view of the module from the normal direction (black) and from an **(c)** oblique direction (red color). **(d)** By applying a picture on the red colored areas an image can be displayed by the module.

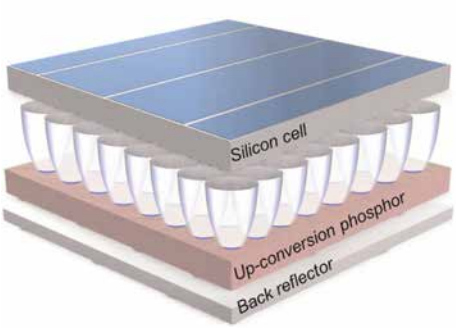

Figure 7.7: The solar cell is placed in front of the concentrator array.[191] Used under ⓒ license.

towards the (apparent) position of the sun. The concentration factors for CPV are generally in the order of 10-2 000×, and thus significantly higher than we suggest to use for the light trapping module (2-10×). The acceptance angle decreases with concentration factor according to eq. 4.1. At low concentration factors the acceptance angle is thus much larger.

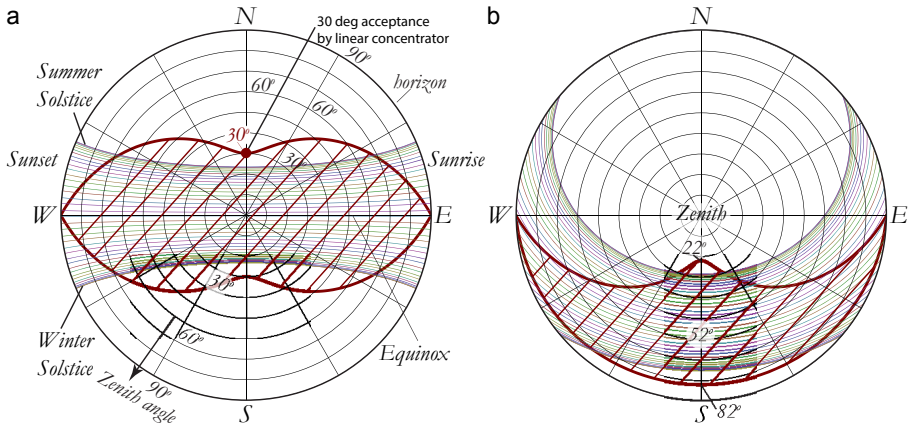

Figure 7.8: **(a)** Polar plot of the path of the sun during one year for a location on the equator. The concentric rings indicate the zenith angle of the sun and the position on the ring is the compass direction. The marked angles indicate angle to the zenith (the zenith marks the point in the sky directly above an observer). If the sun is directly overhead, it is in the center of this polar plot. During the summer and winter solstice, the sun moves along the top most curve and bottom most (thin) curve, respectively. The bold red curve marks the boundary of the acceptance angles for a static, horizontal module with a linear concentrator with an acceptance (half-)angle of 30°. When the sun is within this angular range the light is accepted and outside the angular region the light is rejected. **(b)** Same type of polar plot, but now at a latitude of 52 degrees North, which roughly represent the latitude of The Netherlands. The red area marks the acceptance angular region for a linear concentrator with an acceptance (half-)angle of 30°, that is tilted 52° South.

Currently, tracking is not widely deployed in non-concentrated photovoltaics. A single-axis tracker can improve the efficiency (per module area) by ∼15−20%, and a double-axis tracker lead to an enhancement of ∼25−40%.[97] Tracking systems are mostly used in utility scale ground mounted arrays. As the cost of modules decreased enormously during last decades, the costs of installation and maintenance of the tracking system makes the cost effectiveness of such systems less attractive than in the past. This trade-off changes when the efficiency of modules increases significantly.

Static Module. Because tracking the sun brings additional cost it is of interest to make a static, fixed mount, module that still accepts most of the incoming light. Here, we analyze some potential static designs for the light trapping module. The path of the sun covers only a small geometric area of the sky. Therefore, it is interesting to see whether it is possible to design a (static) concentrator that only collects the light from the part of the sky in which the sun moves.

Path of the Sun. Figure 7.8a shows a polar plot with the yearly path of the sun, as seen from a location on the equator. This position is calculated using the local

time, equation of time and some correction factors.[213–215] At the equator, the sun rises from a direction close to the East and sets at a direction close to the West. The tilt of the earth axis with respect to its orbital plane is ~23.45 degree. Due to the axial tilt of the earth, the path of the sun varies during the year. The axial tilt equals the zenith angle at noon of the summer and winters solstice for a geographic location on the equator. Figure 7.8b shows the yearly path of the sun for a latitude of 52 degrees North.

Matching of Sun Path and Acceptance Region. Most of the direct sunlight can be accepted by using a linear concentrator that is orientated along the East-West direction. For example, the bold red curve Figure 7.8a shows the outer boundary of the geometric acceptance angles for a horizontally orientated module with a linear compound parabolic concentrator (CPC) with an acceptance angle of 30°. This angle corresponds to a hollow concentrator with $C=2\times$ or a glass ($n=1.5$) concentrator with $C=3\times$ (see eq. 7.1). When the orientation of the sun is within this red border the light is completely accepted, otherwise it is rejected (reflected without hitting the solar cell). It can be seen that the matching of this linear concentrator is perfect at noon. However, at the hours just after sunrise and just before sunset the matching is poor. Alternative concentrator designs can improve this matching.

When the acceptance angle of the concentrator is equal to the axial tilt, the direct light is completely collected during each noon of the year. For other times during the day, the light will not be completely collected. By using an acceptance angle that is larger than the axial tilt of the earth, the sunlight can be collected during almost the complete day. As this acceptance angle of 30° is larger than the axial tilt, all light is accepted during noon (sun on direct North or South). During the equinox (sun on East-West line), the direct light of the sun is accepted from sunrise (east) to sunset (west). For other days of the year there is a small cut-off just after sunrise and just before sunset. However, this is only a small fraction of the daytime and moreover the intensity at low elevation (sun close to horizon) on the solar module is low due the long path length through the atmosphere as well as the decrease of the effective intensity on the module due an area projection[173] according to $I=I_{\text{sun}}\cdot\cos(\theta_{\text{i}})$, with θ_{i} the angle of incidence.

7.2.1 Acceptance of Diffuse and Direct Light

To estimate the performance of the external light trapping module we analyze which fraction of the direct and diffuse light is transmitted through the openings in the reflector (see Fig. 7.1). For isotropically distributed incident diffuse light, a fraction $1/C$ is transmitted by the CPC;[113, 162] for example, a $C=2\times$ concentrator thus transmits 50% of the diffuse light. The geographic location of the solar module determines the fraction of diffusely incoming photons. Geographic regions with a

high time-average of clear sky conditions are favorable for external light trapping. Also, it is advantageous to have a geographical location with a short (averaged) optical path length through the atmosphere to reduce Rayleigh scattering to minimize diffuse irradiance. Geographic locations at high elevation that are close to the equator and have only few clouds have therefore the lowest fraction of diffuse light and are thereby best suited for the basic light trapping modules. If the amount of transmitted light is too low, then more advanced designs like that shown in Fig. 7.3 can be used to capture both the direct and diffuse light completely.

For areas around the equator, the fraction of diffuse incoming photons is relatively low. For example, for Tamanrasset, Algeria the diffuse irradiance is ~10% ,[216] and a fraction of $10 \cdot 1/C$ of the total incoming light cannot be transmitted via the openings of the light trapping module. So, when a $C=2\times$ concentrator is used ~5% of the total light falls on top of the reflector. For other geographic areas this loss can be too high and therefore require using the design shown in Fig. 7.3.

Optimal Acceptance Angle. A remaining question is whether there exists an optimal concentration factor depending on the amount of diffuse light. To address this question we first assume that the direct light is accepted completely. When the concentration factor is changed this alters both the trapping performance (of both diffuse and direct accepted light) and the acceptance of diffuse light. In chapter 4 the following formula was derived for direct illumination:

$$A_{\text{trap}} = T_{\text{c}} \cdot \frac{A_{\text{sc}}}{1 - R_{\text{sc}}(1 - C^{-1}) R_{\text{cage}}}. \tag{7.3}$$

This equation can be adapted to include both the direct and diffuse component. For this first order approximation we again assume that the diffuse light is isotropically distributed. However, in reality the intensity (and spectrum) of the diffuse light (in first order) decreases with increase of the angle with respect to the zenith angle (or surface normal), because the path length through the atmosphere increases with this zenith angle.

A fraction f_{d} of the intensity of the incoming light is diffuse and the remaining intensity (1-f_{d}) is direct. A fraction $\frac{1}{C}$ of the diffuse light is transmitted. In that case eq. 7.3 becomes:

$$A_{\text{trap}} = (\overbrace{1 - f_{\text{d}}}^{\text{direct}} + \overbrace{f_{\text{d}} \frac{1}{C}}^{\text{Accepted Diffuse}}) \cdot T_{\text{c}} \cdot \frac{A_{\text{sc}}}{1 - R_{\text{sc}}(1 - C^{-1}) R_{\text{cage}}}. \tag{7.4}$$

This equation is expected to be fairly accurate for a measurement in a laboratory environment. However, due to the assumptions (such as isotropically distributed diffuse light and complete acceptance of the direct light), this equation only gives a rough estimate of the total yearly absorptance of an external light trapping module in the field. Figure 7.9 shows the total absorptance (A_{trap}) of the diffuse, direct

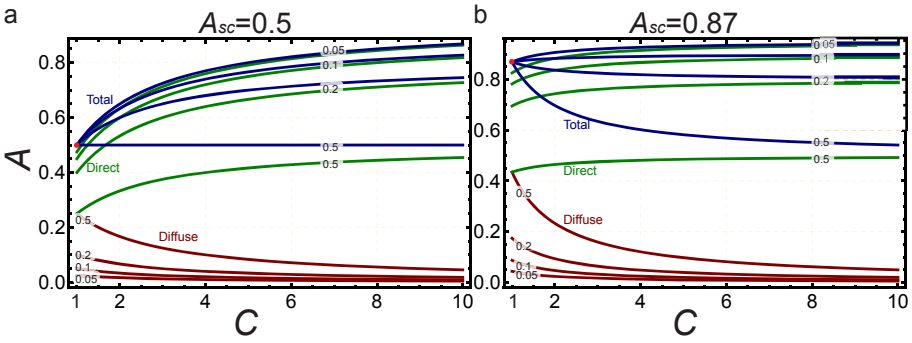

Figure 7.9: Plots of the absorptance by the solar cell with an external light trap for several components of the sunlight as a function of the concentration factor. The absorptance for isotropically distributed diffused light is shown in red, for direct light in green and for the total (diffuse + direct) light in blue. The curves are shown for various fractions of the diffuse light (f_d= 0.05, 0.1, 0.2, and 0.5). Please note that these values depend on many parameters of the irradiance that are not included, and therefore only give a rough indication for the "real" response at "field conditions".

and total irradiance as a function of the concentration factor (C) at a solar cell absorptance (A_{sc}) of 0.5 (Fig 7.9a) and 0.87 (Fig. 7.9b). The value A_{sc}=0.87 represents a typical module absorptance as shown in chapter 6. The different lines indicate the four different fractions (f_d) of diffuse irradiance. Figure 7.9a shows that the absorptance of a module with an absorptance of 0.5 (which is very low) without light trap increases when f_d<0.5 for different concentration factors of the external light trap. The total absorptance increases with concentration factor; so there is no optimal concentration factor as might be expected. Sun tracking is not required at low concentration factors (C<~2.5×) as we discussed in section 7.2.

To realize a significant improvement in absorptance for a more realistic module with an absorptance of A_{sc}=0.87 is more challenging. In this case an efficiency gain is obtained when the diffuse irradiance is less than 10%. Based on our assumption we can therefore conclude that the basic light trapping module has an efficiency enhancing potential in geographical regions with a diffuse irradiance of around 10% and lower. If the diffuse light is not isotropically distributed, but a relative large fraction of the diffuse light comes from the acceptance angle this conclusion is wrong. The basic external light trapping module has commercial potential if it enables the use of solar cells that are for example cheaper (as they can be thinner) and/or have a higher V_{oc} and efficiency (due to less bulk recombination due to reduced thickness and/or less surface recombination of a flat surface, see chapter 6). Alternatively, one can increase the spacing between the solar cells which brings down the c-Si material cost (per unit area) and increase the power output of the module. This inter-cell spacing is increased in some solar modules

fabricated by Trina Solar to improve the module power output.[217]

As the absorption of conventional c-Si solar modules is already fairly good, a larger commercial value of the light trapping module can be generated by its additional features, such as color and/or suitability for integration of tandem solar cells. The use of color for solar modules is certainly interesting for building integrated photovoltaics. However, it is difficult to estimate what price end-customers are willing to pay for such aesthetic modules.

For a good business case of integration of a tandem cell in the light trapping module, the availability of a stable, low-cost, high band gap solar cell is essential. Recently, a high band gap GaInP cell and a c-Si cell were mechanically stacked resulting in an efficiency of 29.8%.[218] Moreover, there is a high potential as high band gap cell coming from perovskite materials.[219, 220] The main benefits provided by the external light trapping module for tandem integration are the 4-terminal contacting, separate cell fabrication and improved light management. These significant advantages can render the external light trapping module as the superior technology for modules with tandem cells.

7.2.2 Suitability of External Light Trapping for Several Solar Cells

Table 7.1 (next page) indicates the suitability of external light trapping for several solar cell technologies. For cells with lower refractive index, a steeper texture is required and thereby it is more difficult to realize internal light trapping. Besides, the internal light trapping limit is relatively low due to the $4n^2$ limit for internal light trapping.[21] The light trapping module can also be used as a hybrid system by integrating (C)PV and solar thermal (heat), similar to previously published concepts.[19] Others demonstrated a hybrid concentrator photovoltaic architecture of CPV and PV for optimal use of the direct and diffuse sunlight.[221] This design might be combined with the light trapping module.

7.3 Fabrication

Type of Concentrator: Lens versus Parabola and their Optical Response. There are several options for the concentrator of the light trap: (Fresnel-) lenses, (compound) parabolic concentrators etc. Microlens arrays, as used in CMOS imaging and wavefront sensors,[222] are not expected to be optimal for the light trapping module due to their relative low transmittance, relative long focal length (f) and low numerical aperture (NA). Small lenses are commonly used in optical cameras, and there is high interest for relatively small lenses for camera integration in mobile phones. The technology developed for fabricating these lenses can be interesting for the fabrication of the lens array of the external light trapping module.

	n	Internal potential ($2n^2$)	Absorption remarks	Reflection Front Side	Radiative recombination[124]	Parasitic absorption indication	Expected Applicability & Remarks
thick c-Si	3.5-4	high	high	✔	✗	<10%	✔
thin c-Si	3.5-4	~	Low for long λ	✔	✗	<10%	✔✔
a- Si & μc-Si	3.5-4.5	high	Low for long λ	✔	✗	0-20% ITO, ZnO, doped layers, Ag (2%)	✔✔
GaAs	~3.5	high	high	✔	✔	low	✔ Gain from radiative recombination. Requires high concentrator transmittance.
CIGS	~ 3		Molybdenum (Parasitic)	✔	✗		? Requires back contact with higher reflectivity than Molybdenum.
OPV Perovskite	~2	✗	Low	~ (low n)	✗		✔✔
Hybrid Tandem				✔			✔ Easy for 4-terminal No current matching required
Thermal	-		high (A>90%)	✔			✔✔ Thermal radiation Improved absorptance
CPV				✔	✔		✔ Combine Concentration & Light trapping
Diffuse & Direct[146]							? More complex, but higher efficiency limit
Hybrid: Thermal & PV							✗Two separate systems can operate better at lower cost

Table 7.1: Overview of several parameters of several solar cells that determine the applicability of external light trapping. The question marks indicate that the applicability of external light trapping depends on a certain aspect of the solar cell.

There is a significant difference between metalized CPCs and dielectric lenses regarding the angular distribution of the light coming out of the lens. A lens refracts the light to a centric cone with a relative small angle around the concentrator axis, indicated by the blue area in Fig. 7.10. In contrast, the light exiting a CPC makes a large angle with respect to the concentrator axis, as indicated by the yellow area. Due to the relatively long focal distance (or low *NA)* of dielectric lenses, a relatively tall cage is needed to prevent light from escaping. This can be illustrated using the f-number of a lens (well known in photography). The f-number ($f\#$) is defined as:

$$f\#=\frac{f}{D}, \tag{7.5}$$

with f the focal length and D the diameter of the lens, see also Fig. 7.10.

Many lenses are not ideal. For these lenses equation 7.1 only gives an upper bound for the obtainable concentration factor (or acceptance angle). Conventional lenses have a less sharp defined acceptance angle than ideal lenses: above at a certain angle the optical efficiency (or transmittance) slowly drops from 100% to e.g. 0%.[125, 204]

Common objective lenses that are used in photography can have an f-number of 1.8 and they consist of a set of several lenses. The focal length is thus 1.8× larger than the diameter of the lens. A ray that travels through the middle of the lens will virtually propagate without being refracted, as shown in Fig. 7.11. For a simple curved lens with focal length f, the dimension of the image (S_2) that is formed of an object extending an angle of 2θ is $S_2=2\cdot f\cdot\theta$, see Fig. 7.11. From this optical ray it can be seen that the associated concentration area (S_2) of the lens is related to the acceptance angle (θ_a) by $S_2=f\cdot 2\cdot\tan(\theta_a)$. This concentration area determines the

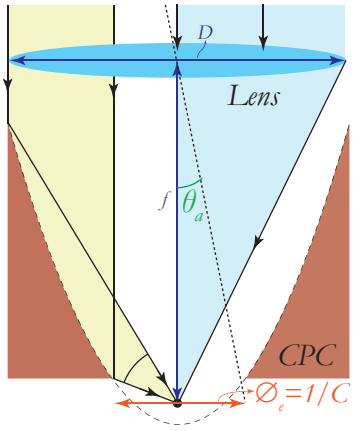

Figure 7.10: Illustration for comparison of a dielectric lens and a parabolic concentrator.

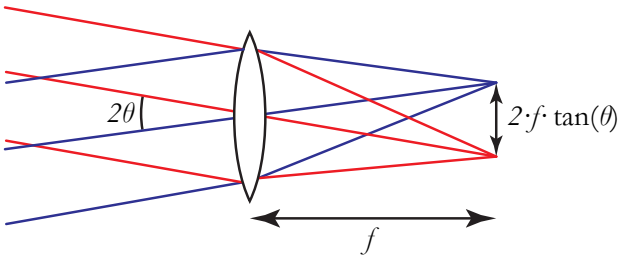

Figure 7.11: An object at infinity spans an angle of 2θ. A lens of focal length f forms an image of this object of size $2f\theta$.

exit diameter that should be used. The maximum concentration factor is related to the f-number according to:

$$C = \frac{D}{S_2} = \frac{D}{f \cdot 2 \cdot \tan(\theta_a)} = \frac{1}{f\# \cdot 2 \cdot \tan(\theta_a)}. \tag{7.6}$$

To realize a high concentration factor, the lens needs to have a low f-number. In practice, this means that the lens will be strongly curved (as can be calculated using the lensmaker equation). This equation cannot be directly applied to the lenses described in this chapter as they only have a curvature on the top side of the glass, instead of two curved sides. Besides, the light propagates in glass (instead of air as considered for the above equation). More research is needed to design dedicated lenses that (better) matches to the path of the sun and to determine their optical performance in terms of concentration factor and acceptance angle. As relatively low concentration factors are required for external light trapping, dielectric lenses are suitable. Fresnel lenses can be used to realize higher concentration factors, but they are hindered by lower transmittance.

Large Area Fabrication. An external light trap for large area applications will not be made by direct milling. Injection molding is a better fabrication option for large areas and large volumes. Generally, the precision molds that are used as master in injection molding processes are fabricated by milling and diamond turning. These highly precise parts are rather expensive (hundreds of thousands of dollars), but as each mold can be used to fabricate millions of items, the costs per item are still relatively low compared to other fabrication techniques. The accuracy of the mold is of extreme importance as this determines the accuracy of the final parts. As we demonstrated in chapter 6, the milling process results in significant artifacts and therefore the use of diamond turning for fabrication of the mold is expected to yield higher accuracy.[197] Alternatively, one can improve the polishing method and/or apply a smoothening coating to realize a smooth surface of the mold and/or the fabricated injection molded parts.

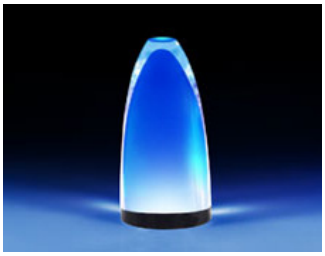

Figure 7.12: Photo of a compound parabolic concentrator.[28] © Edmund Optics

Fabrication Alternatives. There are various alternative types and fabricating methods and sizes for the concentrator.[129, 223–225] Alternatively, dielectric CPCs are interesting as they offer a higher degree of light trapping for a fixed acceptance angle.[28] The geometric concentration factor of a linear (2D) concentrator is given by:

$$C = \frac{n}{\sin(\theta_i)}, \tag{7.7}$$

with θ_i the acceptance angle.[125]

7.3.1 Fabrication & Materials

There are several companies that can be involved in the fabrication of a prototype module and develop mass scale fabrication equipment. For example: LuxExcel, Anterion, Isuzu Glass, VDL, LuxExel, Phillips, Docter Optics, and DSM.

***Ultra-Precision Glass Pressing* for Lens.** The lenses can be made from many materials by several fabrication processes. One option is to use *ultra-precision glass pressing* (also known as precision glass moulding), a process used for fabricating lenses in e.g. photo cameras. The costs of a mold process are much lower than the costs of mechanically processed (e.g. by diamond turning) glass. This process is commonly used for fabricating automotive headlight lenses. In this process (fire-)polished preforms are molded in their final shape such that the surface quality of the preform is preserved. A commonly used mold material is SCHOTT B270 superwite, which has an internal transmission of close to 100%. The only reflection losses occur at the interfaces, and can be minimized using anti-reflection coatings. A lens with an AR-coating still bends the light in (roughly) the same way as a lens without an AR-coating, so this improves the optical efficiency of the lens. The costs of this process are not expected to become sufficiently low; however, the process can be highly suited to fabricate a prototype. Figure 7.12 shows a photo of a commercially available CPC. This type of CPC lenses can be fabricated by Ultra-Precision Glass Pressing at relatively low cost. The transmittance of these CPCs can be more than 99.5% by using a proper AR coating. The optical efficiency of the lens

plays a crucial role. The knowledge of concentrators that was developed for CPV[226] can be used for the relatively low concentration factors used in the light trapping module. The polymer Zeonex® is used in many optical instruments and can be an interesting alternative material. It gives the design freedom of molded plastic and the optical properties of glass. One of the challenges of applying the polymer on top of glass sheet can be de-lamination due to the difference in physical properties of the two materials.

Reflector. The reflector can be fabricated from a highly specular reflective metal or diffuse reflective white paint (e.g. TiO_2). The diffuse or specular reflectivity can have important consequences on the homogeneity of the cell illumination and the light trapping efficiency (Section 6.4.2). The reflector needs to be reflective, but can be less reflective than the concentrator surface while still leading to good results.

Spacer. EVA is normally used as an encapsulation layer. In the light trapping module, the light needs to diverge over a sufficiently large distance after it passes the aperture to assure a certain degree of homogeneity. Moreover, a minimum amount of spacing is needed to assure the light is reflected by the reflector on its upwards path instead of a direct escape that happens if the cage is too short. As we discussed before, the lens should have a focal distance in the order of the thickness of the glass to assure the light is concentrated in the openings of the reflector at the backside of the glass. This condition implies that the required thickness of the EVA coating should be in the order of the thickness of the glass, if a (conventional) lens is used. When a CPC is used instead of a lens, a shorter spacing can be sufficient because the light exits a CPC at much larger outcoupling angles with respect to a lens, see Fig. 7.10.

References

[1] T. Stocker, D. Qin, G.-K. Plattner, M. Tignor, S. K. Allen, J. Boschung, A. Nauels, Y. Xia, V. Bex, and P. M. Midgley, *Climate change 2013: The physical science basis*, Cambridge University Press Cambridge, UK, and New York, 2014.

[2] R. T. Watson, M. C. Zinyowera, and R. H. Moss, *The regional impacts of climate change: an assessment of vulnerability*, Cambridge University Press, 1998.

[3] *Scripps Institution of Oceanography*, https://scripps.ucsd.edu/programs/keelingcurve.

[4] *NREL AM1.5 spectrum*, http://rredc.nrel.gov/solar/spectra/am1.5.

[5] D. Labuhn and S. Kabelac, *The spectral directional emissivity of photovoltaic surfaces*, International journal of thermophysics **22**, 1577 (2001).

[6] L. Zhu, A. Raman, K. X. Wang, M. A. Anoma, and S. Fan, *Radiative cooling of solar cells*, Optica **1**, 32 (2014).

[7] J. Hansen et al., *Earth's energy imbalance: Confirmation and implications*, science **308**, 1431 (2005).

[8] *IEA, World Energy Outlook 2015 - Executive Summary*.

[9] *COP21*, www.cop21paris.org.

[10] R. Schmalensee et al., *The Future of Solar Energy - An Interdisciplinary MIT Study led by the MIT Energy Initiative*, 2015.

[11] Many contributers from industry, *International Technology Roadmap for Photovoltaic (ITRPV), 2014 results*.

[12] M. M. de Wild-Scholten, *Energy payback time and carbon footprint of commercial photovoltaic systems*, Sol Energ Mat Sol C **119**, 296 (2013).

[13] J. N. Mayer, P. Simon, N. S. H. Philipps, T. Schlegl, and C. Senkpiel, *Current and Future Cost of Photovoltaics*, Long-term Scenarios for Market Development, System Prices and LCOE of Utility-Scale PV Systems (Fraunhofer ISE, Study on behalf of Agora Energiewende, Freiburg, 2015) (2015).

[14] M. Cambell, *The Drivers of the Levelized Cost of Electricity for Utility-Scale Photovoltaics (Report by SunPower Corporation)*.

[15] S. B. Darling, F. You, T. Veselka, and A. Velosa, *Assumptions and the levelized cost of energy for photovoltaics*, Energ Environ Sci **4**, 3133 (2011).

[16] *IEA - Statistics*, www.iea.org/statistics.

[17] *SolarGIS*, http://solargis.info.

[18] P. Würfel and U. Würfel, *Physics of Solar Cells: From Basic Principles to Advanced Concepts*, John Wiley & Sons, 2009.

[19] Z. J. Yu, K. C. Fisher, B. M. Wheelwright, R. P. Angel, and Z. C. Holman, *PVMirror: a new concept for tandem solar cells and hybrid solar converters*, Photovoltaics, IEEE Journal of **5**, 1791 (2015).

[20] *Photo Olympic Games, London 2012*, https://twitter.com/L2012PoolCam.

[21] E. Yablonovitch, *Statistical ray optics*, JOSA **72**, 899 (1982).

[22] *Movie of printing process, see Supporting info*, http://onlinelibrary.wiley.com/doi/10.1002/pip.2702/abstract.

[23] *Ultimaker homepage*, www.ultimaker.com.
[24] *OpenSCAD, CAD software*, www.openscad.org.
[25] *Cura, slicer software*, http://software.ultimaker.com.
[26] T. Coenen and A. Polman, *Polarization-sensitive cathodoluminescence Fourier microscopy*, Opt Express **20**, 18679 (2012).
[27] J. M. Bennett, J. Stanford, and E. Ashley, *Optical constants of silver sulfide tarnish films*, JOSA **60**, 224 (1970).
[28] *Edmund Optics, metallic-mirror-coatings*, www.edmundoptics.com.
[29] *HyET Solar*, www.hyetsolar.nl.
[30] A. Gordijn, *PhD Thesis, Microcrystalline Silicon for Thin-Film Solar Cells*, 2005.
[31] S. Okur, M. Güneş, F. Finger, and R. Carius, *Diffusion length measurements of microcrystalline silicon thin films prepared by hot-wire/catalytic chemical vapor deposition (HWCVD)*, Thin Solid Films **501**, 137 (2006).
[32] M. Boccard, C. Battaglia, S. Hänni, K. Söderström, J. Escarré, S. Nicolay, F. Meillaud, M. Despeisse, and C. Ballif, *Multiscale transparent electrode architecture for efficient light management and carrier collection in solar cells*, Nano lett **12**, 1344 (2012).
[33] H. Sai, K. Saito, N. Hozuki, and M. Kondo, *Relationship between the cell thickness and the optimum period of textured back reflectors in thin-film microcrystalline silicon solar cells*, Appl Phys Lett **102**, 053509 (2013).
[34] H. Sai, T. Koida, T. Matsui, I. Yoshida, K. Saito, and M. Kondo, *Microcrystalline Silicon Solar Cells with 10.5% Efficiency Realized by Improved Photon Absorption via Periodic Textures and Highly Transparent Conductive Oxide*, Appl Phys Express **6**, 104101 (2013).
[35] A. Polman, M. W. Knight, E. Garnett, B. Ehrler, and W. C. Sinke, *Photovoltaic materials: Present efficiencies and future challenges*, Science **352** (2016).
[36] Y. Kuang, M. Di Vece, J. K. Rath, L. van Dijk, and R. E. Schropp, *Elongated nanostructures for radial junction solar cells*, Rep Prog Phys **76**, 106502 (2013).
[37] M. Berginski, J. Hüpkes, M. Schulte, G. Schöpe, H. Stiebig, B. Rech, and M. Wuttig, *The effect of front ZnO: Al surface texture and optical transparency on efficient light trapping in silicon thin-film solar cells*, J Appl Phys **101**, 074903 (2007).
[38] J. Bhattacharya, N. Chakravarty, S. Pattnaik, W. D. Slafer, R. Biswas, and V. L. Dalal, *A photonic-plasmonic structure for enhancing light absorption in thin film solar cells*, Appl Phys Lett **99**, 131114 (2011).
[39] H. Tan, E. Psomadaki, O. Isabella, M. Fischer, P. Babal, R. Vasudevan, M. Zeman, and A. H. Smets, *Micro-textures for efficient light trapping and improved electrical performance in thin-film nanocrystalline silicon solar cells*, Appl Phys Lett **103**, 173905 (2013).
[40] Y. Kuang, M. van Lare, L. Veldhuizen, A. Polman, J. Rath, and R. E. Schropp, *Efficient nanorod-based amorphous silicon solar cells with advanced light trapping*, J Appl Phys **118**, 185307 (2015).
[41] R. Franken, R. Stolk, H. Li, C. Van der Werf, J. Rath, and R. E. Schropp, *Understanding light trapping by light scattering textured back electrodes in thin film n-i-p-type silicon solar cells*, J Appl Phys **102**, 014503 (2007).
[42] M. Di Vece, Y. Kuang, S. N. van Duren, J. M. Charry, L. van Dijk, and R. E. I. Schropp, *Plasmonic nano-antenna a-Si:H solar cell*, Opt Express **20**, 27327 (2012).
[43] M. Vanecek, O. Babchenko, A. Purkrt, J. Holovsky, N. Neykova, A. Poruba, Z. Remes, J. Meier, and U. Kroll, *Nanostructured three-dimensional thin film silicon solar cells with very high efficiency potential*, Appl Phys Lett **98**, 163503 (2011).
[44] T. Matsui, M. Tsukiji, H. Saika, T. Toyama, and H. Okamoto, *Influence of substrate texture on microstructure and photovoltaic performances of thin film polycrystalline silicon solar cells*, J Cryst Growth **299**, 1152 (2002).
[45] H. B. Li, R. H. Franken, J. K. Rath, and R. E. Schropp, *Structural defects caused by a rough substrate and their influence on the performance of hydrogenated nano-crystalline silicon n–i–p solar cells*, Sol Energ Mat Sol C **93**, 338 (2009).

[46] R. E. Schropp, J. Rath, and H. Li, *Growth mechanism of nanocrystalline silicon at the phase transition and its application in thin film solar cells,* J Crystal Growth **311**, 760 (2009).

[47] M. Python, O. Madani, D. Dominé, F. Meillaud, E. Vallat-Sauvain, and C. Ballif, *Influence of the substrate geometrical parameters on microcrystalline silicon growth for thin-film solar cells,* Sol Energ Mat Sol C **93**, 1714 (2009).

[48] M. Python, D. Dominé, T. Söderström, F. Meillaud, and C. Ballif, *Microcrystalline silicon solar cells: effect of substrate temperature on cracks and their role in post-oxidation,* Prog Photovolt Res Appl **18**, 491 (2010).

[49] M. Sever, J. Krč, and M. Topič, *Prediction of defective regions in optimisation of surface textures in thin-film silicon solar cells using combined model of layer growth,* Thin Solid Films **573**, 176 (2014).

[50] A. Gordijn, L. Hodakova, J. Rath, and R. E. Schropp, *Influence on cell performance of bulk defect density in microcrystalline silicon grown by VHF PECVD,* J Non-Cryst Solids **352**, 1868 (2006).

[51] G. Bugnon, G. Parascandolo, T. Söderström, P. Cuony, M. Despeisse, S. Hänni, J. Holovskỳ, F. Meillaud, and C. Ballif, *A new view of microcrystalline silicon: the role of plasma processing in achieving a dense and stable absorber material for photovoltaic applications,* Adv Funct Mater **22**, 3665 (2012).

[52] H. Sai, Y. Kanamori, and M. Kondo, *Flattened light-scattering substrate in thin film silicon solar cells for improved infrared response,* Appl Phys Lett **98**, 113502 (2011).

[53] K. Söderström, G. Bugnon, F.-J. Haug, S. Nicolay, and C. Ballif, *Experimental study of flat light-scattering substrates in thin-film silicon solar cells,* Sol Energ Mat Sol C **101**, 193 (2012).

[54] A. Feltrin, T. Suezaki, T. Meguro, and M. Ichikawa, *Advanced super light trapping of high efficiency thin film silicon solar cells,* 4th International Workshop on thin-film silicon solar cell (2012).

[55] M. Schwind, B. Kasemo, and I. Zorić, *Localized and propagating plasmons in metal films with nanoholes,* Nano lett **13**, 1743 (2013).

[56] P. Lacharmoise, N. Tognalli, A. Goñi, M. Alonso, A. Fainstein, R. Cole, J. Baumberg, J. G. de Abajo, and P. Bartlett, *Imaging optical near fields at metallic nanoscale voids,* Phys Rev B **78**, 125410 (2008).

[57] T. H. Reilly III, R. C. Tenent, T. M. Barnes, K. L. Rowlen, and J. van de Lagemaat, *Controlling the optical properties of plasmonic disordered nanohole silver films,* ACS nano **4**, 615 (2010).

[58] N. Rotenberg, M. Spasenović, T. Krijger, B. Le Feber, F. G. de Abajo, and L. Kuipers, *Plasmon scattering from single subwavelength holes,* Phys rev lett **108**, 127402 (2012).

[59] K. Vynck, M. Burresi, F. Riboli, and D. S. Wiersma, *Photon management in two-dimensional disordered media,* Nat Mater **11**, 1017 (2012).

[60] N. N. Lal, B. F. Soares, J. Sinha, F. Huang, S. Mahajan, P. Bartlett, N. Greenham, and J. J. Baumberg, *Enhancing solar cells with localized plasmons in nanovoids,* Opt express **19**, 11256 (2011).

[61] R. B. Dunbar, T. Pfadler, N. N. Lal, J. J. Baumberg, and L. Schmidt-Mende, *Imprinting localized plasmons for enhanced solar cells,* Nanotechnology **23**, 385202 (2012).

[62] S. Y. Chou and W. Ding, *Ultrathin, high-efficiency, broad-band, omni-acceptance, organic solar cells enhanced by plasmonic cavity with subwavelength hole array,* Opt Express **21**, A60 (2013).

[63] V. E. Ferry, M. A. Verschuuren, H. B. Li, R. E. Schropp, H. A. Atwater, and A. Polman, *Improved red-response in thin film a-Si: H solar cells with soft-imprinted plasmonic back reflectors,* Appl Phys Lett **95**, 183503 (2009).

[64] S. A. Mann, R. R. Grote, R. M. Osgood, and J. A. Schuller, *Dielectric particle and void resonators for thin film solar cell textures,* Opt Express **19**, 25729 (2011).

[65] P. Spinelli, M. Hebbink, R. De Waele, L. Black, F. Lenzmann, and A. Polman, *Optical impedance matching using coupled plasmonic nanoparticle arrays,* Nano Lett **11**, 1760 (2011).

[66] P. Spinelli, M. Verschuuren, and A. Polman, *Broadband omnidirectional antireflection coating based on subwavelength surface Mie resonators,* Nat Commun **3**, 692 (2012).

[67] P. Spinelli, V. Ferry, J. Van De Groep, C. Van Lare, M. Verschuuren, R. E. Schropp, H. Atwater, and A. Polman, *Plasmonic light trapping in thin-film Si solar cells,* J Opt **14**, 024002 (2012).

[68] P. Spinelli and A. Polman, *Prospects of near-field plasmonic absorption enhancement in semiconductor materials using embedded Ag nanoparticles*, Opt Express **20**, A641 (2012).

[69] P. Spinelli and A. Polman, *Light trapping in thin crystalline Si solar cells using surface Mie scatterers*, IEEE J Photovolt **4**, 554 (2014).

[70] C. van Lare and A. Polman, *Optimized Scattering Power Spectral Density of Photovoltaic Light-Trapping Patterns*, ACS Photonics **2**, 822 (2015).

[71] J. van de Groep, P. Spinelli, and A. Polman, *Single-step soft-imprinted large-area nanopatterned anti-reflection coating*, Nano Lett (2015).

[72] S. Veprek, F.-A. Sarott, and Z. Iqbal, *Effect of grain boundaries on the Raman spectra, optical absorption, and elastic light scattering in nanometer-sized crystalline silicon*, Phys Rev B **36**, 3344 (1987).

[73] M. Esfandyarpour, E. C. Garnett, Y. Cui, M. D. McGehee, and M. L. Brongersma, *Metamaterial mirrors in optoelectronic devices*, Nat Nanotechnol **9**, 542 (2014).

[74] J. Zhao, A. Wang, and M. Green, *24% efficient PERL structure silicon solar cells*, in *Photovoltaic Specialists Conference, 1990., Conference Record of the Twenty First IEEE*, pages 333–335, IEEE, 1990.

[75] M. A. Verschuuren, *PhD Thesis, Utrecht University, Substrate Conformal Imprint Lithography for Nanophotonics*, 2010.

[76] R. H. J. Franken, *PhD Thesis, Utrecht University, Transparent conducting oxide contacts and textured metal back reflectors for thin film silicon solar cells*, 2006.

[77] V. E. Ferry, M. A. Verschuuren, C. v. Lare, R. E. Schropp, H. A. Atwater, and A. Polman, *Optimized spatial correlations for broadband light trapping nanopatterns in high efficiency ultrathin film a-Si: H solar cells*, Nano Lett **11**, 4239 (2011).

[78] V. E. Ferry, A. Polman, and H. A. Atwater, *Modeling light trapping in nanostructured solar cells*, ACS nano **5**, 10055 (2011).

[79] C. van Lare, F. Lenzmann, M. A. Verschuuren, and A. Polman, *Dielectric Scattering Patterns for Efficient Light Trapping in Thin-Film Solar Cells*, Nano lett **15**, 4846 (2015).

[80] H. Zappe, *Fundamentals of Micro-optics*, Cambridge University Press, 2010.

[81] C. van Lare, F. Lenzmann, M. A. Verschuuren, and A. Polman, *Mode coupling by plasmonic surface scatterers in thin-film silicon solar cells*, Appl Phys Lett **101**, 221110 (2012).

[82] V. E. Ferry, J. N. Munday, and H. A. Atwater, *Design considerations for plasmonic photovoltaics*, Adv mater **22**, 4794 (2010).

[83] L. C. Andreani, A. Bozzola, and M. Liscidini, *The importance of light trapping in thin-film solar cells*, SPIE Newsroom .

[84] C. van Lare, G. Yin, A. Polman, and M. Schmid, *Light Coupling and Trapping in Ultra-thin Cu (In, Ga) Se2 Solar Cells using Dielectric Scattering Patterns*, ACS nano (2015).

[85] B. W. Schneider, N. N. Lal, S. Baker-Finch, and T. P. White, *Pyramidal surface textures for light trapping and antireflection in perovskite-on-silicon tandem solar cells*, Opt Express **22**, A1422 (2014).

[86] N. Vandamme, C. Hung-Ling, A. Gaucher, B. Behaghel, A. Lemaitre, A. Cattoni, C. Dupuis, N. Bardou, J.-F. Guillemoles, and S. Collin, *Ultrathin GaAs Solar Cells With a Silver Back Mirror*, IEEE J Photovolt **5**, 565 (2015).

[87] N. Tucher, J. Eisenlohr, H. Hauser, J. Benick, M. Graf, C. Müller, M. Hermle, J. C. Goldschmidt, and B. Bläsi, *Crystalline silicon solar cells with enhanced light trapping via rear side diffraction grating*, Energy Procedia **77**, 253 (2015).

[88] V. Steenhoff, A. Neumüller, O. Sergeev, M. Vehse, and C. Agert, *Integration of a-Ge: H nanocavity solar cells in tandem devices*, Sol Energ Mat Sol C (2015).

[89] Z. C. Holman, S. De Wolf, and C. Ballif, *Improving metal reflectors by suppressing surface plasmon polaritons: a priori calculation of the internal reflectance of a solar cell*, Light Sci Appl **2**, e106 (2013).

[90] C. Lin, L. J. Martínez, and M. L. Povinelli, *Experimental broadband absorption enhancement in silicon nanohole structures with optimized complex unit cells*, Opt Express **21**, A872 (2013).

[91] C. Wang, S. Yu, W. Chen, and C. Sun, *Highly efficient light-trapping structure design inspired by natural evolution*, Sci Rep **3** (2013).

[92] M. Smeets, V. Smirnov, K. Bittkau, M. Meier, R. Carius, U. Rau, and U. W. Paetzold, *Angular dependence of light trapping in nanophotonic thin-film solar cells*, Opt Express **23**, A1575 (2015).

[93] L. van Dijk, E. P. Marcus, A. J. Oostra, R. E. Schropp, and M. Di Vece, *3D-printed concentrator arrays for external light trapping on thin film solar cells*, Sol Energ Mat Sol C **139**, 19 (2015).

[94] L. van Dijk, U. W. Paetzold, G. A. Blab, R. E. I. Schropp, and M. Di Vece, *3D-printed external light trap for solar cells*, Prog Photovolt Res Appl (2015).

[95] H. Sai, T. Matsui, K. Saito, M. Kondo, and I. Yoshida, *Photocurrent enhancement in thin-film silicon solar cells by combination of anti-reflective sub-wavelength structures and light-trapping textures*, Prog Photovolt Res Appl (2015).

[96] R. Schropp, *Advances in solar cells made with hot wire chemical vapor deposition (HWCVD): superior films and devices at low equipment cost*, Thin Solid Films **403**, 17 (2002).

[97] A. Luque and S. Hegedus, *Handbook of photovoltaic science and engineering*, John Wiley & Sons, 2011.

[98] U. W. Paetzold, *Light trapping with plasmonic back contacts in thin-film silicon solar cells*, Forschungszentrum Jülich, 2013.

[99] V. Khanna et al., *A three diode model for industrial solar cells and estimation of solar cell parameters using PSO algorithm*, Renew Energy **78**, 105 (2015).

[100] J. Robinson and Y. Rahmat-Samii, *Particle swarm optimization in electromagnetics*, IEEE T Antenn Propag **52**, 397 (2004).

[101] S. Mokkapati and K. Catchpole, *Nanophotonic light trapping in solar cells*, J Appl Phys **112**, 101101 (2012).

[102] A. Polman and H. A. Atwater, *Photonic design principles for ultrahigh-efficiency photovoltaics*, Nat Mater **11**, 174 (2012).

[103] U. Rau, U. W. Paetzold, and T. Kirchartz, *Thermodynamics of light management in photovoltaic devices*, Phys Rev B **90**, 035211 (2014).

[104] C.-H. Sun, P. Jiang, and B. Jiang, *Broadband moth-eye antireflection coatings on silicon*, Appl Phys Lett **92**, 061112 (2008).

[105] U. Paetzold, M. Smeets, M. Meier, K. Bittkau, T. Merdzhanova, V. Smirnov, D. Michaelis, C. Waechter, R. Carius, and U. Rau, *Disorder improves nanophotonic light trapping in thin-film solar cells*, Appl Phys Lett **104**, 131102 (2014).

[106] J. Springer, A. Poruba, L. Müllerova, M. Vanecek, O. Kluth, and B. Rech, *Absorption loss at nanorough silver back reflector of thin-film silicon solar cells*, J Appl Phys **95**, 1427 (2004).

[107] F.-J. Haug, T. Söderström, O. Cubero, V. Terrazzoni-Daudrix, and C. Ballif, *Plasmonic absorption in textured silver back reflectors of thin film solar cells*, J Appl Phys **104**, 064509 (2008).

[108] E. Moulin, U. W. Paetzold, J. Kirchhoff, A. Bauer, and R. Carius, *Study of detached back reflector designs for thin-film silicon solar cells*, Phys Status Solidi-R **6**, 65 (2012).

[109] M. van Lare, F. Lenzmann, and A. Polman, *Dielectric back scattering patterns for light trapping in thin-film Si solar cells*, Opt Express **21**, 20738 (2013).

[110] R. Biswas and C. Xu, *Nano-crystalline silicon solar cell architecture with absorption at the classical $4n^2$ limit*, Opt Express **19**, A664 (2011).

[111] K. X. Wang, Z. Yu, V. Liu, Y. Cui, and S. Fan, *Absorption enhancement in ultrathin crystalline silicon solar cells with antireflection and light-trapping nanocone gratings*, Nano lett **12**, 1616 (2012).

[112] P. Campbell and M. A. Green, *The limiting efficiency of silicon solar cells under concentrated sunlight*, IEEE T Electron Dev **33**, 234 (1986).

[113] R. Winston, *Principles of solar concentrators of a novel design*, Sol Energy **16**, 89 (1974).

[114] M. Gaspare, *High yielding solar modulus for the transformation, on photovoltaic cells, of a substantially monochromatic radiation in electric energy*, 1986, EP Patent App. EP19,840,830,013.

[115] A. Goetzberger, J. Goldschmidt, and M. Peters, *Patent, Photovoltaic device and use thereof*, 2012, WO2011098212.

[116] P. Peumans, V. Bulović, and S. Forrest, *Efficient photon harvesting at high optical intensities in ultrathin organic double-heterostructure photovoltaic diodes*, Appl Phys Lett **76**, 2650 (2000).

[117] J. H. Atwater, P. Spinelli, E. Kosten, J. Parsons, C. Van Lare, J. van de Groep, J. Garcia de Abajo, A. Polman, and H. A. Atwater, *Microphotonic parabolic light directors fabricated by two-photon lithography*, Appl Phys Lett **99**, 151113 (2011).

[118] W. Yan, M. M. Hossain, and M. Gu, *High light-directing micrometer-sized parabolic mirror arrays*, Opt Lett **38**, 3177 (2013).

[119] P. Spinelli, B. Macco, M. Verschuuren, W. Kessels, and A. Polman, *Al2O3/TiO2 nano-pattern antireflection coating with ultralow surface recombination*, Appl Phys Lett **102**, 233902 (2013).

[120] J. Zhao, A. Wang, M. A. Green, and F. Ferrazza, *19.8% efficient "honeycomb" textured multicrystalline and 24.4% monocrystalline silicon solar cells*, Appl Phys Lett **73**, 1991 (1998).

[121] E. D. Kosten, J. H. Atwater, J. Parsons, A. Polman, and H. A. Atwater, *Highly efficient GaAs solar cells by limiting light emission angle*, Light Sci Appl **2**, e45 (2013).

[122] E. D. Kosten, B. M. Kayes, and H. A. Atwater, *Experimental demonstration of enhanced photon recycling in angle-restricted GaAs solar cells*, Energ Environ Sci **7**, 1907 (2014).

[123] A. Braun, E. A. Katz, D. Feuermann, B. M. Kayes, and J. M. Gordon, *Photovoltaic performance enhancement by external recycling of photon emission*, Energ Environ Sci **6**, 1499 (2013).

[124] M. A. Green, *Radiative efficiency of state-of-the-art photovoltaic cells*, Prog Photovolt Res Appl **20**, 472 (2012).

[125] R. Winston, J. Miñano, and P. Benítez, *Nonimaging Optics*, Electronics & Electrical, Elsevier Academic Press, 2005.

[126] A. Rabl, J. O'gallagher, and R. Winston, *Design and test of non-evacuated solar collectors with compound parabolic concentrators*, Sol Energy **25**, 335 (1980).

[127] *Solargenix Energy*, www.solargenix.com.

[128] M. Paire, L. Lombez, N. Péré-Laperne, S. Collin, J.-L. Pelouard, D. Lincot, and J.-F. Guillemoles, *Microscale solar cells for high concentration on polycrystalline Cu (In, Ga) Se2 thin films*, Appl Phys Lett **98**, 264102 (2011).

[129] B. H. Jared et al., *Micro-concentrators for a microsystems-enabled photovoltaic system*, Opt Express **22**, A521 (2014).

[130] T. Gu, G. Agrawal, A. Vessey, W. C. Sweatt, B. H. Jared, J. L. Cruz-Campa, R. Goeke, W. K. Miller, D. L. Zamora, E. Langlois, M. Okandan, G. N. Nielson, and M. W. Haney, *Micro-concentrator Module for Microsystems-enabled Photovoltaics: Optical Performance Characterization, Modeling and Analysis, in the proceeding of IEEE PVSC 2015*, (2015).

[131] S. Jutteau, P. F. Paire, Myriam and, L. Lombez, and J.-F. Guillemoles, *Micro solar concentrators: Design and fabrication for microcells arrays, in the proceeding of IEEE PVSC 2015*, IEEE PVSC, 2015.

[132] F. Khan, S.-H. Baek, J. Kaur, I. Fareed, A. Mobin, and J. H. Kim, *Paraboloid Structured Silicon Surface for Enhanced Light Absorption: Experimental and Simulative Investigations*, Nanoscale Res Lett **10**, 1 (2015).

[133] A. Luque and J. C. Miñano, *Optical aspects in photovoltaic energy conversion*, Sol Cells **31**, 237 (1991).

[134] C. Ulbrich, M. Peters, B. Bläsi, T. Kirchartz, A. Gerber, and U. Rau, *Enhanced light trapping in thin-film solar cells by a directionally selective filter*, Opt Express **18**, A133 (2010).

[135] E. D. Kosten et al., *Limiting light escape angle in silicon photovoltaics: ideal and realistic cells*, IEEE J Photovolt **5**, 61 (2015).

[136] W. Shockley and H. J. Queisser, *Detailed balance limit of efficiency of p-n junction solar cells*, J Appl Phys **32**, 510 (1960).

[137] A. Richter, M. Hermle, and S. W. Glunz, *Reassessment of the limiting efficiency for crystalline silicon solar cells*, Photovoltaics, IEEE Journal of **3**, 1184 (2013).

[138] M. A. Green, *Lambertian light trapping in textured solar cells and light-emitting diodes: analytical solutions*, Prog Photovolt Res Appl **10**, 235 (2002).

[139] J. Nelson, *The physics of solar cells*, World Scientific, 2003.

[140] A. Luque, G. Sala, and J. Arboiro, *Electric and thermal model for non-uniformly illuminated concentration cells*, Sol Energ Mat Sol C **51**, 269 (1998).

[141] J. M. Gordon, D. Feuermann, and H. Mashaal, *Micro-optical designs for angular confinement in solar cells*, J Photon Energy **5**, 055599 (2015).

[142] L. A. Weinstein, W.-C. Hsu, S. Yerci, S. V. Boriskina, and G. Chen, *Enhanced absorption of thin-film photovoltaic cells using an optical cavity*, J Opt **17**, 055901 (2015).

[143] J. Woerdenweber, T. Merdzhanova, T. Zimmermann, A. Flikweert, H. Stiebig, W. Beyer, and A. Gordijn, *Cross-contamination in single-chamber processes for thin-film silicon solar cells*, J Non-Cryst Solids **358**, 2183 (2012).

[144] J. M. Gordon, D. Feuermann, M. Huleihil, and E. A. Katz, *New optical systems for the solar generation of nanomaterials*, in *Optical Science and Technology, SPIE's 48th Annual Meeting*, pages 99–108, 2004.

[145] L. Weinstein, D. Kraemer, K. McEnaney, and G. Chen, *Optical cavity for improved performance of solar receivers in solar-thermal systems*, Sol Energy **108**, 69 (2014).

[146] M. Tormen, O. Inganäs, K. Tvingstedt, and S. Zilio, *Photovoltaic device with enhanced light harvesting*, 2010, US Patent App. 12/601,798.

[147] K. Tvingstedt, S. Dal Zilio, O. Inganäs, and M. Tormen, *Trapping light with micro lenses in thin film organic photovoltaic cells*, Opt Express **16**, 21608 (2008).

[148] M. Peters, C. Ulbrich, J. C. Goldschmidt, J. Fernandez, G. Siefer, and B. Bläsi, *Directionally selective light trapping in a germanium solar cell*, Opt Express **19**, A136 (2011).

[149] S. J. Kim, G. Y. Margulis, S.-B. Rim, M. L. Brongersma, M. D. McGehee, and P. Peumans, *Geometric light trapping with a V-trap for efficient organic solar cells*, Opt Express **21**, A305 (2013).

[150] J. Zhao, A. Wang, M. A. Green, and F. Ferrazza, *19.8% efficient "honeycomb" textured multicrystalline and 24.4% monocrystalline silicon solar cells*, Appl Phys Lett **73**, 1991 (1998).

[151] K. Masuko, M. Shigematsu, T. Hashiguchi, D. Fujishima, M. Kai, N. Yoshimura, T. Yamaguchi, Y. Ichihashi, T. Mishima, N. Matsubara, T. Yamanishi, T. Takahama, M. Taguchi, E. Maruyama, and S. Okamoto, *Achievement of More Than 25% Conversion Efficiency With Crystalline Silicon Heterojunction Solar Cell*, IEEE J Photovolt **4**, 1433 (2014).

[152] M. Kerr, J. Schmidt, A. Cuevas, and J. Bultman, *Surface recombination velocity of phosphorus-diffused silicon solar cell emitters passivated with plasma enhanced chemical vapor deposited silicon nitride and thermal silicon oxide*, J Appl Phys **89**, 3821 (2001).

[153] D. Macdonald, A. Cuevas, M. J. Kerr, C. Samundsett, D. Ruby, S. Winderbaum, and A. Leo, *Texturing industrial multicrystalline silicon solar cells*, Sol Energy **76**, 277 (2004).

[154] Z. Tang, W. Tress, and O. Inganas, *Light trapping in thin film organic solar cells*, Mater Today **17**, 389 (2014).

[155] A. Goetzberger, J. Goldschmidt, M. Peters, and P. Löper, *Light trapping, a new approach to spectrum splitting*, Sol Energ Mat Sol C **92**, 1570 (2008).

[156] S. D. Zilio, K. Tvingstedt, O. Inganäs, and M. Tormen, *Fabrication of a light trapping system for organic solar cells*, Microelectron Eng **86**, 1150 (2009).

[157] P. W. Blom, V. D. Mihailetchi, L. J. A. Koster, and D. E. Markov, *Device physics of polymer: fullerene bulk heterojunction solar cells*, Adv Mater **19**, 1551 (2007).

[158] S.-B. Rim, S. Zhao, S. R. Scully, M. D. McGehee, and P. Peumans, *An effective light trapping configuration for thin-film solar cells*, Appl Phys Lett **91**, 243501 (2007).

[159] M. A. Green, *Enhanced evanescent mode light trapping in organic solar cells and other low index optoelectronic devices*, Prog Photovoltaics **19**, 473 (2011).

[160] H. Deckman, C. Roxlo, and E. Yablonovitch, *Maximum statistical increase of optical absorption in textured semiconductor films*, Optics Lett **8**, 491 (1983).

[161] S. Iftiquar, J. Jung, C. Shin, H. Park, J. Park, J. Jung, and J. Yi, *Light management for enhanced efficiency of textured n–i–p type amorphous silicon solar cell*, Sol Energ Mat Sol C **132**, 348 (2015).

[162] A. Rabl, *Comparison of solar concentrators*, Sol Energy **18**, 93 (1976).

[163] S. Forrest, R. Lunt, and M. Slootsky, *Light trapping architecture for photovoltaic and photodetector applications*, 2012, WO Patent App. PCT/US2011/034,971.

[164] *Labsphere website on Spectralon®*, www.labsphere.com.

[165] A. J. Oostra, P. W. Blom, and J. J. Michels, *Prevention of short circuits in solution-processed OLED devices*, Org Electron **15**, 1166 (2014).

[166] M. Lampton, *Trade Study: Why Silver?*, www.ssl.berkeley.edu/~mlampton.

[167] J. Simmons and K. Potter, *Optical Materials*, Electronics & Electrical, Academic Press, 2000.

[168] Y. Xin, Z. Wang, L. Xu, X. Xu, Y. Liu, and F. Zhang, *UV-Ozone Treatment on Cs2CO3 Interfacial Layer for the Improvement of Inverted Polymer Solar Cells*, J Nanomater **2013**, 6 (2013).

[169] D. L. King, J. A. Kratochvil, and W. E. Boyson, *Measuring solar spectral and angle-of-incidence effects on photovoltaic modules and solar irradiance sensors*, 26th IEEE PVSC Conference , 1113 (1997).

[170] T. Mishima, M. Taguchi, H. Sakata, and E. Maruyama, *Development status of high-efficiency HIT solar cells*, Sol Energ Mat Sol C **95**, 18 (2011).

[171] S. C. Baker-Finch, *Rules and Tools for Understanding, Modelling and Designing Textured Silicon Solar Cells*, Thesis Australian National University (2012).

[172] S. C. Baker-Finch and K. R. McIntosh, *Reflection of normally incident light from silicon solar cells with pyramidal texture*, Prog Photovolt Res Appl **19**, 406 (2011).

[173] R. J. Beal, B. G. Potter, and J. H. Simmons, *Angle of Incidence Effects on External Quantum Efficiency in Multicrystalline Silicon Photovoltaics*, IEEE J Photovolt **4**, 1459 (2014).

[174] H. Savin, P. Repo, G. von Gastrow, P. Ortega, E. Calle, M. Garín, and R. Alcubilla, *Black silicon solar cells with interdigitated back-contacts achieve 22.1% efficiency*, Nat nanotechnol (2015).

[175] A. Gabor, *Cell-to-Module gains and losses in crystalline silicon PV, Gabor Photovoltaics Consulting*, July 10, 2013 Intersolar NA .

[176] G. Peharz, W. Nemitz, V. Schmidt, S. Schweitzer, W. Mühleisen, and C. Hirschl, *Investigations on the Photon-Recycling Properties of Different Back-sheets*, in *EUPVSEC*, 2014.

[177] *PVLighthouse - Tracey*, www.pvlighthouse.com.au.

[178] A. Richter, S. W. Glunz, F. Werner, J. Schmidt, and A. Cuevas, *Improved quantitative description of Auger recombination in crystalline silicon*, Phys Rev B **86**, 165202 (2012).

[179] H. Jin and K. Weber, *Relationship between interface defect density and surface recombination velocity in (111) and (100) silicon/silicon oxide structure*, in *EUPVSEC 2008*, volume 244, 2008.

[180] K. Xiong, S. Lu, D. Jiang, J. Dong, and H. Yang, *Effective recombination velocity of textured surfaces*, Appl Phys Lett **96**, 193107 (2010).

[181] M. Green et al., *Limits on the open-circuit voltage and efficiency of silicon solar cells imposed by intrinsic Auger processes*, IEEE Trans Electron Dev **31**, 671 (1984).

[182] *1366 Technologies, direct-wafer technology*, http://1366tech.com.

[183] *NexWafe*, http://nexwafe.com.

[184] *SmartWire Connection Technology*, www.meyerburger.com.

[185] M. F. Schumann, S. Wiesendanger, J. C. Goldschmidt, B. Bläsi, K. Bittkau, U. W. Paetzold, A. Sprafke, R. B. Wehrspohn, C. Rockstuhl, and M. Wegener, *Cloaked contact grids on solar cells by coordinate transformations: designs and prototypes*, Optica **2**, 850 (2015).

[186] P. Verlinden, R. Swanson, and R. Crane, *7000 high-eficiency cells for a dream*, Prog Photovolt Res Appl **2**, 143 (1994).

[187] M. Peters, J. C. Goldschmidt, T. Kirchartz, and B. Bläsi, *The photonic light trap - Improved light trapping in solar cells by angularly selective filters*, Sol Energ Mat Sol C **93**, 1721 (2009).

[188] O. Höhn, T. Kraus, G. Bauhuis, U. T. Schwarz, and B. Bläsi, *Maximal power output by solar cells with angular confinement*, Opt Express **22**, A715 (2014).

[189] R. A. Sinton and R. M. Swanson, *Increased photogeneration in thin silicon concentrator solar cells*, Electron Device Lett, IEEE **8**, 547 (1987).

[190] I. Papakonstantinou and C. Tummeltshammer, *Fundamental limits of concentration in luminescent solar concentrators revised: the effect of reabsorption and nonunity quantum yield*, Optica **2**, 841 (2015).

[191] G. E. Arnaoutakis, J. Marques-Hueso, A. Ivaturi, S. Fischer, J. C. Goldschmidt, K. W. Krämer, and B. S. Richards, *Enhanced energy conversion of up-conversion solar cells by the integration of compound parabolic concentrating optics*, Sol Energ Mat Sol C **140**, 217 (2015).

[192] J. Miñano, A. Luque, and I. Tobias, *Light-confining cavities for photovoltaic applications based on the angular-spatial limitation of the escaping beam*, Appl opt **31**, 3114 (1992).

[193] M. Planck, *The theory of heat radiation (Translation)*, Masius, P. Blackiston's Son & Co, Philadelphia (1914).

[194] *LightTools®*, http://optics.synopsys.com.

[195] C. Van Lare, *Light-trapping in thin-film solar cells using dielectric and metallic nanostructures*, Thesis University of Amsterdam (2014).

[196] B. T. Phong, *Illumination for computer generated pictures*, Communications of the ACM **18**, 311 (1975).

[197] E. L. Church and J. Zavada, *Residual surface roughness of diamond-turned optics*, Appl Opt **14**, 1788 (1975).

[198] A. Parretta, *Optics of solar concentrators Part I: Theoretical models of light collection*, Int J Opt Appl **3**, 27 (2013).

[199] *Labsphere®*, www.labsphere.com.

[200] *Hamamatsu, cell S1337-1010BQ data*, www.hamamatsu.com.

[201] C. Honsberg, *Cherry Award acceptance talk*, in *IEEE PVSC 2015, New Orleans*.

[202] A. Antonini, M. Stefancich, J. Coventry, and A. Parretta, *Modelling of compound parabolic concentrators for photovoltaic applications*, Int J Opt Appl **3**, 40 (2013).

[203] A. Parretta and A. Antonini, *Optics of solar concentrators. Part II: Models of light collection of 3D-CPCs under direct and collimated beams*, (2013).

[204] M. Victoria, C. Domínguez, I. Antón, and G. Sala, *Comparative analysis of different secondary optical elements for aspheric primary lenses*, Opt Express **17**, 6487 (2009).

[205] H. Uzu, M. Ichikawa, M. Hino, K. Nakano, T. Meguro, J. L. Hernández, H.-S. Kim, N.-G. Park, and K. Yamamoto, *High efficiency solar cells combining a perovskite and a silicon heterojunction solar cells via an optical splitting system*, Appl Phys Lett **106**, 013506 (2015).

[206] M. Lamers et al., *17.9% Metal-wrap-through mc-Si cells resulting in module efficiency of 17.0%*, Progress in Photovoltaics: Research and Applications **20**, 62 (2012).

[207] *IEEE - Tapping the Power of 100 Suns*, http://spectrum.ieee.org/green-tech/solar/tapping-the-power-of-100-suns.

[208] T. Bandara, W. Jayasundara, H. Fernado, M. Dissanayake, L. De Silva, I. Albinsson, M. Furlani, and B.-E. Mellander, *Efficiency of 10% for quasi-solid state dye-sensitized solar cells under low light irradiance*, Journal of Applied Electrochemistry **45**, 289 (2015).

[209] J.-H. Jung, J. Yeom, J. Hong, K. Hong, S.-W. Min, and B. Lee, *Effect of fundamental depth resolution and cardboard effect to perceived depth resolution on multi-view display*, Opt Express **19**, 20468 (2011).

[210] *Solaxess*, www.solaxess.ch.

[211] J. Escarre et al., *When PV modules are becoming real building elements: White solar module, a revolution for BIPV*, in *Photovoltaic Specialist Conference (PVSC), 2015 IEEE 42nd*, pages 1–2, IEEE, 2015.

[212] *SunpartnerTechnologies*, http://sunpartnertechnologies.com/smart-cities.

[213] L. Vant-Hull and A. F. Hildebrandt, *Solar thermal power system based on optical transmission*, Solar Energy **18**, 31 (1976).

[214] M. Blanco-Muriel, D. C. Alarcón-Padilla, T. López-Moratalla, and M. Lara-Coira, *Computing the solar vector*, Sol Energy **70**, 431 (2001).
[215] *PVEducation*, www.pveducation.org.
[216] *Meteonorm*, http://meteonorm.com.
[217] *Limit for industrial c-Si solar cells reached in 2030: what next?*, www.pv-tech.org/.
[218] S. Essig, *Realization of GaInP/Si dual-junction solar cells with 29.8 percent one-sun efficiency*, Submitted for publication in the IEEE Journal of Photovoltaics (2016).
[219] *DyeSol*, www.dyesol.com.
[220] *OxfordPV*, www.oxfordpv.com.
[221] N. Yamada and D. Hirai, *Maximization of conversion efficiency based on global normal irradiance using hybrid concentrator photovoltaic architecture*, Progress in Photovoltaics: Research and Applications (2016).
[222] *Thorlabs homepage*, www.thorlabs.com.
[223] D. Mills and J. Giutronich, *Ideal prism solar concentrators*, Sol Energy **21**, 423 (1978).
[224] M. A. Schuetz, K. A. Shell, S. A. Brown, G. S. Reinbolt, R. H. French, and R. J. Davis, *Design and construction of a 7× low-concentration photovoltaic system based on compound parabolic concentrators*, IEEE J Photovolt **2**, 382 (2012).
[225] K. Lee, J. Lee, B. A. Mazor, and S. R. Forrest, *Transforming the cost of solar-to-electrical energy conversion: Integrating thin-film GaAs solar cells with non-tracking mini-concentrators*, Light Sci Appl **4**, e288 (2015).
[226] K. Araki, K. Emery, G. Siefer, A. Bett, T. Sakakibara, Y. Kemmoku, N. Ekins-Daukes, H. Lee, and M. Yamaguchi, *Comparison of efficiency measurements for a HCPV module with 3J cells in 3 sites*, in *Photovoltaic Specialists Conference, 2005. Conference Record of the Thirty-first IEEE*, pages 846–849, IEEE, 2005.

Summary

Renewable energy resources such as wind and solar energy are essential to realize a sustainable society and a clean environment. In virtually all energy prognoses, solar energy will supply a significant fraction of the world energy demand within a few decades. This transition from polluting fossil fuels towards renewable energy will be significantly accelerated when the power conversion efficiency of solar cells further increases. A higher efficiency brings down the costs per delivered unit of energy, and thereby solar cells become even more economically competitive with fossil fuels. The efficiency of solar cells is related to their absorptance. Conventional solar modules do not absorb the incoming sunlight completely; instead they reflect a fraction to outer space. Solar modules therefore require light management to improve their absorptance. This thesis focuses on two solutions for improved absorptance of light in solar modules: internal and external light trapping. Internal light trapping is realized by internal cell modifications that lead to light guiding through the active layer of the solar cell. External light trapping is realized by applying optical elements on top of the solar cell.

Chapter 3 demonstrates enhanced internal light trapping in a thin film hydrogenated nano-crystalline silicon (nc-Si:H) solar cell. We introduce a novel scattering back reflector for flat nc-Si:H solar cells which consists of an array of silica nano-cylinders in a metal sheet. Typically, nc-Si:H solar cells are grown on textured substrates that scatter the incoming light. However, it is challenging to grow defect-free nc-Si:H layers on top of such (nano)-structured substrates. Instead of growing the solar cell on a textured substrate, we first deposited a flat high-quality nc-Si:H semi-cell on a flat piece of glass. This is called the superstrate configuration. On top of the nc-Si:H semi-cell, we applied a plasmonic scattering structure composed of a periodic array of dielectric nano-cylinders, which was overcoated by silver. This flat plasmonic scattering back reflector (PSBR) circumvents silicon growth defects and prevents the associated reduction of the open circuit voltage. At the same time, the geometry and the contrast of the dielectric index of the silicon, glass, and silver enable scattering of light when it interacts with this back reflector. By total internal reflection in the silicon,

most of the scattered light travels back and forth through the cell, similar to light propagating through an optical fiber. The light thereby travels a longer distance through the nano-patterned solar cell compared to a flat solar cell. This leads to an increase of the absorptance and thereby an increase in the short circuit current and efficiency of the solar cell. The PSBR can be fabricated over a large area using substrate conformal imprint lithography. Optical modeling was performed using finite-difference time-domain (FDTD) simulations to determine the absorptance in the active layer of the cell. The particle swarm optimization algorithm is used to optimize the PSBR geometry, such that the photocurrent is maximized. We fabricated a 1 micrometer thick nc-Si:H cell and experimentally demonstrate a current improvement of 32% compared to the flat reference cell, without affecting the open circuit voltage. The PSBR structure is not only effective for nc-Si solar cells, but can also be applied to a wide range of thin film superstrate solar cells.

The second part of this thesis describes various aspects of external light trapping. In an external light trap, a lens (or concentrator) is used to funnel the light through a small aperture in a mirror. This mirror is located above the solar cell. The light that reflects from the solar cell is reflected back to the solar cell by the mirror. Thereby, the light travels a longer distance through the solar cell, which leads to an enhanced efficiency.

Chapter 4 presents the first demonstration of a universally applicable 3D-printed external light trap. The required optical components were not off-the-shelf available and therefore we had to fabricate them. 3D-printing turned out to be excellent for prototyping. The light trap consists of a reflective parabolic concentrator that is placed on top of a reflective cage. The components of the light trap are 3D-printed and made of smoothened, silver coated thermoplastic. Due to the external light trap, the efficiency of a thin-film nanocrystalline silicon (nc-Si:H) solar cell improved by 15%. The trapped light traverses the solar cell several times within the reflective cage, and thereby the total absorption in the cell increases. Consequently, the trap reduces optical losses and enhances the absorption over the entire spectrum. In contrast to conventional light trapping methods external light trapping leaves the material quality and the electrical properties of the solar cell unaffected. To explain the theoretical operation of the external light trap, a model is introduced that predicts the absorption enhancement in a solar cell with an external light trap. The corresponding calculated path length enhancement shows good agreement with the empirically derived value from the opto-electrical data of the solar cell. Moreover, the influence of the angle of incidence on the parasitic absorptance is analyzed to improve the understanding of the trap performance.

Chapter 5 explores the potential of external light trapping for larger solar cell areas. The light trap is tested on organic solar cells, which have a major need for proper light trapping and can therefore significantly benefit from external light trapping. Scaling a single external light trap such that it covers a large solar panel

has disadvantages in terms of the height and cost. These disadvantages can be overcome by deploying an array of concentrators as the top part of the external light trap. We presented an optimization study of concentrator arrays for external light trapping. We fabricated 3D-printed external light traps with a square, hexagonal, and circular compound parabolic concentrator and tested their suitability for concentrator arrays. The 3D-printed traps were placed on top of an organic solar cell, which significantly enhanced the external quantum efficiency. The theoretical and experimentally determined optical performance of the different concentrators is compared and design guidelines for large scale concentrator arrays are given.

Chapter 6 moves one step beyond the realm of the previous chapters by considering the potential of external light trap on module level. A unique feature of using external light trapping on module level is the capability to simultaneously recycle the broadband reflection from the metal front grid, the front interfaces, the reflective backside of the cell, and the white back sheet in between the cells. A 64% reflectance reduction of a bare crystalline silicon (c-Si) solar cell is demonstrated. In contrast to conventional light trapping methods, external light trapping does not induce any damage to the active solar cell material. Moreover, this is a universally applicable technology that enables the use of thin and planar solar cells of superior electrical quality that were so far hindered by limited optical absorption. We milled a series of prototype millimeter-scale external metal light traps and applied these on a c-Si solar cell. We determined the concentrator transmittance and analyzed the effect of both the concentration factor and cage height on the absorptance and spatial intensity distribution on the surface of the solar cell.

Chapter 7 completes this thesis by considering several applications of external light trapping. We illustrate a basic design of a light trapping module that has a higher absorptance and higher power conversion efficiency. This module design is angular selective, which means that light coming from some angles does not make it to the solar cell. For some solar applications, the module has to track the sun to work efficiently and this brings additional cost. We show a configuration of the lenses that enables the module to be placed in a fixed position, while it captures most of the direct light during the each day of the year. Diffuse light comes from all angles and can therefore not completely be absorbed. We showed how the ratio of diffuse light (determined by the geographical position) affects the final module performance. After introducing this basic design, we show several potential upgrades for the light trapping module. For example, we show how two different solar cells can be integrated in the light trapping module. This allows the individual cells to be separately fabricated and contacted, leading to various fabrication and efficiency advantages. Also, we show how a layer of paint can be integrated in the light trapping module to show an arbitrary color, and even a picture can be shown. Depending on various cell properties and the geographical location of the solar module this can be realized while the efficiency of the module

is still enhanced. For geographical locations with a high degree of diffuse light the module performance will decrease slightly, but less severe than for other colored module concepts.

This thesis explored some designs that can be used to improve the efficiency of solar panels. Internal light trapping was shown to improve the efficiency of a thin film solar cell. Besides, we demonstrated the universal applicability of external light trapping by showing significant efficiency enhancement for several types of solar cells. Furthermore, the introduced light trapping module enables several new features for solar modules. External light trapping is therefore a serious candidate for a new generation of solar modules.

Samenvatting

Onuitputtelijke energiebronnen zoals wind- en zonne-energie spelen een essentiële rol bij de totstandkoming van een duurzame inrichting van onze samenleving. In bijna alle voorspellingen over de levering van energie in de toekomst zal zonne-energie in een aanzienlijk deel van de wereldwijde energiebehoefte voorzien binnen enkele tientallen jaren. De transitie van vervuilende fossiele brandstoffen naar duurzame bronnen kan aanzienlijk versneld worden wanneer de omzetting van licht naar elektriciteit (nog) verder toeneemt. Een hogere omzettingsefficiëntie verlaagt immers de kosten per geleverde energie-eenheid, waardoor zonnepanelen sterker concurreren met fossiele brandstoffen. De efficiëntie van een zonnepaneel is gerelateerd aan de hoeveelheid licht die het absorbeert. Zonnepanelen absorberen het zonlicht niet helemaal, een deel van het licht komt daardoor weer de module uit en gaat verloren. Het is daarom belangrijk om het pad van het licht zodanig te manipuleren dat het een zo lang mogelijke afstand door het actieve materiaal aflegt. In dit proefschrift worden hiervoor twee methodes gepresenteerd: interne en externe lichtopsluiting.

Hoofdstuk 3 geeft een demonstratie van interne lichtopsluiting in een dunne film waterstofhoudende nano-kristallijn silicium (nc-Si:H) zonnecel. We laten zien hoe een vierkant rooster van glazen nano-cilinders in een metalen film als een verstrooiende achterreflector in een vlakke nc-Si:H zonnecel gebruikt kan worden. Vaak groeit men nc-Si:H zonnecellen bovenop een getextureerd substraat. De textuur zorgt voor goede verstrooiing van het licht, maar het verslechtert de elektronische kwaliteit van het nc-Si:H. Daarom hebben we de fabricage omgedraaid en zijn met de bovenkant (de glaszijde) van de zonnecel begonnen, dit wordt de “superstraat configuratie” genoemd. Hiervoor hebben we eerst een vlakke, hoogkwalitatieve nc-Si:H (semi-)cel op glas gegroeid. Boven deze laag hebben we een vierkant rooster van glazen nano-cilinders aangebracht en deze met een laag zilver gecoat. Deze vlakke, verstrooiende achterreflector (PSBR) voorkomt groeifouten in het nc-Si:H en voorkomt daardoor dat de open-klemspanning van de cel verslechtert. De geometrie en het brekingsindexcontrast van het silicium, glas en zilver zorgen ervoor dat het inkomende licht in vele richtingen verstrooid

wordt door deze structuur. Door totale interne reflectie in het silicium zal een groot gedeelte van het verstrooide licht heen en weer door de cel reizen, net zoals in een glasvezel. Door deze lichtopsluiting legt het licht een langere afstand af. Dit heeft als gevolg dat de absorptie toeneemt en daarmee nemen ook de opgewekte stroomdichtheid en efficiëntie toe. De nanostructuur kan gefabriceerd worden op een groot oppervlak door gebruik te maken van een rubber stempel.

Met behulp van computersimulaties konden we een model van de absorptie in de zonnecel maken. Met het zwervende-deeltjes (ZD) algoritme konden we de geometrie van de nano-structuur efficiënt optimaliseren. Een eenvoudig algoritme, zoals het "brute kracht algoritme", probeert alle mogelijkheden en selecteert de beste geometrie. De rekentijd hiervoor kan echter vele dagen in beslag nemen op een supercomputer. Het ZD algoritme kan dit veel sneller doen. Eerst berekent het ZD algoritme de absorptie van een aantal random gekozen geometrieën. In de volgende stap selecteert het algoritme de beste geometrie en past de overige geometrieën aan zodat ze steeds meer gaan lijken op de (tot dan toe) beste geometrie. Dit voorkomt het doorrekenen van onnodig veel structuren en gaat dus veel sneller dan andere algoritmes. Een zonnecel met een dikte van 1 micrometer werd gefabriceerd. Door de aangebrachte nano-structuur op deze cel was de stroomdichtheid 32% hoger dan dat van de vlakke referentiecel. Bovendien werd er geen (nadelig) effect op de open-klemspanning gemeten. De ontwikkelde nano-structuur is niet alleen toepasbaar voor nc-Si:H cellen maar ook voor andere dunne film superstraat cellen.

Het tweede deel van dit proefschrift behandelt diverse aspecten van externe lichtopsluiting. In een externe lichtval wordt het licht dat uit de zonnecel komt en dreigt te ontsnappen teruggezonden naar de zonnecel. Dit wordt bereikt door een spiegelende kooi met een klein gaatje aan de bovenkant bovenop de zonnecel te plaatsen. Het zonlicht wordt met een lens (zoals een vergrootglas of een parabolische spiegel) gebundeld zodat het licht, via het gaatje in de kooi, de zonnecel bereikt. Doordat het grootste gedeelte van het gereflecteerde licht hierna nogmaals door de zonnecel gaat krijgt de zonnecel effectief een hogere efficiëntie. Een groot voordeel van deze manier van lichtopsluiting is dat het de werking van de zonnecel niet aantast, terwijl dit voor veel andere opsluit methodes wel het geval is. Bovendien worden de diverse bronnen van reflectie van een zonnecel in slechts één stap aangepakt en is de methode geschikt voor alle type zonnecellen.

Hoofdstuk 4 toont de eerste succesvolle demonstratie van een lichtval op een nc-Si:H zonnecel. Aangezien de benodigde parabolische spiegel en lichtkooi niet standaard verkrijgbaar zijn, hebben we de onderdelen met behulp van een 3D-printer gefabriceerd. Deze printer verhit een thermoplastic dat vervolgens vloeibaar wordt en een object laagje-voor-laagje opbouwt. Na het printen is het oppervlak nog ruw. Door het oppervlak kortstondig met een oplosmiddel vloeibaar te maken worden de kleine oneffenheden verwijderd. Na het verdampen van het

oplosmiddel blijft een spiegelglad oppervlak over. Daarna werd een dunne laag zilver aangebracht. Door de lichtval verbeterde de efficiëntie van de zonnecel met 15%. Met behulp van een theoretisch model hebben we uitgerekend hoeveel verbetering te verwachten was, en dit bleek zeer goed te kloppen met de metingen. Daarnaast is het effect van de hoek van inval op de zonnecel geanalyseerd om zo een beter begrip van de externe lichtval te krijgen.

Hoofdstuk 5 laat zien hoe deze technologie opgeschaald kan worden. Het gebruik van één enkele grote lichtval is onpraktisch en vereist bovendien veel materiaal. Deze problemen kunnen worden opgelost door een rooster van concentratoren te gebruiken. Dit hebben we gedemonstreerd met een organische zonnecel. We hebben onderzocht hoe dit zo optimaal mogelijk gerealiseerd kan worden. Hiervoor hebben we vierkante, hexagonale en ronde concentratoren gemaakt en hun prestatie gemeten. Daarnaast hebben we uitgerekend wat de minimale transmissie van de parabolische spiegel moet zijn om een gewenste efficiëntieverbetering te behalen.

Hoofdstuk 6 gaat een stap verder door te kijken naar de mogelijkheden voor lichtopsluiting op het niveau van het zonnepaneel. In een c-Si zonnepaneel reflecteert er licht op het metalen netwerk aan de voorkant van de cel (voor de elektrische geleiding), de materiaalovergangen, de achterkant van de zonnecel en het witte vlak tussen de zonnecellen (herkenbaar aan de witte strepen op een zonnepaneel). Het gebruik van de lichtval maakt het mogelijk om al deze reflecties in één stap terug naar de cel te sturen. Tevens wordt het mogelijk om dunnere c-Si cellen te gebruiken die betere elektrische eigenschappen hebben. Een goedkope manier om op grote schaal plastic voorwerpen te fabriceren is door ze te gieten in een mal, dit wordt spuitgieten genoemd en wordt industrieel toegepast voor de fabricage van bijna alle dagelijkse plastic voorwerpen. Deze techniek wordt bijvoorbeeld gebruikt voor het maken van optische componenten zoals lenzen voor brilglazen en lenzen op autokoplampen en zou tevens voor de fabricage van de externe lichtval gebruikt kunnen worden. De nauwkeurigheid van de metalen mal is van groot belang voor de gefabriceerde plastic onderdelen. Met een industrieel freesproces hebben we verschillende metalen concentrators gemaakt die aangepast zouden kunnen worden om als mal te gebruiken. Door het freesproces ontstonden kleine groeven in het oppervlak van de concentrator die de reflectie behoorlijk nadelig bleken te beïnvloeden. Daarnaast hebben we onderzocht wat het effect is van de concentratiefactor (de grootte van de opening in de kooi) en de hoogte van de kooi op de mate van lichtopsluiting en op de verdeling van het licht op de zonnecel.

Tot slot beschrijft hoofdstuk 7 diverse opties voor het commercieel toepassen van externe lichtopsluiting. De tot nu toe beschreven lichtvallen moeten worden aangepast om ze eenvoudig en goedkoop te kunnen integreren in een zonnepaneel. Aan de voorkant van een (standaard) zonnepaneel zit een glazen ruit. Op het

oppervlak van deze ruit kunnen we (op diverse manieren) lenzen aanbrengen. Aan de achterkant van de ruit maken we een reflecterende laag van bijvoorbeeld witte verf of een metaal zoals zilver of aluminium. In deze reflecterende laag maken we gaatjes waardoor de lens het licht kan focusseren. Hierna zit het licht gevangen tussen deze reflecterende laag en de zonnecel en daardoor verbetert de efficiëntie. Dit basisontwerp kan relatief eenvoudig in een zonnepaneel geïntegreerd worden omdat het maar weinig afwijkt van het standaard ontwerp van een zonnepaneel.

Het basisontwerp brengt veel nieuwe mogelijkheden met zich mee. Zo kunnen twee verschillende zonnecellen worden ingebouwd waardoor het zonnespectrum beter benut kan worden. De individuele zonnecellen kunnen los van elkaar worden geproduceerd en gecontacteerd, wat de fabricage vergemakkelijkt en een hogere efficiëntie in het vooruitzicht stelt. Daarnaast laten we zien dat een gekleurd zonnepaneel gemaakt kan worden door een laag verf aan de bovenkant van de reflecterende laag aan te brengen. Dit maakt het zelfs mogelijk om een afbeelding weer te geven. De techniek die we hiervoor bedacht hebben lijkt op die van lenticulaire ansichtkaarten, ook bekend als 3D-ansichtkaarten. Op deze kaarten zitten lijnvormige lenzen met daaronder verschillende afbeeldingen die in dunne stroken afgewisseld worden. Onder elke lens zit een geheel aantal stroken. Elke lens buigt het licht naar één focuslijn op de kaart. Als de kijkhoek verandert, dan verschuift de positie van de focuslijn. Indien het licht op een andere strook valt dan zal een andere afbeelding worden weergegeven. Op een zonnepaneel kunnen ook lijnvormige lenzen aangebracht worden. Hierdoor kan het (meeste) zonlicht via de gaten in de reflector naar binnen gaan en opgesloten worden en gelijktijdig kan het zonnepaneel één (of zelfs meerdere) afbeeldingen naar keuze laten zien voor verschillende kijkhoeken. In geografische gebieden met veel direct zonlicht kan deze afbeeldingstechniek gelijktijdig voor lichtopsluiting zorgen waardoor het zonnepaneel ook efficiënter wordt. In gebieden met veel diffuus licht zal de efficiëntie van het zonnepaneel iets afnemen. Elders in ontwikkeling zijnde concepten voor gekleurde of afbeelding vertonende zonnepanelen hebben een grotere negatieve impact op de omzettingsefficiëntie.

Samenvattend heeft dit proefschrift een aantal grensverleggende mogelijkheden verkend waardoor de efficiëntie van zonnepanelen nog beter kan worden. Door gebruik te maken van interne lichtopsluiting werd een hogere efficiëntie gemeten. Daarnaast hebben we laten zien hoe externe lichtopsluiting voor elk type zonnepaneel gebruikt kan worden en bovendien een voor een hogere theoretische efficiëntie zorgt. Bovendien maakt externe lichtopsluiting het mogelijk om het inkomende zonlicht beter te manipuleren, waardoor het zonnepaneel bijvoorbeeld een kleur of zelfs een afbeelding kan vertonen. Externe lichtopsluiting is daarmee een kanshebber voor een nieuwe generatie zonnepanelen.

List of Publications

This thesis is based on the following scientific publications:

- *Plasmonic Scattering Back Reflector for Light Trapping in Flat Nano-Crystalline Silicon Solar Cells*, L. van Dijk, J. van de Groep, L. W. Veldhuizen, M. Di Vece, A. Polman, and R. E. I. Schropp, ACS Photonics, (2016). **(Chapter 3)**

- *3D-printed external light trap for solar cells*, L. van Dijk, U. W. Paetzold, G.A. Blab, R. E. I. Schropp, and M. Di Vece, Progress in Photovoltaics: Research and Applications **24**, pages 623–633, (2016). **(Chapter 4)**

- *3D-printed concentrator arrays for external light trapping on thin film solar cells*, L. van Dijk, E. A. P. Marcus, A. J. Oostra, R. E. I. Schropp, and M. Di Vece, Solar Energy Materials and Solar Cells **139**, pages 19–26, (2015). **(Chapter 5)**

- *Universal External Light Trap for Photovoltaic Modules*, L. van Dijk, J. van de Groep, M. Di Vece, and R. E. I. Schropp, Submitted (2016). **(Chapter 6)**

- *Concepts for External Light Trapping and its Utilization in Colored and Image Displaying Photovoltaic Modules*, L. van Dijk, J. van de Groep, L. W. Veldhuizen, M. Di Vece, and R. E. I. Schropp, Submitted (2016). **(Chapter 7)**

The work described in Chapters 2 and 4-7 of this thesis was carried out at Utrecht University and Solliance[†] under the supervision of Prof. dr. R.E.I. Schropp and Dr. M. Di Vece. The work described in Chapter 3 was carried out at the FOM Institute AMOLF in Amsterdam, Utrecht University, and Solliance under the supervision of Prof. dr. A. Polman, Prof. dr. R.E.I. Schropp and Dr. M. Di Vece.

[†]Solliance is a partnership between TNO (the Netherlands Organisation for Applied Scientific Research), Eindhoven University of Technology, Holst Centre, the Energy research Centre of the Netherlands, IMEC, the Forschungszentrum Jülich, Delft University of Technology, and the University of Hasselt, and focuses on research and development of thin-film photovoltaic technologies.

Conference Proceedings

- *Light Trapping in μc-Si Solar Cells by Flat Plasmonic Scattering Back Reflector*, L. van Dijk, J. van de Groep, M. Di Vece, A. Polman, R. E. I. Schropp, Proceedings 29th European Photovoltaic Solar Energy Conference and Exhibition, WIP Germany, page 4298, (Amsterdam, 2014).

- *3D-printed external light traps for solar cells*, L. van Dijk, L., U. W. Paetzold, G. A. Blab, E. A. P. Marcus, A. J. Oostra, J. van de Groep, A. Polman, R. E. I. Schropp, and M. Di Vece, Proceedings 42nd IEEE Photovoltaic Specialist Conference (PVSC), pages 1-3, (New Orleans, 2015).

Other Publications

- *Heat transfer model of an iCVD reactor*, R. Bakker, V. Verlaan, A. D. Verkerk, C. H. M. Van der Werf, L. van Dijk, H. Rudolph, J. K. Rath, and R. E. I. Schropp, Thin Solid Films, 517(12), 3555-3558 (2009).

- *Plasmonic nano-antenna a-Si:H solar cell*, M. Di Vece, Y. Kuang, S. N. van Duren, J. M. Charry, L. van Dijk, and R. E. I. Schropp, Optics Express, 20(25), 27327-27336 (2012).

- *Elongated nanostructures for radial junction solar cells*, Y. Kuang, M. Di Vece, J. K. Rath, L. van Dijk, and R. E. I. Schropp, Reports on Progress in Physics 76.10: 106502 (2013).

I was just guessing at numbers and figures; pulling the puzzles apart
Questions of science; science and progress; do not speak as loud as my heart
[...] Nobody said it was easy; No one ever said it would be this hard.
Coldplay - The Scientist

Dankwoord

De mogelijkheid voor een promotieonderzoek is een geschenk waar ik dankbaar voor ben en waar ik erg van genoten heb! De afgelopen jaren werden getypeerd door een mix van fascinatie, frustratie, tumult, inzicht, verhuizingen, (de)monteren, kalibreren, teleurstellingen, eureka momentjes en doorzettingsvermogen. Ik heb op drie locaties mogen werken en daar veel inspirerende mensen leren kennen. Zonder hen was dit proefschrift nooit voltooid. Ik wil iedereen bedanken die hier een bijdrage aan heeft geleverd.

Als eerste wil ik mijn begeleiders bedanken. Ruud Schropp, bedankt voor je begeleiding door deze stormachtige tijden! We delen een passie voor high-efficiency: niet alleen voor efficiënte zonnecellen, maar ook voor efficiënt autorijden. Fijn dat je de vrijheid gaf voor zelfstandig onderzoek in een nieuwe richting. Marcel Di Vece, bedankt voor alle hulp die je gegeven hebt! De dagelijkse begeleiding werd er door de verhuizing niet makkelijker op, maar toch is het gelukkig allemaal goed gekomen. Dank voor jouw persoonlijke betrokkenheid, kritisch meedenken en vertrouwen in mijn onderzoeksideeën! Albert Polman, je bent een inspirerende professor voor mij geweest. Mijn dank is groot voor jouw enthousiaste begeleiding, positieve aanmoedigingen, gastvrijheid, persoonlijke aandacht en de groepsuitjes die we naast ons wetenschappelijk werk gedaan hebben! Jatin Rath, bedankt dat je altijd de tijd nam om mijn vragen te beantwoorden!

Daarnaast wil ik mijn collega's bedanken. Yinghuan Kuang, during the countless hours we shuttled between Zeist and Eindhoven, I enjoyed our diverse discussions. I got to know you as an extraordinary Chinese. Thanks for our collaboration, enjoyable moments and dinners. Let's make sure that we stay in touch for many years to come! Pim Veldhuizen, je bent een bescheiden, prettige collega en tevens een gezellige reispartner. Onze duik met zee-schildpadden zal ik niet snel vergeten. Dank voor de samenwerking, de diepgaande gesprekken en de fotoshoots! Ioannis, bedankt voor jouw enorme inzet. Thanks to the other colleagues that made the *Physics of Devices* group a social and pleasant work environment: Kees Landheer, Henriette Gatz, Akshatha Mohan, Dibya Koushik, Caterina Prastani, Minne de Jong, Diederick Spee, Zachar Krumer, Xin Jin, Jessica de Wild, Silvester Houweling, and Riny de Haas. Although we experienced challenging times after the movement of our lab, I felt strong social cohesion and perseverance. Kuang, Pim, Henriette, Akshatha, thanks for trusting me as your driver! Jan-Willem Schüttauf, fijn dat je altijd leven in de brouwerij bracht; jammer dat we maar zo'n

korte tijd collega's waren. Dick van Dam, Dayinta Perrier en Pepijn Marcus, ik vond het leuk om jullie te begeleiden, bedankt voor jullie bijdrage! Also thanks to the other students: Jamie, Sjors, Friso, Arjan, Tjeerd, Boudewijn and Stephan. Pieter Bons, dank voor onze lunchexpedities! Wim Westerveld, jouw enthousiasme maakte het assisteren van *practicum natuurkunde* een plezierige bezigheid.

Mijn Amolf collega's van de *Photonic Materials group* heb ik leren kennen als een sterk team met een aangename werkatmosfeer. Jorik van de Groep, van Kuznetsov tot en met Amolf hebben we veel samengewerkt. Hartelijk dank voor het delen van jouw helder inzicht, jouw belangrijke inhoudelijke bijdrage aan dit proefschrift en de gezellige momenten! Mark Knight, Bonna Newman, Claire van Lare, Piero Spinelli, Timmo van der Beek, Sander Mann, and Sebastian Öner, thanks for your help and the interesting brainstorms that we had on the future of solar energy! Benjamin Brenny, Ruben Maas, Marie Anne van de Haar, Toon Coenen en Rutger Thijssen: het was motiverend om bij jullie in het team te zitten!

Graag wil ik de mensen bedanken die ondersteuning bij het onderzoek leverden en er voor zorgden dat de fabricage en analyse apparatuur 'gesmeerd' bleef lopen. Van Universiteit Utrecht bedank ik: Caspar van Bommel, Martin Huijzer, Karine van der Werf, Ioannis Poulios, Bart Sasbrink, Arjen de Waal, Pieter Jan Dingemans, Jos van Gemert, Dave van den Heuvel en Judith Wijnhoven. Van Amolf bedank ik: Dimitry Lamers, Hans Zeijlemaker, Dion Ursem, Hinco Schoenmaker, Andries Lof, Henk-Jan Boluijt, Dirk-Jan Spaanderman en Menno Borsboom.

Ulrich Peatzold, Jolt Oostra and Gerhard Blab thanks for our smooth collaboration! Joep Bos-Coenraad, Dick de Boer, Mark Steltenpool en Marc Verschuuren, ik waardeer jullie bijdrage. Ik dank Radu Surdeanu en de rest van het team voor de interessante *Physics with Industry* week.

Door de verhuizing van ons lab kreeg ik vele nieuwe collega's binnen Solliance. Van ECN bedank ik Tristram Budel, Dong Zhang, Maarten Dörenkämper, Hans de Neve en Wim Soppe. Klaas Bakker, bedankt voor jouw hulp bij mijn veeleisende experimenten! Kostas Sinapis, thanks for our conversations. Roland Valckenborg, hartelijk dank voor het delen van jouw PV ervaringen in Afrika! Wiep Folkerts, Corry de Keizer en Menno van den Donker, bedankt voor jullie positieve bijdragen aan onze werkplek. Ruud Bakker, Bas van Aken en Wim Sinke, dank voor de uitstekende uitrusting die jullie meegegeven hebben.

Verder wil ik mijn vrienden en familie bedanken. Heren van Vaccae Conspectus en Maeradith, bedankt voor jullie gezelligheid! Mijn ouders dank ik voor de vrijheid, liefde en zorg die ze mij gaven. Pa, als klein kind was ik gefascineerd door de Crookes radiometer en vroeg wat licht precies is. Het antwoord kon jij niet geven, behalve dan dat licht iets complex is. Ik weet het antwoord nog steeds niet, maar ik weet nu wel hoe je er nuttige dingen mee kan doen. Roelof, Huibert en Jaap, jullie zijn de geweldigste broers die ik kan wensen!

Lieve Elmarie, bedankt voor jouw steun, betrokkenheid en onvoorwaardelijke liefde! Fijn dat jij mij regelmatig afleiding van mijn werk gaf, maar bovenal dat je met mij besloot om samen verder door het leven te gaan!

About the Author

Lourens van Dijk was born in Leusden, The Netherlands, on January 7, 1987. From his early youth he has been interested in miraculous phenomena that occur in nature and he has been trying to understand what's going on using Physics and Mathematics. Lourens obtained his high school diploma from *Guido de Brès*, Amersfoort, in 2005. He continued his scientific quest by studying Physics at Utrecht University with a solar energy related bachelor research. During his Master on Nanomaterials he wrote his thesis *Modeling and Optimization of Hydrogenated Amorphous Silicon Photovoltaics* at the Energy Research Centre of the Netherlands (ECN) under supervision of Dr. Bas van Aken and Prof. Dr. Wim Sinke. In 2011 he returned to Utrecht for his PhD research under supervision of Dr. Marcel Di Vece, Prof. Dr. Ruud Schropp, and Prof. Dr. Albert Polman.

During his PhD, Lourens supervised many students and assisted various experimental physics courses and summerschools. Furthermore, he was a member of the PhD committee of the Debye Institute of Nanomaterial Science. He presented his work at international conferences and collected several awards including the *FOM Film challenge award* (2012); a presentation and collaboration award at ACEEES (Los Angeles, 2013); the 1st poster award at INC10 (NIST, Maryland, 2014), NanoCity (Utrecht, 2014), and SunDayNL (Arnhem, 2014); and the poster award for "New Materials and Concepts for Solar Cells and Modules" at EUPVSEC (Hamburg, 2015). Lourens gave several interviews on his research in various media including Technisch Weekblad, NanoNextNL magazine and the JSP jaarverslag 2014. Moreover, he contributed to several solar cell related articles on Wikipedia and gave input for www.pvlighthouse.com.au.

In his free time, Lourens enjoys mountaineering, solving puzzles, photography, traveling and running. Although it is a tough challenge to change the energy use by nations, Lourens plans to continue his work on developing renewable energy technologies and policies to secure the energy supply of the future.